AN ABSTRACT OF THE THESIS OF

Duncan Stark for the degree of Master of Science in Civil Engineering presented on April 28, 2009.

Title: Experimental and Analytical Investigation of Ponding Load Effects on a Steel Joist Roof System

Abstract approved:

_____

Christopher C. Higgins

Ponding of water on roof systems leading to collapse causes expensive damage and jeopardizes the life safety of building occupants. Current building codes and design specifications for flat roof systems offer minimal guidance in designing for ponding loads. The present research investigated ponding load effects on a long span, lightweight roof system. A numerical study confirmed the established ponding stability theory and found that pitch does not provide large benefits until it becomes steeper than required by current specifications. Two full-scale roof systems consisting of steel joists, steel decking, rigid insulation, lateral bridging and roofing membrane (one flat and one on a 1/48 pitch) were designed, built, and loaded to failure under ponding water to permit detailed investigation of ponding load effects. Experimental results showed that the responses of both roofs were similar, that failure in both cases resulted from buckling of the joist top chord angles near midspan and that the total load on the roofs exceeded the specified strengths. Recommendations for future designs include proportioning the roof structure to support accumulated water to the level of the parapet wall and designing decking for the maximum water load that can accumulate at the lowest elevation of the roof.

Experimental and Analytical Investigation of Ponding Load Effects on a Steel Joist Roof System

by
Duncan Stark

A THESIS

Submitted to

Oregon State University

In partial fulfillment of
the requirements for the
degree of

Master of Science

Presented April 28, 2009
Commencement June 2009

Master of Science thesis of Duncan Stark presented on April 28, 2009.

APPROVED:

_____

Major Professor, representing Civil Engineering

_____

Head of the School of Civil and Construction Engineering

_____

Dean of the Graduate School

I understand that my thesis will become part of the permanent collection of Oregon State University libraries. My signature below authorizes release of my thesis to any reader upon request.

_____

Duncan Stark, Author

ACKNOWLEDGEMENTS

I owe thanks to many people for help with this project. First, thanks to Dr. Higgins for his guidance and patience with me on this project. Thanks also to Dr. Miller and Dr. Scott for their help with the project, and to all the professors I had for class over the last three years. This project would not have happened without the support of the Honors College, the College of Engineering and the Opportunity Plus program.

Thanks to Margaret Mellinger and the staff at the Valley Library who helped me find Academic Search Premier, Compendex, and a variety of information I would have been very frustrated without, as well as the CCE staff in the wave lab and in Owen and Kearney halls. Manfred Dittrich of the ECE department lent his skills, and Professor Robert Schultz lent equipment.

The completion of the lab work for this project would have been impossible without a few extra sets of hands. I owe thanks to several undergraduate assistants, including Edwin Safo-Kwakye, Kate Bradbury, Jake Goebel, Eric Goodall, and especially Ewan Stark. I also had help from some of the graduate research assistants in the lab and in the office, including Gautam Sopal, Josh Goodall, Quang Nguyen, Mary Ann Triska, Tugrul Turan, Ekin Senturk, Murat Hamutcuoglu and Thomas Schumacher. I also had occasional help from a couple friends, in particular, Andrew Stice and Ben Palmer.

Finally, thanks to the industry professionals and their employers for assistance with this project. Thanks to Mr. John Ashbaugh of Steven Schaefer Associates, Mr. Richard Davis of FM Global, Mr. Tim Holtermann of Canam, and Dr. Perry Green of the Steel Joist Institute.

TABLE OF CONTENTS

TABLE OF CONTENTS (Continued)

TABLE OF CONTENTS (Continued)

Page

TABLE OF CONTENTS (Continued)

Page

LIST OF FIGURES

LIST OF FIGURES (Continued)

Figure Page

LIST OF FIGURES (Continued)

Figure Page

LIST OF FIGURES (Continued)

Figure Page

LIST OF TABLES

LIST OF APPENDIX FIGURES

PREFACE

This is my Master's Thesis project. Through the Opportunity Plus program at Oregon State, offered by the College of Engineering and the University Honors College, I began this research as an undergraduate and wrote my Honors College thesis on the same topic. Much of what is contained here comes from that report. The research has been updated, expanded and completed, and the changes made here reflect that. There have been small updates to the literature review and numerical analysis sections, the experimental design section has been updated to reflect actual testing procedures, and the experimental results and conclusion sections are new.

EXPERIMENTAL AND ANALYTICAL INVESTIGATION OF PONDING LOAD EFFECTS ON A STEEL JOIST ROOF SYSTEM

INTRODUCTION

Despite consideration of a variety of loads, most building codes and design specifications provide only minimal guidance to design and construction professionals on the effects of ponding. The lack of dedicated space in code is not reflective of the importance or complexity of this type of loading. Ponding related roof collapses are common, destructive, and potentially life threatening. They often occur without warning, and can be difficult to predict (Blaauwendraad, 2007). They have occurred on roofs made of a variety of materials, including wood, steel, concrete and aluminum (Haussler, 1962) (Moody and Salama, 1967). Failures due to these loads have occurred across America, in both northern and southern regions, regardless of climate. This type of loading and the continued collapse of engineered roof systems under such conditions demand more research, a better understanding of the phenomena, and more prescriptive design provisions in building codes.

Definition

The ponding condition can be defined simply as progressive deflection and resulting accumulation of load until either stability or collapse is reached. In a typical scenario, a nearly flat roof will collect a certain amount of load in the form of snow or standing water, which will cause deflection. Assuming water is available, it can fill this deflection to a certain height (to at least the height of the supports), and the deflection will create a still

larger volume for the water to fill. As more water flows in, the deflection increases, and the water level continues to rise. This process can continue to one of three end cases. First, the roof system could reach stability, in which case excess water will flow over the edges, leaving collected water to eventually drain or dry out later. Second, the roof system could approach stability, but reach an overload condition before stability, and fail because the loads are too large. Third, in the most dangerous case, the roof deflections could become large and unbounded rapidly so that the roof system will never reach stability. In this case, the roof will fail eventually due to overload.

Ponding Stability

There are two phenomena that lead to failure under ponding loads: overload due to load amplification, and instability. While the overload condition will be experimentally tested, as it is more common, stability is also investigated. Ensuring stability of a roof system is not a simple matter, as the literature demonstrates. Many factors play a role, including the effects of two way systems, support conditions, sloped roofs, camber, and the geometry of the system. The work done in the area has shown that ponding stability or instability can be determined and that there are various methods of doing so. The most simple and widely cited ponding stability criterion was initially published by Robert Haussler in 1962, for a flat, simply supported beam. This generally represents the worst case, and a safe way to ensure stability. It is reproduced in modified form here:

$$\pi^4 EI > \gamma B L^4 \tag{1.1}$$

Where E is the modulus of elasticity, I is the moment of inertia, L is the length, B is the spacing between beams and γ is the unit weight of the fluid ponding on the roof. It is worth

noting that the ponding problem is purely geometric. In general, the stability of a system will depend on the properties of the members and their layout in the system. The properties that determine stability are internal to the system and do not include external factors, such as the initial load.

If a system is stable, then as the load and deflections increase, they will approach a limit. This limit may be above or below the critical load to cause failure, but if an infinitely strong, yet flexible system is assumed, then a stable system will come to equilibrium and not fail. If a system is unstable, the load and deflection will increase unboundedly until failure is reached. In this case, if an infinitely strong yet flexible system is assumed, then it will simply deflect to infinity. This means that for an unstable system with water available, any initial imperfection or deflection that allows water to begin to collect will cause collapse.

Causes of Ponding

Ponding loads can be caused by either rain or snow loads. It is common for snow on a roof to melt as heat passes through the building membrane, which can lead to the ponding effect. Additionally, snow on a roof often acts as a sponge, absorbing rainfall, and increasing the loads on a roof. Rain after a snowstorm may produce some of the heaviest loads a roof will experience, and can lead to ponding.

Several things must be present in a roofing system for it to be susceptible to ponding loads. First, it must be a relatively flexible roof. Without this quality, the roof will not deflect

enough to collect additional water to create a ponding situation. Also, a roof must either be relatively flat or sloped with some form of a parapet that allows collection of runoff water. Other issues that can exacerbate the problem include blocked, misplaced, or missing drains or scuppers and initial sag due to mechanical units or other unexpected dead loads. One problem to be aware of is that often, drains are placed near columns (Kaminetzky, 1991). This can be a problem because as the roof deflects under load, the points at columns will be the high points, and there is little sense in providing a drain at a high point.

Over the last century, there has been a trend in construction towards stronger materials. By using high strength materials such as steel, more efficient, long span roofs made of smaller, shallower and more slender building components have been possible (Bohannan and Kuenzi, 1964). This trend is epitomized in the efficiency provided by open web steel joists: very slender elements made of strong but ductile materials can lead to very efficient but very flexible structural units. While they allow for more efficient designs, high strength materials and flexible roofs require careful attention to detail to prevent ponding.

Prevention

It may appear to be a simple matter to ensure that a roof is stable and strong enough to withstand these loads, yet buildings continue to collapse under ponding loads. The problem in practice is that systems that are stable under the criteria provided in the literature and in the design specifications still experience ponding effects. A beam that is close to the critical ratio will be subjected to an amplification of the loads it experiences. A beam that is stable and strong enough to hold loads will still deflect, allowing larger loads to collect

on the system. The problem in design is that this amplification factor is not accounted for in roof systems that provide a slight pitch. The two simplest ways to avoid ponding are to either increase the pitch of the entire roof, or to provide more drainage in better locations (midspan), and conduct regular maintenance and inspection of the drainage systems. While not a cure for the problem, providing additional camber to steel joists or to the roofing system will help to reduce the effects of ponding loads. A cambered roof will collect water first at the edges, instead of at midspan, which produces much smaller bending moments and stresses in the system. This can easily be the difference between a failed and a safe roof.

Data Collection

The first thing any researcher will find regarding structural failures is that it is incredibly difficult to get data. It is hard to find any relevant, important, accurate data at all, let alone a comprehensive collection of information on the subject. It seems as though failures do not like exposure. In an article published in June 1981, a forward looking author wrote about the lack of available information on structural failures (ENR, 1981):

> "Large-scale structural failure is a nightmare that haunts the construction industry. The financial devastation, the demolished reputations and the loss of life that could result from collapse have troubled the sleep of probably every architect, engineer, contractor or owner at some time.
> This frightening quality of failures almost guarantees that they will continue to happen. Fear, embarrassment and the gag of interminable lawsuits have kept information on failures from traveling quickly enough, what little of it gets into general circulation at all.
> The way to dispel a nightmare is to attack it with hard fact, with eyes open wide and the mind alert…
> …A more promising development is the Engineering Performance Information Center. Its developers hope eventually to set up repositories for information on all types of failures, in a standardized format that would permit the comparisons necessary to develop an understanding of how

> failures can be prevented. This availability of complete and accurate information could be the first step towards shaking the dread of collapse."

The result of this work was the Architecture and Engineering Performance Information Center, established at the University of Maryland in 1982. The center no longer exists in this form, and could not be found elsewhere. It is likely that the "Fear, embarrassment and gag of interminable lawsuits" kept support from reaching the volume required to make it useful. A data center as described here would be incredibly valuable, and could lead to fewer structural failures in the future.

The best information obtained regarding failures, roof collapse and ponding loads came from the Factory Mutual Insurance Company (FM Global). They provide public data sheets on their webpage regarding the safety of a variety of commercial buildings and equipment. FM Global Public Data Sheet 1-54 provides information relevant to structural roof collapses, and some important statistics. An employee was also contacted for more specific information.

According to FM Global statistics, more than 1700 roof failures occurred over the twenty years from 1977 to 1996 (FM Global, 2006). FM Global states that the primary cause of overloading that leads to these failures is ponding of water in roof depressions. Their statistics show that the majority of these failures occur on flat roofs, and that blocked or inadequate drainage systems are a large contributor to the ponding problem. In a phone conversation with an employee at FM Global, it was noted that roof collapse is a serious problem, and that roof failures are typically very expensive, but that the number of deaths is small. It was also pointed out that the majority of roof collapses are due to snow and

rain, and that collapse is a much larger problem in the southern states, as rainfall intensity is higher, and resistance to loads is often lower, due to lower design snow loads.

FM Global also provided financial data on the costs involved in roof collapse. The data provided is representative of all roof collapses that were insured by FM Global, and provides the data both by number of failures and by the costs of those failures. This data shows that the average cost of a roof failure is around $770,000 and the total cost in 2007 dollars over the last 20 years is almost a billion dollars, which illustrates how costly these failures are. In the first set of data, the failures are divided by the type of load; in the second set, they are divided by type of construction. From the first set, shown in table 1, it can be seen that the two most damaging loads, by expense, are snow and rain. From the second set of data, shown in table 2, it can be seen that the two most damaged roofing systems, by cost, are metal buildings and steel decking on a steel frame, indicating that flexible materials more often lead to failures. Together, this data indicates that the ponding effect is a very strong contributor to roof collapse.

Table 1: Roof Collapse Data by Load, 1986-2005:

Probable Overload Cause	No. of Losses	Indexed Gross 2007$
SNOW, ICE, HAIL	730	$588,739,011
RAIN, ETC	255	$219,910,829
FIXED EQUIPMENT LOAD	16	$40,473,920
MISCELLANEOUS OVERLOAD	90	$33,761,599
CEMENT, SAND	15	$13,511,047
SNOW, ICE EQUIPMENT OVERLOAD	21	$12,988,698
STORAGE	55	$10,788,188
MISCELLANEOUS MATERIAL	4	$4,526,282
SAWDUST, CHIPS	9	$4,434,785
TEMPORARY EQUIPMENT LOAD	16	$4,006,022
Grand Total	1,211	$933,140,380

Table 2: Roof Collapse Data by Construction, 1986-2005:

Type of Construction	No. of Losses	Indexed Gross 2007$
All Metal Buildings	116	$369,027,896
Steel Deck on Steel	141	$207,629,811
Not Classified by Construction Type	779	$181,675,505
Concrete on Steel (Exposed)	22	$49,147,899
Boards on Joists	81	$42,292,682
Plank on Timber or Steel	24	$30,942,251
Plywood on Laminated Beam	23	$25,914,381
All Concrete (No exposed steel)	11	$14,050,841
Plank on Laminated Timber	7	$8,990,095
Miscellaneous	7	$3,469,019
Grand Total	1,211	$933,140,380

To put this data in perspective, it is important to note that it only represents losses from the companies FM Global ensures, which include about one third of S&P 1000 companies. FM global does not track deaths in their statistics, but other estimates indicate that roof collapses cause about 20 deaths yearly (Senteck, 2008). They also lead to huge financial costs and delays to companies, which could force some smaller companies to close.

Case Study: New OSU Energy Center

The best way to get a good practical understanding of how these types of roofs (steel deck, steel joist) are put together is to look at an actual example. The new OSU Energy Center, which is a replacement and upgrade to the old facility, will have about 23 thousand square feet (2137 square meters) of building space and produce enough energy to power about half of campus. This facility provides an interesting example of steel joist roof design. A typical roof will be pitched to the edge so that rain runs off into gutters. This roof, however, is pitched in both directions, so the rain from either side collects in the middle of the building.

The structure will use a steel deck roof supported on steel joists. The membrane roofing system will consist of a two ply SBS modified bitumen roofing system on ½ inch (12.7 mm) Georgia Pacific DensDeck insulation. Based on the design drawings, the joists of the highest roof are 30 ft (9.14 m) 16K9 joists spaced at 7.5 ft (2.29 m), and are welded to their supports. These joists are shorter than typical, but their strength is representative of roof loads in the area. Figure 1 shows the roof after the joists have been installed and figure 2 shows the roof with the deck, then insulation installed.

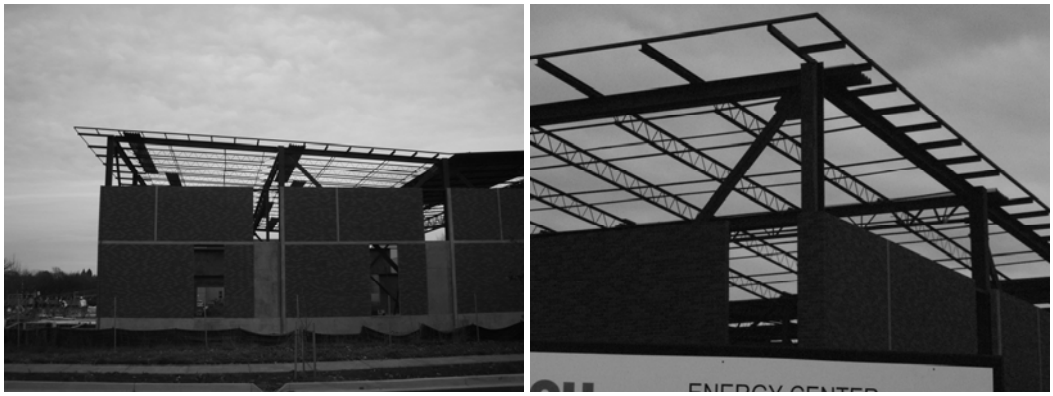

(a) (b)

Figure 1: OSU Energy Center, (a) November 15, 2007 (b) November 15, 2007

(a) (b)

Figure 2: OSU Energy Center, (a) November 30, 2007 (b) February 25, 2008

Research Goals

While there is a lot of knowledge in the literature regarding ponding loads, little of it has been incorporated into the design code. The ponding checks given in the code are brief when compared to the number of observed failures and the incurred costs over the past twenty years. It is hoped that this research will help create a better understanding of the ponding phenomenon, including how a roof deflects and how the loads are carried. Hopefully, the results will illustrate the joist deflection and strength, how the roof structure fails, what the load distribution looks like at failure, and what contribution the ponding effect makes to the load. A better understanding of ponding could reduce the number of failures, reduce costs, and prevent deaths by improving roof designs.

BACKGROUND

Literature Review

Although roof collapses have been a major concern for quite some time, collapse due to this specific load scenario was not studied until the 1960s. The literature comes from a variety of sources, and variables are defined differently by different authors. For this reason, all variables will be defined with the equations containing them.

The first paper written on the topic was published in 1962 by Robert W. Haussler (Haussler, 1962). In this paper, the author begins by assuming that the roof structure is a simply supported beam, and that deflections can be approximated by a half sine wave. Many authors use this approximation, as it makes the mathematics much simpler, and is only slightly conservative. He also assumes that the ponding fluid is not held by any wall, but only rises to the level of the supports. Using this as a starting point, he finds that for a stable system under water loads:

$$\frac{EI\pi^4}{L^4} > \gamma \tag{2.1}$$

Where E is the modulus of elasticity, I is the moment of inertia per inch of width, L is the length and γ is the unit weight of the fluid. If a roof is flat, provided with adequate drainage, and meets this stability requirement, then it will be safe from ponding loads. He also states that any roof built on an adequate slope will not experience ponding loads, as water will simply run off.

Haussler provides a very simplified method for calculating the required slope for a safe roof. He suggests the designer choose an initial slope, then use local rainfall data to estimate a depth at the low end. By assuming this depth is constant across the roof (a very conservative and simple assumption), an end rotation can be calculated. This rotation can then be used as a conservative value for the safe pitch of the roof.

Finally, Haussler notes that the analysis of complex roof structures (those with primary and secondary members) could be handled by using the sum of individual deflections. A designer could apply a 5 psf (239 Pa) load (approximately one inch or 2.54 cm of water), then sum the resulting deflection of each system. If this deflection is greater than an inch (2.54 cm), then ponding will probably be a problem. He also considers long span systems, and concludes that the common code live load limit of a fraction of the length (live load deflection limited to L/360) is meaningless with respect to ensuring ponding stability. The equation Haussler arrived at, equation 2.1, is not dependant on the live load at all. A better limit to ensure ponding stability would be a ratio of deflection to load (1/2 inch per 5 psf or 1.27 cm per 239 Pa).

Two years later, analysis of ponding loads superimposed on existing load cases was done (Bohannan and Kuenzi, 1964). The authors began by assuming linear elastic behavior and a sinusoidal deflected shape. Using energy methods, the authors determine that the work done by the load will be less than the energy in the beam if:

$$\frac{EI\pi^4}{a^4} > k \tag{2.2}$$

Where E is the modulus of elasticity, I is the moment of inertia, a is the length and k is the unit weight of the fluid times the beam spacing. They conclude that if the inequality is not satisfied, then the work done by the load will be greater than the bending energy, and the beam is unstable. This is essentially a confirmation of the work of Haussler. The authors continue, however, to expand the work to the case of an original distributed load in addition to the ponding load due to the deflection. The midspan deflection resulting from both loads can be calculated as:

$$\Delta = \frac{5w_0 * a^4}{384EI\left(1 - \frac{ka^4}{EI\pi^4}\right)} \tag{2.3}$$

Where w_0 is the initial uniform distributed load and all other variables are as previously defined. Note that this equation is simply a combination of the critical ponding criteria and the deflection due to a uniform distributed load. It is also good to notice that as a system approaches the limits for stability as defined in equations 2.1 and 2.2, this expression goes to infinity, and that the ponding effect amplifies the deflection due to initial loads by the factor:

$$\frac{1}{1 - \frac{ka^4}{EI\pi^4}} \tag{2.4}$$

As a result, the stresses in the materials are also increased by the same factor. The authors also go on to solve the problem for the case of a point load with additional ponding effects, and they repeat the analysis for both loading cases under fixed end conditions instead of the simply supported case. The theory was then tested with small aluminum beams. The experiment was set up with three cases. In the first, the total deflection should have been twice that under dead load alone, in the second, four times, and in the third case, the beam

was designed to be unstable and deflect to failure. The experiment verified the theory. The largest difference between the predicted and experimental results was the discrepancy between the theoretical and actual deflections under uniform loading, signaling that the greatest uncertainty was not in the ponding theory.

Less than a year later, a paper regarding the failure due to overload of these simply supported flat roofs under ponding loads was published (Chinn, 1965). The author expands on the problem of overload of stable roofs. First, Chinn determines that the final deflection of a beam under ponding loads is:

$$D = \frac{d}{1 - \frac{\gamma L^4}{\pi^4 EI}} \tag{2.5}$$

Where d is the initial deflection, γ the fluid unit weight times the beam spacing, L the length, E the modulus of elasticity of the material and I the moment of inertia. As in the Kuenzi and Bohannan paper, it is clear that as the system approaches the limits of the requirements for a stable system as outlined in equations 2.1 and 2.2, the final deflection will go to infinity. Chinn then solves for the maximum stress in a beam under ponding loads:

$$F = \frac{M_0 c}{I} + \frac{\gamma L^2 \pi^2 Ecd}{\pi^4 EI - \gamma L^4} \tag{2.6}$$

Where M_0 is the moment due to the initial loads, c is the distance from the neutral axis to the extreme fiber, and all other variables are as previously defined. This assumes that a beam will fail when it becomes inelastic. This equation allows an engineer to calculate when a stable system will fail due to overload, and could be used by a designer to choose an appropriate value for the moment of inertia of a member to prevent this failure mode.

The theory was then expanded to consider the effects of a two way system (Marino, 1966). Until now, all equations only considered a one way system bending independently of the supports. This paper treated the system as one with secondary members holding the load and supported by primary members that collect the load and transfer it to columns.

In a two way system, the primary members hold up the secondary members. The secondary members are more closely spaced, and have less strength than the primary members. The critical secondary member is the one at the center of the span of the primary member because it will be at the lowest elevation, thus incurring the greatest load. The author assumed that all of the primary members will deflect together so that a single bay can be analyzed as a unit, and that all deflections are sine waves. He also assumed that a theoretically stable system will not fail in overload conditions. From his analysis, Marino concludes that:

$$\Delta_w = \frac{\alpha_p\left(\Delta_0 + \frac{\pi}{4}\delta_0\right) + \frac{\pi}{4}\alpha_p\alpha_s\left(\delta_0 + \Delta_0\right)}{1 - \frac{\pi}{4}\alpha_p\alpha_s} \tag{2.7}$$

And:

$$\delta_w = \alpha_s\left(\delta_0 + \frac{\pi^2}{8}\Delta_0\right) + \frac{\pi^2}{8}\alpha_p\alpha_s\frac{\Delta_0 + \frac{\pi}{4}\delta_0 + \frac{\pi}{4}\alpha_s\delta_0 - \frac{2}{\pi}\alpha_s\delta_0}{1 - \frac{\pi}{4}\alpha_p\alpha_s} \tag{2.8}$$

Where Δ is the midspan deflection of a primary member, and δ is the midspan deflection of the critical secondary member. Subscript w indicates after the fluid load, subscript 0

indicates before the fluid load. The parameters α are defined in terms of flexibility constants:

$$\alpha_s = \frac{C_s}{1 - C_s} \tag{2.9}$$

$$\alpha_p = \frac{C_p}{1 - C_p} \tag{2.10}$$

And these flexibility constants are defined in terms of the properties of the system, reflecting the critical ponding criteria already outlined in previous literature:

$$C_s = \frac{\gamma S L_s^{\,4}}{\pi^4 E I_s} \tag{2.11}$$

$$C_p = \frac{\gamma L_s^{\,4} L_p}{\pi^4 E I_p} \tag{2.12}$$

Where s indicates secondary and p primary, S indicates the spacing between secondary members, L the length of the members, E the modulus of elasticity, I the moment of inertia, and γ the unit weight of the fluid.

Marino went on to make simplifying assumptions that make these equations easier to work with, and, using a factor of safety of 1.25, creates design aides based on the important properties of these systems. This analysis is now the basis of the improved AISC steel manual check for ponding. Marino concludes by stating that the easiest method of preventing this type of collapse is to provide sufficient slope to adequate drainage. He claims that 1/8 inch per foot (3.175 mm per 30.5 cm) should be sufficient, but notes that roof drainage can be complex and should be analyzed in more detail for roofs of this pitch.

Soon thereafter, the theory was expanded to cover several variations on the ponding problem (Moody and Salama, 1967). The authors expand the theory to include beams with different support conditions, ponding loads on plates, and they are the first to draw a connection between the ponding problem and steady state vibrations.

They begin by restating Haussler's inequality for a simply supported beam, rearranged to identify the critical stiffness. The authors go on to calculate the critical stiffness for beams and plates with varied supports. Throughout, the authors use superposition and a set of differential equations with appropriate boundary conditions. They solve the problem of the critical stiffness under ponding loads for a beam with supports that are simple-fixed, fixed-fixed, continuous over three supports with fixed ends, and continuous over any number of supports with simple supports. They also solve the problem for plates simply supported on all edges, simply supported on two edges and fixed on the others, fixed on all edges, and continuous over several simple supports. The results are summarized in figure 3:

TABLE 1.—SUMMARY OF THE MINIMUM CRITICAL STIFFNESSES FOR BEAMS AND PLATES

Boundary conditions	Minimum critical stiffness
(*a*) Beams	
Simple-Simple	$(E\,I)_{cr} = \frac{\bar{\gamma} L^4}{\pi^4}$
Simple-Fixed	$(E\,I)_{cr} = \frac{\bar{\gamma} L^4}{(3.927)^4}$
Fixed-Fixed	$(E\,I)_{cr} = \frac{\bar{\gamma} L^4}{(4.73)^4}$
Continuous over 3-supports (outside ends are fixed)	$(E\,I)_{cr} = \frac{\bar{\gamma} L^4}{(3.927)^4}$
Continuous over any number of simple supports	$(E\,I)_{cr} = \frac{\bar{\gamma} L^4}{\pi^4}$
(*b*) Plates	
Simple, four sides	$D_{cr} = \frac{\gamma}{\pi^4\left(\frac{1}{a^2} + \frac{1}{b^2}\right)^2}$
Simple along two opposite sides of length b, and fixed along two sides of length a	$D_{cr} = \frac{\gamma}{\left[\left(\frac{5.789}{b}\right)^2 - \left(\frac{\pi}{a}\right)^2\right]^2}$
Four sides fixed each of length a	$D_{cr} = \frac{\gamma a^4}{1.303.76}$
Continuous over any number of spans. All edges are simply supported	$D_{cr} = \frac{\gamma}{\pi^4\left(\frac{1}{a^2} + \frac{1}{b^2}\right)^2}$

Figure 3: Critical stiffnesses by boundary conditions (Moody and Salama, 1967)

Where $\bar{\gamma}$ is the unit weight times the beam spacing, L is the length, and a and b are the edge dimensions of a plate. The authors also note that the ponding problem is analogous to steady state forced vibrations. They relate the idea of the critical stiffness to the natural frequency of the member. This is useful, they assert, because there has been much more work done on the problem of steady state vibrations than ponding, so to relate the two would open up additional approaches for study of the ponding problem. In this analogy, the critical stiffness is analogous to harmonic vibration: as the period of a forcing function approaches the natural frequency, deflection becomes unbounded, just as deflection becomes unbounded when the stiffness of a beam or plate equals the critical stiffness. From this analogy, it is concluded that the critical stiffness can be calculated if the natural frequency of the beam or plate is known:

For Plates: $$\left(\frac{\gamma}{D}\right)_{cr} = \frac{m\omega^2}{D} \tag{2.13}$$

For Beams: $$\left(\frac{\gamma}{EI}\right)_{cr} = \frac{m\omega^2}{EI} \tag{2.14}$$

Where γ is the unit weight of the liquid, D and EI represent flexural rigidity, m is the mass per unit length or unit surface area, and ω is the natural frequency. The authors conclude by comparing the critical stiffness value for beams to the Euler buckling load for columns, and suggest that it should be used similarly as a critical design value.

Authors began attempting to create simple aides for designing for ponding (Sawyer, 1967). Donald Sawyer starts by re-deriving Haussler's original inequality. Sawyer sets the ponding critical stiffness criteria equal to a new value he terms the Criterion Ratio:

$$R = \frac{\gamma B L^4}{\pi^4 EI} \tag{2.15}$$

If the Criterion Ratio (R) is greater than unity, then Sawyer calls the beam supercritical. If the criterion ratio is equal to one, the beam is critical, and if it is less than that, it is subcritical.

Supercritical beams will fail with sustained rain or snow that allows the roof to continually deflect and collect load. This analysis of supercritical beams is only applicable for a set amount of water, that is, if conditions are such that water is not continually entering the system. Based on the criterion ratio and the design plots provided in figure 4, a designer should be able to calculate maximum moments, maximum deflection, and maximum weight.

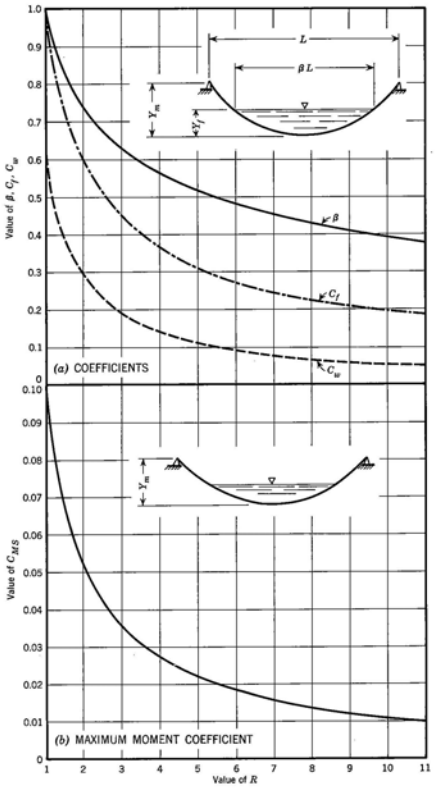

FIG. 1.—(a) COEFFICIENTS FOR SUPERCRITICAL BEAMS, (b) MAXIMUM MOMENT COEFFICIENT FOR SUPERCRITICAL BEAMS

Figure 4: Design guide (Sawyer, 1967)

After getting the values from the plots, the important properties of the supercritical beam can be calculated:

$$W_f = C_{ws}\gamma BY_s L \tag{2.16}$$

$$Y_m = \frac{W_f}{C_{ws}\gamma BL} \tag{2.17}$$

$$Y_f = C_f Y_m \tag{2.18}$$

$$M_m = C_{ms}\gamma BL^2 Y_m \tag{2.19}$$

Where W_f is the total weight of the load, Y_m is the maximum deflection, Y_f is the midspan liquid depth, M_m is the maximum moment. Y_s is the end depth of the liquid, γ is the unit weight of the liquid, B is the spacing, L is the length of the beams and the parameters C_{ws},

C_f and C_{ms} are from figure 4. This analysis is somewhat limited in the fact that it only applies to the situation where a set amount of liquid sits on the structure. For this specific case, this method makes the calculations simpler from a design standpoint.

It is more interesting, however, to study subcritical beams to determine when they will or will not fail, especially because most practical beams are subcritical. A general solution should allow for any depth, initial camber or sag, pitch, and include the effects of a two way system. The author constructs some curves that help identify parameters regarding subcritical beams. The use of the plot in figure 5 requires the designer to calculate both the Criterion Ratio, as well as a parameter, α, as defined individually in each plot, based on the degree of camber of the beam. From the plot shown in figure 5, a designer can find C_y for cambered or non-cambered beams, and C_w and C_m for cambered beams:

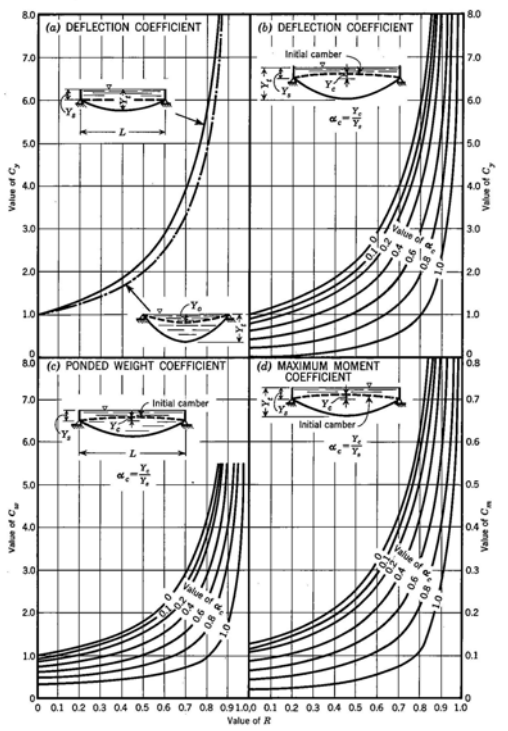

FIG. 2.—(a) DEFLECTION COEFFICIENT FOR INITIALLY FLAT BEAMS, (b) DEFLECTION COEFFICIENTS FOR CAMBERED BEAMS, (c) PONDED WEIGHT COEFFICIENTS FOR CAMBERED BEAMS, (d) MAXIMUM MOMENT COEFFICIENTS FOR CAMBERED BEAMS, (e) TOTAL REACTION COEFFICIENTS FOR SLOPED BEAMS, (f) MAXIMUM MOMENT COEFFICIENTS FOR SLOPED BEAMS

Figure 5: Design guide (Sawyer, 1967)

From these parameters, important properties of the subcritical beam can be calculated:

$$W_f = C_w \gamma B Y_s L \tag{2.20}$$

$$Y_t = C_y Y_s \tag{2.21}$$

$$M_m = C_m \gamma B Y_s L^2 \tag{2.22}$$

Where W_f is the total weight of the load, Y_t is the midspan deflection, M_m is the maximum moment, Y_s is the height of the liquid above the supports, and C_y, C_w and C_m are values pulled from the plots. The values are important because they will let a designer determine whether a beam will fail under ponding loads, even if it is part of a subcritical system.

It is clear that initial upward camber is beneficial to preventing ponding from occurring, but the author notes that caution should be used. Camber should not be used to replace the additional benefits provided by increasing the beam stiffness because as the depth of water approaches the height difference provided by the initial camber, the rate of deflection increases rapidly. For this reason, some roofs could perform well in some events, but fail under slightly heavier loads, depending on how close to this tipping point the system gets.

Sawyer also provides plots that allow a designer to calculate the maximum shear and moments in a beam on a slope, which is useful, as many sloped roofs should also be checked for ponding problems. He notes that in the current AISC specifications, (1963 Ed.) the check for ponding stability was disregarded for anything but a completely flat roof. He points out that some sloped roofs, if the slope is shallow enough, will still experience the ponding effect, and it is unacceptable to ignore this loading because a nominal pitch is specified. Sawyer argues that if it is reasonable to expect the water level to rise above the high end of the roof by at least one half of the depth at the low end, then the roof should be treated as flat. The plots he provides again require the user to calculate the Criterion Ratio and a parameter α based on the initial camber. The plots are shown in figure 6:

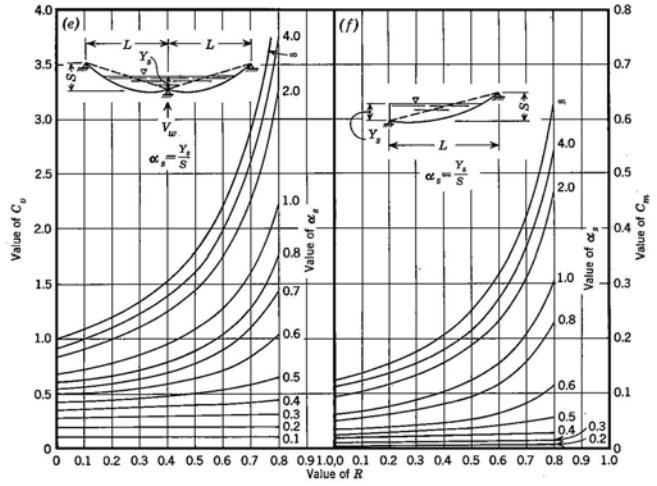

FIG. 2.—*CONTINUED*

Figure 6: Design guide (Sawyer, 1967)

Based on the values for the coefficients C_v and C_m from these plots, the maximum shear and moments can be calculated by equations 2.23 and 2.24:

$$M_m = C_m \gamma B Y_s L^2 \tag{2.23}$$

$$V_f = C_v \gamma B Y_s L \tag{2.24}$$

Sawyer goes on to discuss roof systems under ponding loads. Roof systems are more complicated than the simple one member case for several reasons. The variables are essentially compounded and interact in various ways. Sawyer treats the system in pairs of framing members. In each pair, he assigns a host (supporting members) and a parasite (supported members), and uses the properties of the parasite to modify those of the host. His procedure calls for the modification of the host Criterion Ratio by a factor of the parasitic member's C_w. First, R values are calculated. Next, starting at the top of the system, a C_w value is found for the parasite, and multiplied by the host's R to find the host's effective R value. This new R is then used in the next iteration when the host is treated as the parasite. In this way, the modifications of the Criterion Ratio compound, and

a system that looks sound at first glance may by further analysis not be adequate. This method is more involved than the one presented by Marino for two way systems.

Later, Salama and Moody expanded their study of beams and plates (Moody and Salama, 1967) to those with a nonlinear response (Moody and Salama, 1969). Following a complex analysis, they outlined an iterative procedure for calculating the response of these members. They conclude that for these nonlinear-elastic members, the initial load is an important factor on the final response, which is in contrast to what other authors have shown for linear-elastic beams and plates. It is doubtful that much of this work would be useful in a design situation, as materials are generally assumed to be linear elastic. The authors outline a complex iterative analysis technique, but provide no simple method of analysis.

That same year, an article was published that investigates subcritical beams with various loading conditions and the effect of initial imperfections on the ponding factor (Adams, Chinn and Mansouri, 1969). The authors begin with the usual assumptions, and analyze a simply supported beam with a fluid filling the depression formed in the middle of the span. They solve the governing fourth order linear non-homogeneous differential equation, and arrive at the same equation Haussler published years earlier. The authors provide equations for the maximum deflection, maximum moment, and beam end rotations for beams with ponded water superimposed with a point load, a distributed load, applied end moments, and nothing. The equations published are long and numerous; they will not be reprinted here.

The authors go on to investigate the effects of initial imperfections on ponding loads. They express the deflection in a Fourier sine series, which shows that the critical ponding factor is not dependant on the type of loading. They point out that a numerical solution would require truncating the series to the dominant term to get an approximate value of the internal forces. A more accurate method would be to treat the loads from the liquid in the depression separately from everything else. It has been shown that deflection is linear with initial imperfections and loads, so this analysis would work by superposition of all sources of deflection (Moody and Salama, 1967).

Again, engineers began trying to make the analysis simpler and more suitable for use in design, this time for two way systems (Burgett, 1973). The author simplified the existing plots and equations, which were based on the work of Marino, and produced just two simple equations. Roof framing systems were identified as stable if:

$$C_p + 0.9C_s \leq 0.25 \tag{2.25}$$

$$I_d \geq 25S^4 10^{-6} \tag{2.26}$$

Where I_d is the moment of inertia of the deck, S is the spacing, and C_p and C_s are defined:

$$C_p = \frac{32L_s L_p{}^4}{10^7 I_p} \tag{2.27}$$

$$C_s = \frac{32SL_s{}^4}{10^7 I_s} \tag{2.28}$$

Where L is span length, I moment of inertia, and the subscripts p and s represent the primary and secondary systems, respectively. Burgett also included graphical representations of these expressions for both deck and framing checks. This approach has

now been incorporated into the AISC code, in appendix 2, design for ponding, as the simplified design for ponding.

The same year, a paper was published that focused specifically on truss behavior under ponding (Chao, 1973). The author studied a specific structure: warren, pin connected, simply supported trusses. Using a set of differential equations, Chao solves for the joint displacements in the x and y directions for every node of the truss. The solution for the nodal displacements lists the displacements as functions of several variables: several parameters, a, defined in equations 2.29 to 2.34, the number of panels in the truss, n, and an arbitrary constant C.

$$a_0 = \frac{\gamma s d^2}{2 A_w E_w} \sec(\Theta) \csc^2(\Theta) \tag{2.29}$$

$$a_1 = \cot(\Theta) \tag{2.30}$$

$$a_2 = 2 \frac{A_w E_w}{A_t E_t} \cos^3(\Theta) \tag{2.31}$$

$$a_3 = 2 \frac{A_w E_w}{A_b E_b} \cos^3(\Theta) \tag{2.32}$$

$$a_4 = a_2 \tan(\Theta) \tag{2.33}$$

$$a_5 = a_3 \tan(\Theta) \tag{2.34}$$

Where γ is the fluid unit weight, s is the spacing of the trusses in the one way roof, d is the width of a panel, A is the cross sectional area, E is Young's Modulus, and Θ is the angle between chord and web members. The subscript w is for web, t for top chord, and b for bottom chord. The truss geometry and parameters are illustrated in figure 7:

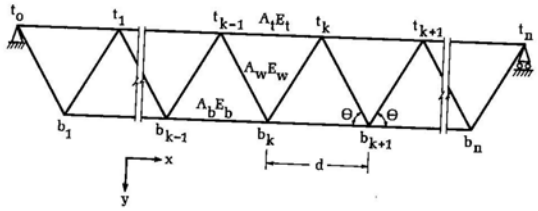

Figure 7: Truss (Chao, 1973)

With these parameters established, the solution for the nodal displacements is:

$$u_t(k) = Ca_0a_4 \cot\left(\frac{\pi}{2n}\right)\left(\cos\left(\frac{k\pi}{n}\right)-1\right) \tag{2.35}$$

$$u_b(k) = -Ca_0a_4 \cot\left(\frac{\pi}{2n}\right) - Ca_0a_5 \csc\left(\frac{\pi}{2n}\right)\cos\frac{(k-0.5)\pi}{n} \tag{2.36}$$

$$v_b(k) = C\cos\left(\frac{\pi}{2n}\right)\left(4\sin^2\left(\frac{\pi}{2n}\right)-a_0a_2\right)\sin\left(\frac{(k-0.5)\pi}{n}\right) \tag{2.37}$$

$$v_t(k) = 4C\sin^2\left(\frac{\pi}{2n}\right)\sin\left(\frac{k\pi}{n}\right) \tag{2.38}$$

Where u and v are the displacements in the x and y directions, respectively. The parameter k is an index that represents the number of the panel point node. The subscripts t and b indicate either the top or bottom chord. Chao goes on to determine a stability condition requirement for trusses under ponding loads. He defines this condition in terms of the parameter β:

$$\beta = 1-\frac{1}{4}\left(a_0(2-a_2)+\left({a_0}^2(2-a_2)^2+16a_0(a_2+a_3)\right)^{\frac{1}{2}}\right) \tag{2.39}$$

Based on this value of β, stability is mathematically assured if:

$$\beta < \cos\left(\frac{\pi}{n}\right) \tag{2.40}$$

By making some simplifying assumptions, this equation can be shown to be equivalent to the stability equation other authors have found (equations 2.1, 2.2, 2.15 etc.) These simplifying approximations are shown to be reasonable for large values of both n and the ratio A_wE_w/A_tE_t. Chao was the first to note that the typical 15% reduction in the moment of inertia to account for shear deformations may not be appropriate, and suggested that a better approach would be to use n and A_wE_w to adjust the critical load.

More analysis was published on the topic of two way systems (Avent and Stewart 1975). The stated goal of the paper was to come up with an analysis method that was more accurate than the work of Marino, but more efficient for design use by the typical engineer. The general approach was the formulation of a set of differential equations solved by Fourier series analysis. The result of this analysis is an inequality that provided a check for the stability of the primary members. As the authors point out, the stability of the secondary members should still be checked by the same criteria that other authors have published. By these calculations, the primary members of a two way system are stable if equation 2.41 is true:

$$J < \frac{\pi^3\left(108{\sigma_k}^2 - \left(3-\sigma_k\right)^3 H\right)}{36\left(2-\sigma_j\right)\left(3-\sigma_k\right)^2 H} \tag{2.41}$$

Where H is the Criterion Ratio as defined by Sawyer, and σ values are defined as:

$$\sigma_j = 1 - \cos\left(\frac{\pi}{n}\right) \tag{2.42}$$

$$\sigma_k = 1 - \cos\left(\frac{\pi}{m}\right) \tag{2.43}$$

Where n is the number of bays parallel to the secondary members and m is the number of bays parallel to the primary numbers. This solution provides a simple check for ponding stability in the primary members and is, according to the authors, more accurate than any other previous approach. The authors go on, using the same method, to find the maximum moment in a primary member. The equation they developed was a double summation, and would take time to use as an office tool. When used, however, it would help a designer determine whether a member would fail from a typical load combined with ponding, even if it meets the stability criteria.

Richard Avent published another article on the topic the following year. He analyzes the deflection of steel joists under loads, including ponding loads (Avent, 1976). He notes that the deflection of these structural units is often important, and that not much work has been done on the subject. He analyzes the idealized warren truss, which is the configuration used in most joists today. The configuration as illustrated by the author is shown in figure 8:

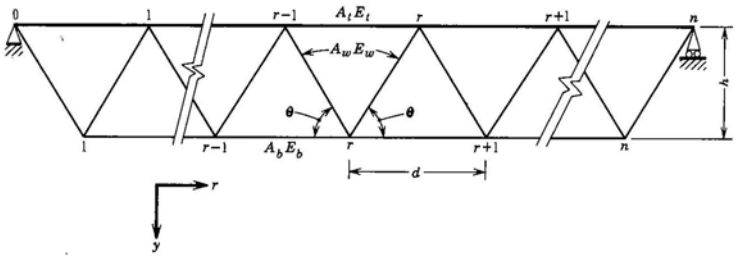

Figure 8: Joist (Avent, 1976)

The author began by improving what had been the equation for calculating the effective moment of inertia in a way he claimed was much more accurate than previous methods. He used this and calculated equations that govern the motion of each of the nodes in the truss with increasing load. The resulting equations resemble those published by Chao in 1973.

There are equations for the displacement of a node on each axis, for top and bottom nodes. The results produced the same stability criteria for joists as found by Chao. The author noted that stability can be determined, but that designers should calculate deflection and stresses to ensure that a stable system does not fail. To increase the ease of these calculations, the author determined simple equations to be used in design that very closely approximate the maximum chord and web member forces. The maximum top or bottom chord force is:

$$F_{\max} = \frac{M_s}{h(1-G)} \tag{2.44}$$

And the maximum web bar force is:

$$S_{\max} = \frac{V_s \sin\theta}{1-G} \tag{2.45}$$

Where M_s is the maximum moment due to non-ponding loads, V_s is maximum reaction due to non-ponding loads, h and Θ are as defined in figure 8, and G is the Criterion Ratio as defined by Sawyer. These equations provide simple estimates for the forces experienced by the members in a warren truss, and should be useful to steel joists designers.

Thus far, analysis of ponding loads on sloped roofs has been minimal. Bin Chang and Ken Chong presented a paper on this topic to the World Congress on Space Enclosures in 1976 that was published the next year in the Forest Products Journal (Chang and Chong, 1976) (Chang and Chong, 1977). In the paper, the authors assume that the height of ponded water at the low end of the sloped roof is zero, allowing for water to collect only in the deflected shape below the low support point. This is limiting in that the analysis only allows for this single load case. The results of this analysis show that the deflection due to the ponding

effect is dependent on the initial loads and deflection. However, no results are given as to how the stability of such a system changes from that of the flat case.

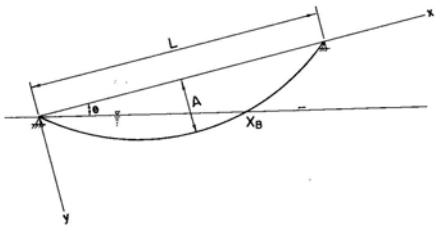

Figure 1. — Ponding of a sloped beam.

Figure 9: Sloped beam ponding setup (Chang and Chong, 1977)

Based on the geometry shown in figure 9, the authors determine that the deflection due to ponding loads only, y_p, can be expressed as a function of the total deflection, A, the angle theta, the length, L, the stiffness, EI, and the unit weight times the spacing, λ:

$$EIy_p = \frac{\lambda L^4}{1440}\left(14\left(A\right) - 9L\Theta\right) \tag{2.46}$$

It can be shown that when the angle is zero, this expression reduces to that found by Chinn (equation 2.5). It should also be noted that by increasing the angle, the deflection due to ponding is decreased. In fact, if the angle is increased to 14A/9L then there will be no deflection due to ponding. Because A is typically very small compared to L, the angle required to eliminate ponding deflection effects is typically very small. In general, a slight pitch should be sufficient to avoid these loads. This equation allows some insight to the ponding problem on sloped roofs, but is limited, as it does not provide an explicit equation for the stability criteria of a sloped roof.

A new set of stability equations designed for office use were formulated and became candidates for inclusion in the specifications, and some engineers spent some time evaluating them (Carter and Zuo, 1999). The source of the new equations is cited as a letter

from author K. P. Milbradt to an AISC representative in February 1995. The equations proposed by Milbradt are candidates for replacement of the specifications based on the work of Marino in the AISC code (Marino, 1966). It is suggested that these equations may provide greater ease and accuracy, as they are calculation based, as opposed to Marino's graphically based solution. The proposed equations for checking the primary and secondary systems are equations 2.47 and 2.48, respectively:

$$C_p \le 1.04 - 0.97C_s - 1.27\frac{f_0}{F_y} \tag{2.47}$$

$$C_s \le 1 - 1.07C_p - 1.25\frac{f_0}{F_y} \tag{2.48}$$

Where C_s and C_p are as defined by Burgett in equations 2.27 and 2.28, F_y is the yield stress, and F_o is the maximum extreme fiber stress in the member due to all loads except ponding (Burgett, 1973). The authors' conclusion regarding the comparison of Milbradt's equations with those of Marino is that they are close but different. No conclusions about relative accuracy were drawn.

In his discussion of the article, Milbradt argues that his equations should replace both the ponding analysis based on the work of Marino and the simplified method based on the work of Burgett (Milbradt, 2000). His argument is that the equations are more accurate than the simplified ones, and because his method is calculation based, it is easier and better than Marino's method. Milbradt also discusses the effect of f_0, residual stresses, and the trouble with calculating effective moments of inertia for joists. He argues that the equation provided in the Steel Joist Institute Design Manual 3 only represents an average

approximation and in some cases is unconservative (SJI, 1971). Milbradt suggests that all of this should be included in the commentary of the AISC code.

A paper that presented and discussed ponding loads and a numerical model was presented to the second European conference on steel structures, in Prague (Colombi and Urbano, 1999). The authors present no new results here, but the paper leads to a published article the following year that presents a new method of analyzing ponding loads (Urbano, 2000). In this paper, the author treats a beam under ponding loads as two equal length beams connected by a spring at midspan, as shown in figure 10:

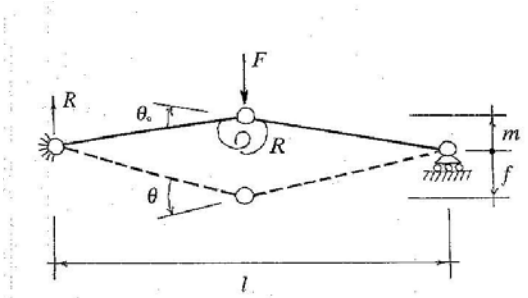

Fig. 2. Static model with one degree of freedom

Figure 10: One DOF bar-spring model (Urbano, 2000)

The author defines a factor he terms the influence coefficient, α, which is a property of the system and defined as the ratio of the displacement f due to a corresponding applied force F. Using this value, Urbano derives equations for the displacement of the system, as well as the moment carried in the spring:

$$f_0 = \alpha F_0 \tag{2.49}$$

$$f = f_0 \left(\frac{1 - \frac{m}{f_0}}{1 - Y\alpha} \right) \tag{2.50}$$

$$M_0 = \frac{Yh_0 l}{4} \tag{2.51}$$

$$M = M_0 \frac{1 - mY\alpha / f_0}{1 - Y\alpha} \tag{2.52}$$

Where f, F, m and l are as defined in figure 10. The naught subscript indicates a value that is due to loads before ponding effects occur. Alpha is as previously defined, Y is the unit weight of the fluid times the spacing of the beams, and h is the height of the water on the system. For this system, Urbano determines that the critical value for the ponding effect occurs when αY = 1. For a system to be stable, it should be ensured that this value is less than one by whatever factor of safety is desired.

Urbano goes on to incorporate the typical code serviceability requirements of restricting deflection to some fraction of the length into his equations. This is interesting, but adds little. He also adds the effect of shear on the deformation by repeating the analysis with three springs, as shown in figure 11:

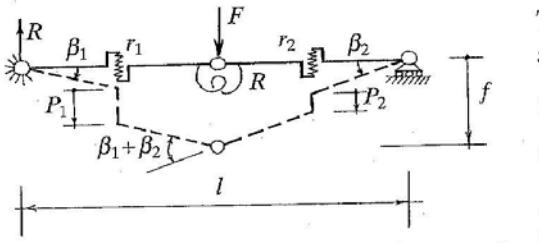

Fig. 6: Static model with three degrees of freedom

Figure 11: 3 DOF bar-spring model (Urbano, 2000)

Based on this analysis, he finds that the deflection can be calculated by the equation:

$$f = \frac{Yh_0\left(\frac{1}{2r}+\frac{l^2}{16k}\right)}{1-Y\left(\frac{1}{2r}+\frac{l^2}{16k}\right)} \tag{2.53}$$

Where r is the spring constant for the springs in shear, and k is the spring constant for the spring in flexure. He also continues to expand these ideas to a two way roofing system, shown in figure 12:

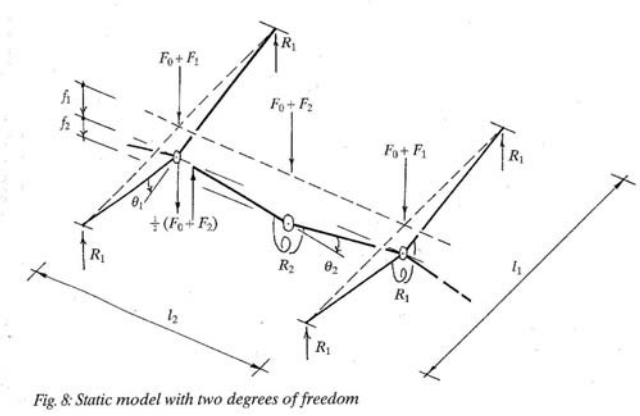

Figure 12: 2-way bar-spring model (Urbano, 2000)

Based on this analysis, Urbano calculates the ratios of moments due to additional ponding load to moment due to initial load for both framing systems as functions of the influence coefficients and Y. This is equivalent to the amplification factors discussed previously (Bohannan and Kuenzi, 1964). The factor amplifies both the displacements and the moments equally. The factors are solved for explicitly, and plots are provided (shown in figure 13) for clarity:

$$\frac{M_1}{M_{01}} = \frac{f_1}{f_{01}} = \frac{1-\alpha_{22}Y/2}{1-2\alpha_{11}Y-\alpha_{22}Y+\alpha_{11}\alpha_{22}Y^2} \tag{2.54}$$

$$\frac{M_2}{M_{02}} = \frac{f_2}{f_{02}} = \frac{1}{1-2\alpha_{11}Y-\alpha_{22}Y+\alpha_{11}\alpha_{22}Y^2} \tag{2.55}$$

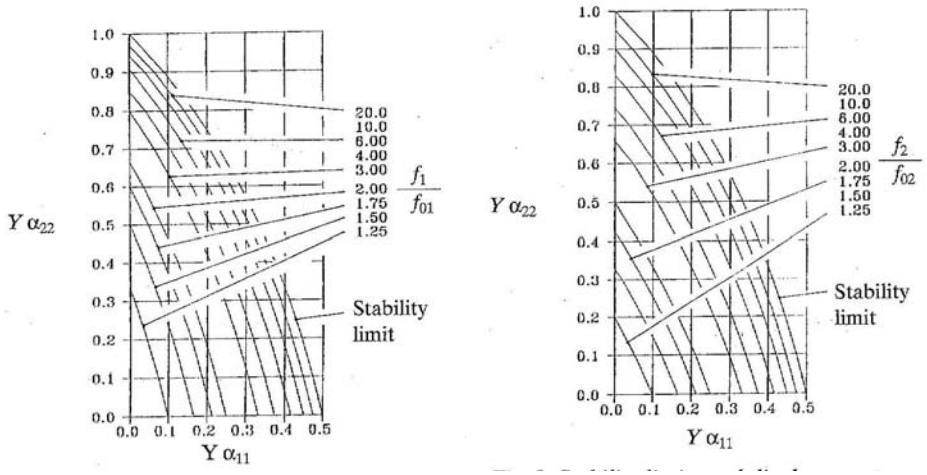

Figure 13: Design guides (Urbano, 2000)

This analysis is good because it is the most comprehensive analysis provided in a single source. The results are equations and graphs that are simple and easy to understand and use. The only drawback is that the author provides no indication of how accurate his initial assumption of a spring connecting two beams is. The equations are simple enough for design use, but need to be evaluated for accuracy. In practice, constants would need to be derived for the spring coefficients and the influence coefficient, so more work is required before this approach can be useful.

Work has been done on members with different end conditions, but it took quite a while before the ideas were expanded to cantilevered members. This is eventually done so that designers can take advantage of the benefits of a cantilevered system derived from balanced moments leading to smaller overall deflections (Bergeron, Green and Sputo, 2004). The authors begin by defining a variable n as the ratio of the deflection of a simply supported system to the deflection of another system (cantilevered in most of this paper) under the same loading conditions. They define the parameter C_p, as used in previous literature (Burgett, 1973), as:

$$C_p = \frac{32 L_s L_p^{\,4}}{10^7 n I_p} \tag{2.56}$$

The authors then proceed to outline a method for determining n. They begin by showing that the midspan deflection of a cantilever is approximately equal to the maximum, and use this as a simplifying assumption. Based on the setup shown in figure 14, the maximum deflection will be at midspan, but will be less than for the simply supported case due to the negative moments caused by the point load on the cantilevered end.

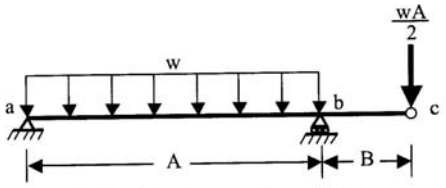

Figure 5. Cantilever beam with applied loads

Figure 14: Cantilevered end (Bergeron, Green and Sputo, 2004)

Based on this methodology, it is then shown that the value of n can be calculated by equation 2.57:

$$n = \frac{1}{\left(1 - \frac{2.463 BA}{C^2}\right)} \tag{2.57}$$

This is the appropriate value of n for this condition only. The authors go on to calculate the value of n for a beam with both ends cantilevered with point loads, as shown in figure 15:

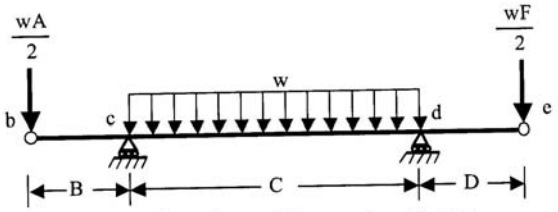

Figure 6. Cantilever beam with unequal cantilevers

Figure 15: Two cantilevered ends (Bergeron, Green and Sputo, 2004)

$$n = \frac{1}{\left(1 - \frac{2.463(BA + DF)}{C^2}\right)} \tag{2.58}$$

The authors have provided equations for appropriate stiffness factors for two common cantilever setups. This allows designers to take advantage of the additional capacity of the cantilever system, and eliminates some of the unnecessary conservatism in the code on this topic.

In another paper, the concept of partial ponding (ponding due to a given amount of water) was expanded (Colombi, 2005). Instead of water accumulating while a roof deflects, the water simply moves as the load changes and the deflected shape is adjusted. The author begins with an analysis of the traditional ponding problem, and based on the simply supported beam with residual camber, as shown in figure 16, he produces an equation for the deflected shape of the beam under water loads:

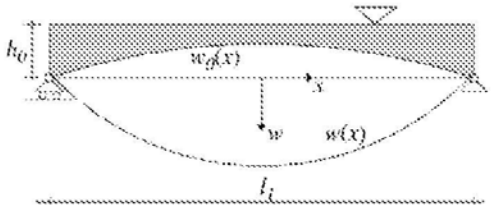

Fig. 3. Simple supported beam under full ponding effect.

Figure 16: Full ponding (Colombi, 2005)

$$w(x) = \frac{h_0}{2}\left(\frac{\cosh(\omega x)}{\cosh\left(\frac{\omega l_1}{2}\right)} + \frac{\cos(\omega x)}{\cos\left(\frac{\omega l_1}{2}\right)} - 2\right) - \frac{m}{1 - \left(\frac{\omega l_1}{\pi}\right)^4}\cos\left(\frac{\pi x}{l_1}\right) \tag{2.59}$$

Where all variables are as defined in figure 17 and m is the residual precambering parameter, the height of the beam at midspan over the straight line. The solution of the partial ponding problem is also found:

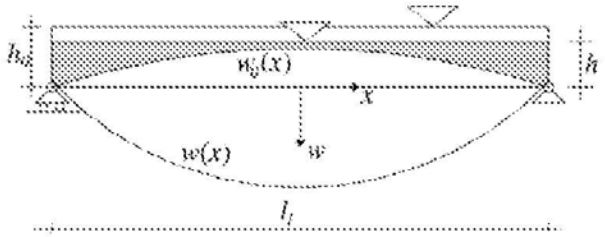

Fig. 6. Simple supported beam under partial ponding effect.

Figure 17: Partial ponding (Colombi, 2005)

$$w(x)=\frac{h_0}{2}g\omega l_1\left(\frac{\cosh(\omega x)}{\cosh\left(\frac{\omega l_1}{2}\right)}+\frac{\cos(\omega x)}{\cos\left(\frac{\omega l_1}{2}\right)}-2\right)-\frac{m}{1-\left(\frac{\omega l_1}{\pi}\right)^4}\cos\left(\frac{\pi x}{l_1}\right) \qquad (2.60)$$

The author then goes on to outline the numerical approach he will use to solve some of the problems in the rest of the paper. He uses an iterative solution technique that evaluates the initial deflection due to the initial load, and then calculates the subsequent deflection due to the additional ponding load. He divides the surface into a grid to facilitate this analysis, and calculates the deflection of every section of the grid to determine an overall deflected shape. After outlining the procedure used to set up the numerical analyses, Colombi runs through three examples of how the analysis works in practice.

The partial ponding condition is important, as it is representative of what can happen in the field. Often, a set amount of water will collect on a roof during a rainstorm, and will remain for some time afterward. It is concluded that the partial ponding condition cannot

lead to ponding instability. The deflected shape equations produced and the numerical analysis procedure described are the most useful results of this analysis.

Most recently, the methods for approaching a ponding analysis were again expanded. By approaching the problem from a new angle, many problems become simplified. The author notes that "…true insight appears to be missing on the very nature of the ponding phenomenon." (Blaauwendraad, 2007) In his paper, he outlines two new ways of approaching the problem of ponding analysis: the piston spring model and the bar spring model for stiff and flexible roof systems, respectively. The difference in the two models is that with stiff roofs, deflections will be small and the roof will likely be completely covered, whereas with a more flexible system, deflections will be larger and water may not completely submerge the roof. These models consider the effects of pitch, camber, slope, and various end conditions on the full ponding problem.

The analysis begins by assuming a sinusoidal deflected shape and accumulated water load. It is then shown that the average accumulated water load is eighty percent of the maximum, and this simplification is used throughout. The author then outlines his piston-spring model for stiff systems, shown in figure 18:

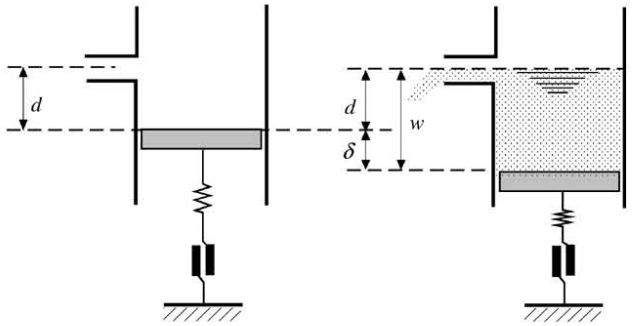

Fig. 3. Piston–spring model of a roof member. Left without, right with water.

Figure 18: Piston-spring model (Blaauwendraad, 2007)

Where d is the original depth of water on the roof and δ is the average additional load, eighty percent of the maximum in the deflected shape of the roof. He then describes three relevant variables: W, the weight of a meter of water on the roof, D, the spring stiffness, and F_p, the overall total strength of the support structure:

$$W = \gamma a l \tag{2.61}$$

$$D = 96EI / l^3 \tag{2.62}$$

If the support structure remains linear elastic, and F_p is not reached, then the deflection δ can be calculated:

$$\delta = \frac{1}{n-1} d \tag{2.63}$$

Where n is the ratio of D to W. Based on this result, it can be seen that for a very stiff roof (D >> W), the additional deflection and load, δ, will be small. When the ratio approaches unity however, the additional deflection becomes large. This is essentially the same as the original stability inequality published by Haussler (Haussler, 1962). This ratio, n, determines whether a system will be strength dominated or stability dominated. If n is greater than one (D greater than W), then the system will be strength dominated. This is because successive deflections will be smaller, and the system will eventually fail due to

overload. If n is less than one, then the system is stability dominated and will fail under pure ponding loading conditions. By analyzing the piston-spring system under a force equal to the maximum strength of the system, the author determines that an ultimate value of W can be calculated:

$$\frac{1}{W_u} = \frac{1}{D} + \frac{d}{F_p} \tag{2.64}$$

As W is a function of the fluid unit weight, spacing and length, and because fluid unit weight and length are typically known, this equation essentially limits the spacing of the beams in the system. It is shown that this method can easily include the effects of initial deflection or camber. This is done by using, as before, an average load or loss of load due to these effects of eighty percent of the maximum under the deflected shape. The deflection parameter, d, is modified by eighty percent of the midspan height change due to camber or initial deflection. The solution is also expanded to include the effects of a two or three way roofing system. To do this, the approach is identical but the formulation of D and W change:

$$\frac{1}{D} = \frac{1}{D_p} + \frac{1}{D_s} + \frac{1}{D_{sh}} \tag{2.65}$$

$$W = \gamma l_p l_s \tag{2.66}$$

Where the subscripts p, s and sh stand for primary, secondary and metal sheet systems, respectively.

The author also outlines a simple method for performing this analysis on systems with end conditions that are not simply supported. The only change required is that the effective

stiffness will be modified by a factor. The factors for several common support conditions are shown in figure 19:

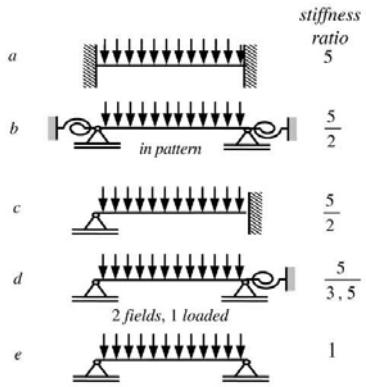

Figure 19: Stiffness ratios (Blaauwendraad, 2007)

The author also outlines a simple method for taking slope into account. If the depth at the low end of the member is d, then the effective depth over the sloped member is:

$$d = d_w - c\alpha l \tag{2.67}$$

Where α is the angle from horizontal and c is a parameter based on how deep the ponded water is. For water that completely submerges the beam, c is one half. For water that does not completely submerge the beam, c is defined in figure 20:

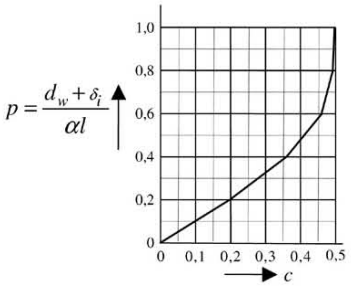

Figure 20: Design guide (Blaauwendraad, 2007)

Blaauwendraad continues by turning to more flexible systems and the bar-spring system as outlined by Urbano (Urbano, 2000), but expands the previous work to treat sloped roof

systems. He starts off by defining the location of the spring at the midspan of the horizontal projection of the submerged portion of the beam, as shown in figure 21:

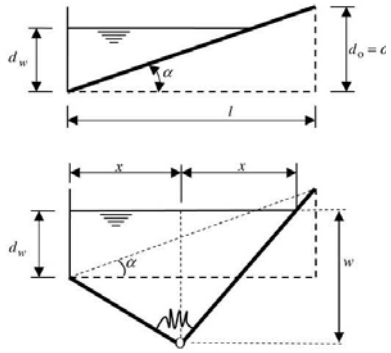

Fig. 11. The bar–spring model, an alternative.

Figure 21: Bar-spring model (Blaauwendraad, 2007)

To complete this analysis, the author finds the rotational stiffness of the spring in terms of E, I, and l, and treating the entire load due to water as an equivalent point load on the system at the spring. He goes on to check the results of both the piston-spring model and the bar-spring model at the point where water rises to the high end of the member, and finds that they give the same result. Based on the model as it is set up and a series of algebraic and geometric derivations, the author outlines the results for determining a stable system. He summarizes his findings in figure 22:

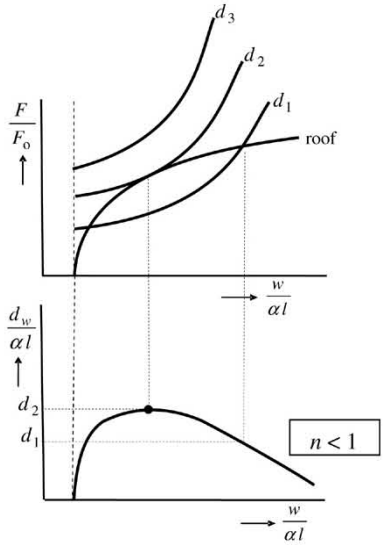

Figure 22: Design guide (Blaauwendraad, 2007)

Figure 22 shows that for given values of roof strength or d_w, as the ratio w/αl (equivalent to the ratio of the height of the water at the shallow end to the height of the high end) increases, so does the ratio of final load after ponding to initial load. The curve labeled roof in figure 22 indicates the ultimate load allowable on a roofing system in terms of F/F_0, while the curves labeled d indicate the maximum induced load on a roofing system in terms of F/F_0 for a given set of geometric parameters. It can be seen that for low values of d_w such as d_1, stable systems exist, and there are two critical points where systems transition from stable to unstable. For high values of d_w such as d_3, the system will always be unstable. The quantity d_2 in figure 22 is the critical value for d_w, the highest value it can be while not eliminating the possibility of a stable system. The second plot in figure 22 shows a summary of the curves in the first. Any system that fits under the curve shown is stable, while any system fitting above is unstable.

While these curves are instructive and conceptual, the author provides no simple way of mathematically determining where a system fits on these plots. As with the Chang paper

(Chang and Chong, 1977), work could still be done in the area of providing a simple, accurate, equation based method of determining stability of sloped roof systems. The author finishes by expanding the method for sloped members to include initial camber or sag, then works through some examples.

Recent research has been nearly exclusively conducted in the Netherlands. Blaauwendraad has published a modification to his method that changes the way the accumulated water on simply supported secondary members is calculated in the piston-spring model (Blaauwendraad, 2009). Several additional articles have been recently published in the Journal, Heron, which describes itsself as "a joint publication by TNO Built Environment and Geosciences, Delft, and the Netherlands School for Advanced Studies in Construction." (Heron, 2009) Five recent articles have been published in this journal in English on the ponding topic. They cover topics such as numerical modeling of ponding loads (Schouten, Locht and Derks, 2006), structural design for ponding loads (Van Herwijnen, Snijder and Fijneman, 2006), investigation of actual failures (Vambersky, 2006), and more.

The theory of ponding loads has covered many areas. It started as a paper that outlined the stability criteria for a flat, simply supported beam under water and has been expanded to cover two way systems, various support conditions, amplification effects, slope, initial imperfections, camber, partial ponding, nonlinear response, creep, trusses, and uses varied approaches and simplifications. It has been pointed out (Chinn, 1980) that the amplification factor, as discussed by Kuenzi and Bohannan (equation 2.4), is the important part of the ponding theory, and the important use of the Criterion Ratio. Most roof systems

will be stable by the theory, but all roof designs should include secondary loading due to ponding in the determination of roof loads. All roofs must be designed with this important loading in mind, whether the end result is additional drains or a steeper, stiffer or stronger roof.

While this represents a summary of the theory developed for ponding loads thus far, the ideas have been expanded into some other fields. Probabilistic studies have been done on the reliability of wood members subject to ponding loads and creep (Folz and Foschi, 1990) (Fridley and Rosowsky, 1993). Studies have also been done on ponding effects on floating membranes (Katsikadelis and Nerantzaki, 2003), more details on the effects of initial imperfections on roof behavior (Ahmadi and Glockner, 1984), and mapping flat roofs that may be prone to ponding (Avrahami, Doytsher, Raizman and Yerach, 2007). Other research has been done in the area of hydrology to determine how ponding is affected by specific rain storms (Sawyer, 1968). The work of Marino has been expanded to determine the excess concrete required when pouring on a flexible flooring system due to the ponding effect (Ruddy, 2005). This work is not directly related to the science of ponding loads, but is good background information. Despite this apparent interest in the nature of these loads, full-scale test results have never been reported. This is a partial motivation for the research at hand.

Building Code Review

While there is an abundance of information available on the subject of ponding, most structural engineers do not know this background and the evolution of the field. A small

fraction of the information available is published in building codes and design specifications. The following is a summary of what a designer who has done no independent research but uses the codes and specifications will know of ponding loads.

International Building Code (IBC) 2006

The model building code that is used throughout most of the United States has relevant provisions for rain and ponding loads. For roof drainage, the IBC requires that both a primary and a secondary drainage system be provided. For rain loads, the code requires a designer to assume there is standing water at the depth it would reach if the primary drainage system fails. To ensure ponding stability, the code requires that a designer provide adequate slope (at least 1/4 on 12) or else verify adequate stiffness to prevent ponding. For guidance on these calculations, the IBC refers designers to section 8.4 of ASCE 7.

American Society of Civil Engineers (ASCE) 7-05

This guide provides information collected by experts in the field of structural engineering and provides guidelines for structural designers. These guidelines require that two independent drainage systems be provided, each with the same capacity. It also requires that design of a roof system provide adequate strength to hold standing water to the height it would reach if the primary system failed. For stability against ponding, section 8.4 requires either a sufficient slope (at least 1/4 on 12), or investigation to ensure adequate stiffness against progressive deflection. It is suggested that the larger of the snow and the rain load be used, and that the primary drainage system should be assumed to be blocked

for this investigation. The commentary for this section suggests that the guidelines in the AISC specifications for steel construction be used to perform this investigation.

AISC Steel Construction Manual

Section B3.8 of the AISC specification requires that the ponding problem be considered. It requires that a designer do one of three things to ensure ponding stability. Either adequate slope should be provided (at least ¼ on 12), adequate drainage be provided, or the ponding investigation be performed as outlined in appendix 2. This is more lenient than the requirements in the IBC and the ASCE 7, so those documents will typically control, and providing adequate drainage alone, as allowed by the AISC specification, will not be sufficient to satisfy ponding requirements.

Appendix 2 in the AISC specification is the only place where a general and useful method of investigating ponding is presented in code or specifications. Two independent methods are presented: a simplified, conservative check, and a more in depth method. The simplified method is taken from Burgett, and allows for a factor of safety of four against instability (Burgett, 1973). When using this method for trusses and joists, it is required that the moment of inertia be reduced by fifteen percent to find the effective moment of inertia. This modification accounts for the part of deflections due to shear deflection. Also, within this method, steel decking should be considered a secondary member when it is supported directly by the primary members alone. The in depth analysis method is taken from Marino (Marino, 1966).

AISC Design Guide 3

AISC publishes design guides in addition to the Steel Construction Manual. Design Guide 3, which contains information relevant to ponding loads, is now in its second edition. It provides a good summary of what is contained in the building codes and the AISC appendix 2, but does not, however expand on any of the ideas or add much to help a designer do a ponding check.

Steel Joist Institute Standard Specifications

This document provides a list of standardized steel joists and should be used by anyone specifying a joist, and any company producing standard steel joists. It also provides some requirements on design, fabrication, and erection of steel joists. In section 5.10 of these specifications, the SJI requires that a ponding investigation be performed by the specifying professional, but provides for no method of performing such an investigation. There are three sections relevant to this research, the "Accessories and Details," the "Standard Specifications for Open Web Steel Joists, K-Series" and the "Code of Standard Practice for Steel Joists and Joist Girders." These will be investigated further in the design background section of this report.

SJI Technical Digest 3

This document provides more details on how to perform the investigation required by section 5.10 of the SJI standard specifications. It contains a summary of code related to ponding, and notes that it lacks in some areas, especially for atypical roofing systems. The

digest suggests ways of expanding the AISC analysis to fit additional systems. It suggests that a good general procedure for a ponding analysis is that outlined in the AISC specifications, but that more detailed methods are available. This digest presents methods for doing a ponding analysis for members with both flexible and rigid supports.

For roof systems with flexible supports, it is suggested that the AISC method be used, but a special equation is provided for the calculation of F_0, the initial extreme fiber stress. For systems with rigid supports, the digest recommends two checks, one for the capacity of the joist, and one for the capacity of the support, as the bearing seats of the joists are also limited in their capacity. The method starts by calculating three values by equations 2.68 to 2.70.

$$C_s = \frac{32L^4}{10^7 I_E} \tag{2.68}$$

$$\Delta_C = 0.00042L^2 + 0.0625L \tag{2.69}$$

$$w = w_D + \left(w_R \text{ or } w_S\right) \tag{2.70}$$

Where L is the length, S the spacing, I_e the effective moment of inertia, w_d the dead load, w_r the impounded water load, and w_s the snow load. By using these values and estimating a height of water, h, above the supports, the centerline deflection can be calculated:

$$\Delta = \frac{C_S}{1 - C_S}\left(0.244w + 1.27h - \Delta_C\right) \tag{2.71}$$

Using this value, both the end reaction and the final maximum load can be calculated:

$$R_1 = SL\left[0.375w + 1.95h + 1.24\left(\Delta - \Delta_C\right)\right] \tag{2.72}$$

$$w_1 = S\left[0.75w + 3.9h + 3.16\left(\Delta - \Delta_c\right)\right] \tag{2.73}$$

These values must then be checked to ensure safety. The distributed load must be less than the capacity of the joist, while the reaction must be less than one half the product of the distributed load and the length. If both of these requirements are met, then the joist is stable and strong enough to support the loads, including the ponding effect.

Conclusion

In general, design codes require that adequate slope and adequate drainage be provided. The IBC and ASCE 7-05 do not provide a method for investigation of ponding stability; this is published in the AISC Steel Construction Manual instead. An additional method is presented by the SJI in a technical digest, but does not replace or add to the method presented in AISC. For a structural engineer interested in ponding loads, the single section of code that must be known is appendix 2 of the AISC specifications. Both the simplified method and the improved method are good ways to ensure stability, and are taken straight from the literature.

The methods provided in the design specifications are somewhat limited. They work only for flat roofing systems with structural members of the same length, strength and stiffness, with identical adjacent framing plans and simply supported members. The design methodology provided by the AISC specifications could use expansion to make the method applicable to a wider variety of roofs. The biggest problem is that the specifications treat roofs as either flat or pitched, and assume that if a roof is pitched, then it is safe. Often, pitched roofs can still suffer from ponding loads, and should be investigated correspondingly.

It has also been suggested in the literature that serviceability limit requirements for the deflection to span ratio of roof and floor systems are not as helpful as they could be. It has been suggested that a good replacement to these requirements for roofs where ponding is an issue would be a limit on deflection per unit load (Haussler, 1962). This would be a simple, effective method to eliminate unstable systems from designs. The method would require that a designer analyze the roof system with a live load of 5 psf (239 Pa) (approximately the weight of one inch or 2.54 cm of standing water). Then, if the resulting deflection is greater than an inch (2.54 cm), it is clear that the system is dangerous and possibly unstable.

Design Background

Physical tests will be conducted on roofs built with steel joists and steel decking. Some important background on these materials and their implementation is included here. For full explanation of all design decisions and details, see the experimental design section.

Open Web Steel Joist Design

Open Web Steel Joists are proprietary products that are designed and manufactured according to industry standards established by the Steel Joist Institute (SJI). The Institute provides load tables that specify designations and strengths for a variety of joists. Any designer can chose steel joists as framing members, and by finding the required strength in the load tables, choose a joist from the SJI Standard Specifications. Joists come in several forms. The K-Series joists are the typical framing members that support steel decking. A

more specific category of K-Series joist is the KCS joist, which is designed for a wider variety of load cases. Longer span, stronger joists are available in the LH and DLH categories. Joist Girders are designed to be the framing members that support the joists. The K-Series joists are the most typical framing members, and come in designations such as 30K7, indicating a joist that is 30 inches (76.2 cm) deep and stronger than a 30K6 but weaker than a 30K8. The second number is the section number, but indicates nothing more than relative size within a family of joist depths.

When these joists are purchased by a contractor for construction, the manufacturer can build the joist in a variety of ways, provided it meets the strength and other requirements from the specifications. Typically, K-Series joists are modified warren trusses, with vertical members providing additional support and bracing for the top chord. This reduces the effective bending length of these members, allowing larger uniform loads. In general, joists are fabricated from angle and channel sections, as well as solid round bars. The flanges are generally paired angles, while the web is made from channels and the last web member is a solid round bar. Joists are typically given camber during fabrication based on an arc radius of about 3,600 ft (1.10 km). This allows the joists to deflect slightly under dead loads and still be flat (SJI and SDI, 2008). The SJI specifications indicate that joists should be designed with a factor of safety of 1.67 over their listed strength, and that they should be built with 50 ksi (345 MPa) steel.

Designing with joists is fairly straightforward. A roof design load is calculated as usual, and a framing plan is drawn. Based on the tributary width each joist will support, the load on each joist can be found in force per length. Using the Standard Specifications, joists can

be chosen. If a desired strength is not available or if a joist will be supporting an unusual load pattern (not a uniform load), then custom joists can be ordered. This is often done in practice (SJI and SDI, 2008). There are other considerations to take into account. When a pitched roof is required, it is more economical to pitch the joists themselves rather than the chords. In this case, the span is taken as the diagonal length. Joists are typically not designed for uplift. If this is required, then special joists may have to be ordered. Finally, it is usually more economical for joists to span the longer dimension of a bay, while the joist girders span the short dimension.

Joists are slender and require significant lateral bracing in the form of bridging. Joists should be connected to each of the adjacent joists to ensure stability. Based on the length and the section number, the number of rows of bridging can be determined. Bridging is typically horizontal, but based on location of the selected joist in the load table, one set may be required to be diagonal. The design of these members is outlined in the Standard Specifications.

Open web steel joists are usually simply supported structural members. In the field, the end of the top chord (the joist seat) is typically welded to the supporting member, forming a hinge and making the supports a pin-pin system. With the addition of a bottom flange extension, however, they can easily be built with fixed ends to resist moments as well.

By looking at existing structures, it is easy to get an idea of what typical joist framing looks like. Decking is supported by joists, which are supported by joist girders, which are supported by columns. Warehouses in the Portland, Oregon area were investigated to see

what range of values is typical. All numbers here are approximate, as exact measurements could not be taken.

- The Fry's Electronics store in Wilsonville has 60 ft (18.3 m) joists spaced at 5½ ft. (1.68 m).
- The IKEA store in Portland has a complex system of joists and joist girders. There are at least two sets of joists, one being 60 ft (18.3 m) joists spaced at about 8 ft (2.44 m), the second being 36 ft (11.0 m) joists spaced at 7½ ft (2.29 m). These are all supported on joist girders about 110 ft (33.5 m) long, spaced at 77 ft (23.5 m). These are supported on steel columns.
- The Best Buy store in Tualatin has joists that span 50 ft (15.2 m) and are spaced at 7 ft (2.13 m).
- The Costco location in Tigard has joists that span 38 ft (11.6 m) and are spaced at 4.5 ft (1.37 m).

From this, it is clear that there are a variety of ways to deploy an open web steel joist roof.

Bridging

Steel joist roofs must be laterally braced to prevent system-wide lateral buckling. The supports used to accomplish this are refered to as the bridging members. Bridging is installed to connect both the top and bottom chords, and should be continuous over the length of the structure, with splices where needed between joists. Both chords are supported as either could be in compression. Under dead, rain or snow loads, the top chord should be in compression, but in high wind conditions, uplift can produce compression in the bottom chord as well. The bridging prevents buckling by reducing the effective length

of the bending members and ensures that the design assumption of two dimensional pin connections remains valid. Per the Standard Specifications for Open Web Steel Joists, K-Series, 4.41 (a), 145 times the least radius of gyration of the chord angle sections should be greater than their length. Thus, by including more bridging members, increasingly slender angle sections are allowed.

The number of sets of required bridging can be found in the SJI code in table 5.4-1. This table will provide a designer with the required number of rows of top chord bridging, and the code specifies that "The number of rows of bottom chord bridging shall not be less than the number of top chord rows" (SJI, 2005)

Steel Decking

Designing with steel decking is straightforward. If the roof pressure and span conditions are known, then steel decking can be selected. The Steel Deck Institute (SDI) publishes a Design Manual that includes load tables based on span, support conditions and type of decking. Generally, decking is continuous over three spans between joists, but the design manual allows for one, two or three spans per section of decking. Based on the number of supports and the space between them, four types of decking can be chosen: narrow rib, intermediate rib, wide rib and deep rib. By far the most commonly used is the wide rib decking. These load tables are all unfactored strength, so they must be given a factor of safety.

Summary

A steel joist, steel deck roof will provide an excellent system with which to test the effects of ponding. These roofs are commonly used in practice, so it should be easy to acquire the materials and to seek advice on their use. These tests should allow investigation of some of the important principles of ponding outlined in this background information.

NUMERICAL ANALYSIS

The ponding effect is a simple idea that can become complex rather quickly. There are several variables involved, and there are numerous variations on the problem. Because there are a variety of factors influencing this phenomenon, a solution for the deflected shape of a member under ponding loads cannot be easily and accurately found. A closed form solution to the problem would be long, tedious, and difficult, due to varied system properties, loads, and the iterative nature of the problem. Since it would be useful, however, to have a tool that could calculate the deflections under these loads, a computer program has been written to do just that.

Approach

The simplest case, a prismatic beam with walls built at the ends will accumulate load as water collects first behind the walls, then into the deflected area. This case has been analyzed using a numerical model in MATLAB. For simplicity, linear elastic behavior is assumed, and the program is set up only to analyze beams that are flat, or slope up in one direction. The program is set up only to analyze beams that are simply supported with displacements due only to bending moments induced by the water loads. Additional assumptions are that the ponding fluid is the only load, the beam is initially perfectly straight, and that the water will always rise to the specified height. Shear deformation contributions to the deflection are ignored.

Even simplifying the problem to a simply supported single linear elastic prismatic beam can get complicated. Identifying the appropriate design approach to this problem took

some careful consideration. Problems arise with a simply supported beam for several reasons. First, if a simply supported, sloped beam is loaded with water, then the question arises: are the walls connected to the beam, or are the walls independent of the supports? Each setup presents difficulties and complications. In the case of independent supports, the load is shown in figure 23:

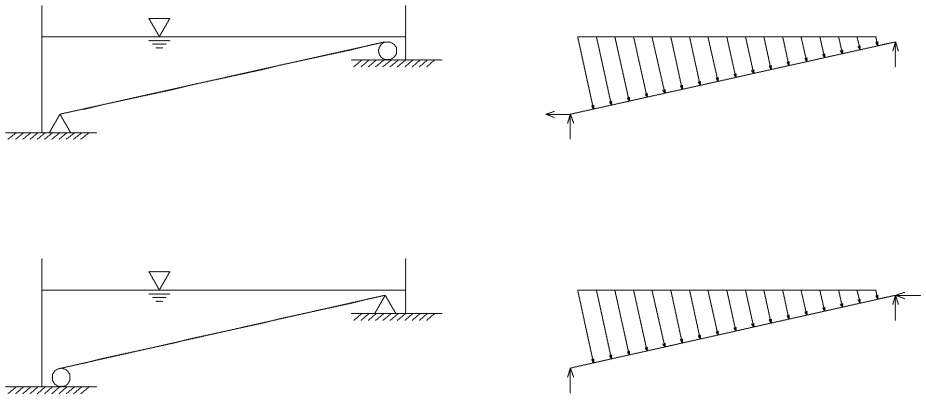

Figure 23: Supports independent of walls

Here it can be seen that if the pinned connection is made at the low end, then the beam will experience tension, and the roller support will be pushed outward. If the pinned connection is made at the top, however, the opposite occurs: the beam experiences compression and the roller support will tend to move inward. These forces will induce second order effects and induce additional bending moments in the beam. These may be small, but should be noted. In the case of walls attached to the beam, the loads are shown in figure 24:

Figure 24: Walls attached to beam

Here it can be seen that the problem of tension/compression in the beam has been eliminated, as the setup has changed, and the horizontal reactions are eliminated as they

balance within the tank itself. It is now essentially a solid tank with simple supports. A complication arises here, as the walls will experience pressure themselves. If the beam is isolated, then at the supports, where the walls meet the beam, bending moments will be induced from the walls. As before, this effect is small, but should be noted.

Thus far, all of the designs have appropriately noted that the water pressure acts perpendicular to the surface it rests on, and increases linearly as a function of depth. This creates serious complications as the beam deflects. After the first iteration of an analysis, the beam may be deflected as shown in figure 25:

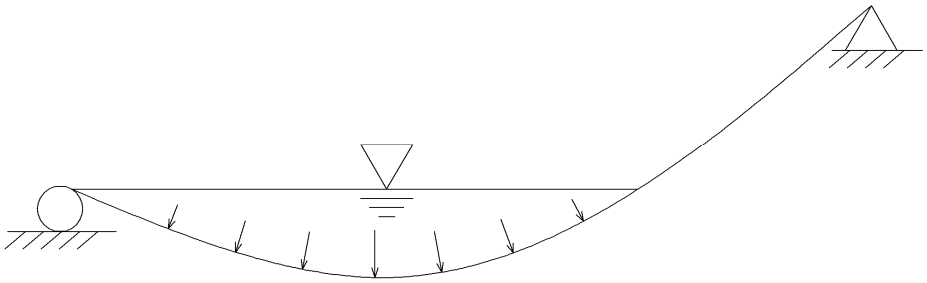

Figure 25: Water pressure on deflected beam

The problem here is that the orientation of the pressure, acting perpendicular to the surface at all points, is difficult to determine. The direction of the resulting forces on the beam will be hard to find, and will change with position along the beam and with each iteration. This effect may be small, depending on the total deflection of the beam, but should be noted.

There are different setups for this design, and there are complications to the analysis. Due to these issues, a simplified case, shown in figure 26, was chosen for the analysis:

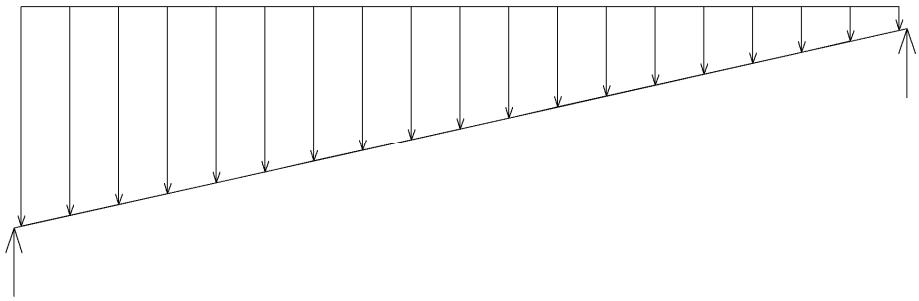

Figure 26: Assumed conditions for numerical analysis

This setup ignores the effects of induced tension/compression on the bending moments in the beam, and ignores the possible end moments from the walls. This design also neglects to consider the water pressure as perpendicular to the surface, instead taking it as a vertical load at all times. This is justifiable by a small angle approximation, as the roofs to be analyzed here are usually on a very shallow pitch. This is further illustrated in figure 27:

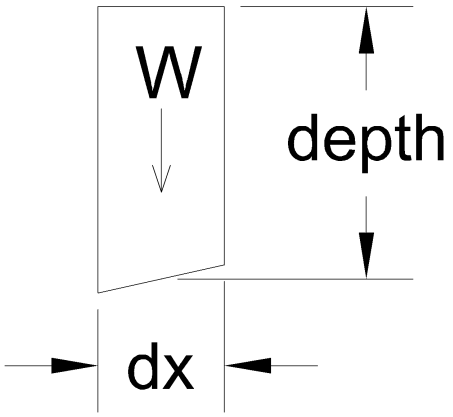

Figure 27: Loading for Numerical analysis

The analysis from here will be done by a numerical integration process. The use of a Gaussian Integration method was considered, but decided against in part because it would be impractical to implement. As the load in each iteration of the analysis depends on the deflection in the previous iteration, each cycle of the analysis will add four to the degree of the polynomial that best describes the deflection. A simple midpoint rule numerical

integration seems the simplest, and after testing, provides accurate results in little computation time.

Method

This program calculates bending moments, rotations, and deflections iteratively using a double numerical integration. The core of the problem is fairly simple. After the input has been collected, the program first finds some of the basic, important values, including the necessary geometric properties and variables, end depths, and more. The program then divides up the beam into very small pieces and calculates the load on each. Based on the locations of these slices and the loads on them, the program calculates the moment at each slice. Once the moments are known, the program numerically integrates them, then determines and subtracts out the constant of integration. This determines the curvature at each point. The program then integrates again to calculate the deflection at each point. The deflected shape is now known, and the load for the next iteration is calculated based on this. The program simply repeats this process for the specified number of iterations, and the whole process is repeated for each beam being analyzed.

Variables

There are seven variables that go into the ponding analysis, most of these are geometric. These include the length, angle, spacing, modulus of elasticity, and moment of inertia. The final two have to do with the load: the unit weight of the ponding fluid and the initial height. The initial height represents the height of water that sits on the beam, and

determines the initial load. It is assumed that the water level will remain constant throughout deflection at this height.

Variations

There are four analysis options built in to the program. The first is the basic ponding analysis. The computer takes input regarding the system properties and loads for any number of beams, does the ponding calculations, and outputs the results (numerically) and the deflected shapes (graphically) for each iteration. This analysis will usually make it clear whether the system is stable or not, but will not indicate whether the system will fail under the given loads. The second option in the program checks the strength. By asking the user for a value for the strength of the beam, and comparing this to the moments induced by the loads, the program will determine whether the beam will fail.

A third and very useful option has also been built in. It allows the user to input all but one of the variables for a ponding setup, then determines the value of the last variable that will put the system exactly at the point of instability. This option has been expanded into a fourth, in which the program will repeat the derivation of the critical value as for as many (closely related) setups as desired. This saves a lot of time, and was used to find the output that led to the conclusions of this section. In these analyses, it is important to note that an initial guess at the correct value for the variable is required. Based on the method of analysis, a final result that is more than twice this value will never be found. Results must be checked to ensure that the results are reasonable and that they are less than twice the initial guess.

Excel

The analysis program was written in MATLAB but also created in Excel. While the MATLAB code allows the more involved analyses to be run, the Excel spreadsheet allows quick analyses to be run and all variables to be viewed. It provides a more convenient interface for simple analyses.

Errors and Accuracy

The results from the MATLAB program have been checked against results from the Excel spreadsheet, and hand calculations. The results of the MATLAB program and Excel are identical when MATLAB is using ten iterations and 100 divisions as the spreadsheet does.

Hand calculations can only be done for the first iteration, as successive iterations get complicated for analysis by hand. Also, for the pitched case, the only setup analyzed by hand for checking accuracy was the first iteration of the case where water fills exactly to the high support, as this provides a simple load pattern. For the first iteration of the flat case, when the programs are compared to the hand calculations, the results are very close. It turns out that the error is independent of all but one of the variables (the pitch), and mostly depends on the number of divisions used in the analysis. The results of the analysis of the accuracy are shown in table 3:

Table 3: Errors in Numerical Analysis:

Divisions:	100	99	75	50	35	25	20	10	2
% Difference:	0.016	0.00408	0.00711	0.064	0.033	0.064	0.4	1.6	40

Where the divisions are all fairly small numbers, and the percent difference represents the percentage difference between the hand calculated values for maximum displacement from equations as provided in the AISC steel manual, and the value for the maximum displacements from the MATLAB and Excel program.

Based on these numbers, it can be seen that errors are very small for a small number of divisions. Also, it can be noted that the error gets smaller at a rate proportional to the square of the rate of the increase in divisions. This can be shown by comparing the errors at 100 and ten divisions. Another important property to notice is that an analysis with an odd number of divisions is much more accurate than an analysis with an even number. In fact, if an odd number is used, only half as many divisions are needed. This can be seen by comparing the accuracies of the analyses with 50 and 25 divisions.

Finally, by checking analyses of sloped beams, it was found that the results from the program are slightly small, but that it is still very accurate. Analyses of sloped beams show that the errors seem to be about 3.5 times larger than the corresponding flat case, regardless of slope. Because the MATLAB program allows large numbers of divisions with little problem, this error is insignificant. In some cases, analyses were run with more than 10,000 divisions, which would put the worst case error at less than one part in ten million.

Results

The program outputs results both in numerical and graphical forms. For the results discussed here, the numerical data is more useful, but the graphical data often gives a better understanding of the behavior. Shown in figure 28 are three plots from MATLAB.

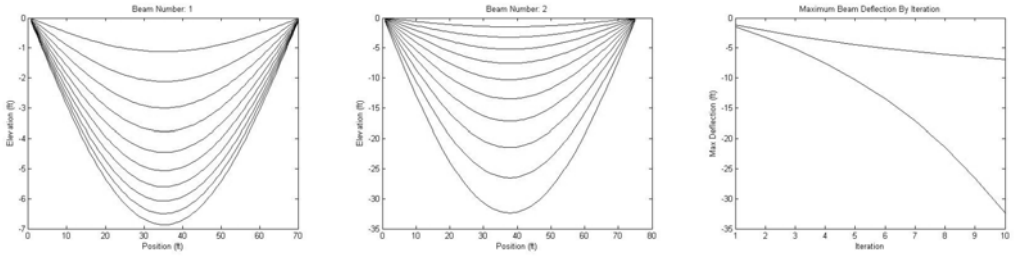

(a) (b) (c)

Figure 28: Beams analyzed by numerical analysis

Figure 28(a) represents a stable system. The successive deflections get bigger, but the rate of deflection increase decreases. This beam is approaching stability and will not deflect indefinitely. Figure 28(b) represents an unstable system. Successive deflections get increasingly larger, and will continue to infinity. Figure 28(c) represents a simplified version of both the other plots. The top curve represents the stable system, as the total deflection approaches a fixed value. The bottom curve represents the unstable system, as the deflection becomes unbounded.

The results of the program, aside from it being a useful tool itself, are the results of the determination of the critical values of variables that put the system exactly at stability. Based on the results, it has been shown that this numerical analysis checks with the stability criteria in the literature, first presented by Haussler in 1962.

Using the program option to find a series of critical points, sets of ten such points were found. One variable, the unit weight, was isolated and varied between 100 and 10 pcf (15.7 kN/m^3 and 1.57 kN/m^3). Based on the critical values, results for the critical values of each other variable were found in turn. Based on these, it was confirmed that unit weight is proportional to the moment of inertia and modulus of elasticity, inversely proportional to the spacing and inversely proportional to the fourth power of the length. These proportionalities all reflected the equation published by Haussler (Haussler, 1962).

Both flat and pitched roofs were checked for the effect of the initial depth of water on the ponding stability and it was found that the critical point was not dependant on the initial load at all in either case. For the sloped case, it was found that the relationships between the variables remain unchanged, with the exception of length. The unit weight is still proportional to the modulus of elasticity and the moment of inertia, and inversely proportional to the spacing. The relationship between these variables, the length and the pitch angle is not known quite as well for a non-flat beam. The two variables in question, length and angle, were checked against each other to determine a relationship at the critical value for stability. For a beam with 110 pcf (17.3 kN/m^3) unit weight, 6 ft (1.83 m) spacing, 2 ft (0.61 m) depth, 500 in^4 (12.0 cm^4) moment of inertia, and 29000 ksi (200 GPa) modulus of elasticity, the results are shown in figure 29:

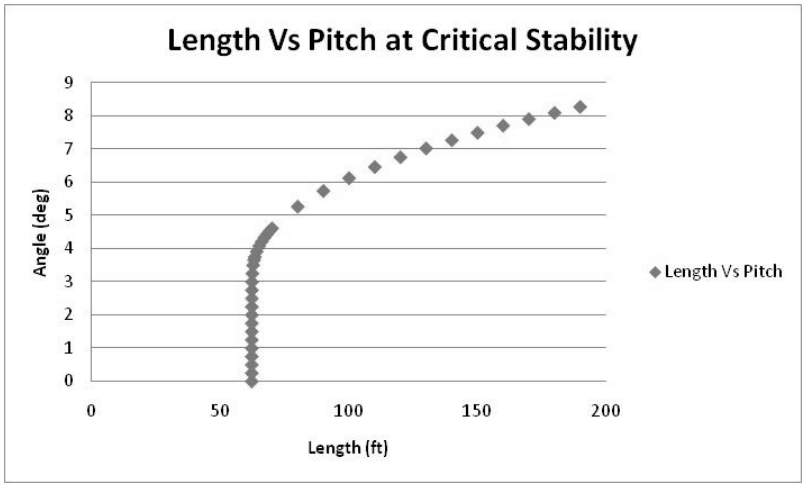

Figure 29: MATLAB output

This typifies the plots of several different sets of the variables. They all have a vertical asymptote that crosses the length axis at the critical length for a flat beam with the other variables constant. It curves up quickly at first, but the growth of the angle with length slows down. This plot does not hit an upper bound, but simply continues up increasingly slowly as the length increases.

Figure 29 illustrates an important fact of the ponding problem. Putting a roof on a pitch will always make it more stable, but it is interesting to note that, in this case, a pitch up to four degrees does not make the allowable length longer. The benefits come as the pitch rises above five or six degrees. Building codes and design specifications only require ponding analysis for roofs that have a pitch below ¼ on 12 or about 1.2 degrees. This requirement is based on ideology completely separate from this analysis. The basis of that angle is that for a pitched roof, the water can simply run off. The analysis presented here, however, assumes it cannot. It is more conservative to assume that the water will be blocked at the low end of a roof, and use the analysis presented here.

Conclusions

Based on this analysis, there are seven variables that determine the deflection of a beam under ponding loads, six of which determine the stability criterion. The result presented by Haussler was verified for the flat case. The sloped case, however, is more complicated. The relationship of the variables length and angle to the other variables is unknown. In two different papers, the authors approach the problem of the sloped roof under ponding loads (Chang and Chong, 1977) (Blaauwendraad, 2007). While they both show that ultimate deflection depends on initial load, neither determines whether stability depends on initial load or not. Also, neither paper presents a simple method for calculating a stability factor. This analysis has shown that the initial load does not affect the stability, and has shown some insight into how the angle affects stability.

It would be good for building codes and design specifications to include the pitch of a roof in the criteria beyond simply to provide a method of drainage. It would be safer to assume that the water draining will be blocked at least to the height of the secondary drainage system, and that this could initiate ponding. Requiring a ponding analysis for sloped roofs to a higher pitch would do a much better job of ensuring safe roof systems.

EXPERIMENTAL DESIGN

The experiments were designed to provide data that will enable better understanding of ponding effects on light weight, long span roof systems. The vast majority of roofs that fail due to water overload and ponding are stable according to design specifications, but collapse due to overload as a result of ponding effects. The experiments were designed to measure the roof response under increasing water load to collapse.

Structural Design

Two roofs were tested to failure: the first was flat; the second was identical except for a 1:48 pitch, the code minimum to allow exclusion of ponding checks in design. The basic design of the specimen was three steel joists simply supported on heavy rolled steel sections. The design intended to isolate the center joist as a typical roofing member within a roof continuum and testing, instrumentation and results focused on this joist for each test. Roofs were designed to be typical of current practice. Loading was accomplished by building walls around all four sides of the roof, placing a waterproofing membrane over the entire system, and allowing water to collect until collapse.

Facilities

The long wave channel at the O.H. Hinsdale Wave Research Laboratory at Oregon State University provided an effective setting to conduct these tests. The channel is 15 ft (4.57 m) deep, nominally 12 ft (3.66 m) wide and effectively infinitely long. It provides one inch (2.54 cm) threaded inserts on 12 by 8 inch (30.5 by 20.3 cm) grids every twelve ft (3.66 m)

to anchor supports into the walls. These enabled the supporting brackets for the roof system to be anchored to the concrete wall. This facility created two restrictions on the experimental design: the length of the roof had to be a multiple of twelve ft (3.66 m) to facilitate convenient supports, and the roof slice had to be twelve ft (3.66 m) wide.

Joists

Steel joists were selected for testing because they provide an economical, light weight, long span roof system that is widely used throughout the country. Many large warehouse, office and commercial buildings deploy roofs built with steel joists and steel decking.

Based on the facilities and materials available, a design consisting of three 48 ft (14.6 m) joists spaced a little less than 6 ft (1.83 m) apart was chosen. In this configuration, the center joist supports approximately twice as much load as the edge joists. By tributary areas of loading, the center joist suppports an area 67 inches (1.70 m) wide, the edge joists, 38 inches (0.965 m) wide. Because the center joist supported more weight, if all joists were of equal stiffness, it would have had a greater deflection than the edge joists. To illicit a one way joist response, two different joists were used. The center joist was the standard 24K9 (one of the most commonly used joists in practice), while the edge joists were specially designed to be approximately half as stiff, and to hold a slightly higher amount of water than the center joist, to ensure that they would not fail first. See appendix B for a comparison of the strengths (which are directly proportional to their stiffnesses), and a check to ensure the center joist would fail first. This modification ensured that the roof would provide more uniform deformations, consistent with a continuum roof system.

The center joists were 24K9 joists with a design capacity of 211 plf (3.08 kN/m). The design live load capacity was 101 plf (1.47 kN/m) and the moment of inertia including the fifteen percent reduction for shear deformations was 309.33 in^4 (7.43 cm^4). The edge joists were 24KSP121/58 joists with a total design capacity of 121 plf (1.77 kN/m), a design live load of 58 plf (0.846 kN/m) and a moment of inertia of 187.74 in^4 (4.51 cm^4). The joists were built with an extra two inches (5.08 cm) seat length at each end to facilitate support for the tests. The required 1.67 design factor of safety and typical one inch (2.54 cm) total camber were built into the joists. Materials used were nominally 50 ksi (345 MPa) steel. Post-test material testing was conducted in accordance with ASTM E8 on undamaged sections of the joists. These tests gave the material properties shown in tables 4 and 5. The larger double angle section was used in the top chord, the smaller in the bottom chord. The bar was used as the last web members and the 1-3/8" channels as the third web member from wither end. The remaining web members that angle up toward the center were made of the U sections, and the rest were made of the 1" channels.

Table 4: Material Strengths, Flat Joist

	F_y ksi (Mpa)	F_u ksi (Mpa)	% Elongation
LL2x0.166	60.3 (416)	90.2 (622)	25.7
LL2x0.142	60.1 (414)	90.1 (621)	26.5
BR15/16	52.0 (359)	90.0 (620)	27.0
C1x0.8x0.09	61.4 (423)	70.8 (488)	22.0
C1-3/8x1.27x0.118	64.2 (443)	75.4 (520)	28.2
U1x1.1x0.118	59.0 (407)	70.9 (489)	26.2

Table 5: Material Strengths, Pitched Joist

	F_y ksi (Mpa)	F_u ksi (Mpa)	% Elongation
LL2x0.166	60.0 (414)	90.4 (623)	26.2
LL2x0.142	58.3 (402)	85.9 (592)	27.0
BR15/16	52.4 (361)	90.4 (623)	29.3
C1x0.8x0.09	63.2 (436)	73.3 (505)	19.8
C1-3/8x1.27x0.118	64.6 (445)	76.6 (528)	28.0
U1x1.1x0.118	58.6 (404)	71.0 (490)	26.5

The purpose of the experiments was not to investigate ponding stability theory, as to do so would require very flexible joists, in part because the AISC specifications require a factor of safety of four against ponding. Custom joists would have be required, and they would have been unrealistically understrength and flexible, and would not have been representative of practice. The fact that none of the standard joists would be unstable against ponding loads in the facilities available demonstrates that common joist designs are theoretically safe for ponding stability. This does not mean, however, that it is not possible to design steel joists that will be unstable for ponding loads. For example, by increasing the spacing between joists enough, any joist could exhibit ponding instability. A comparison of the ponding stability of the chosen joist to the specified criteria is shown in appendix B.

Roofing System

The roofing system consisted of the steel joists, steel decking, insulation and waterproofing membrane, shown in figure 30:

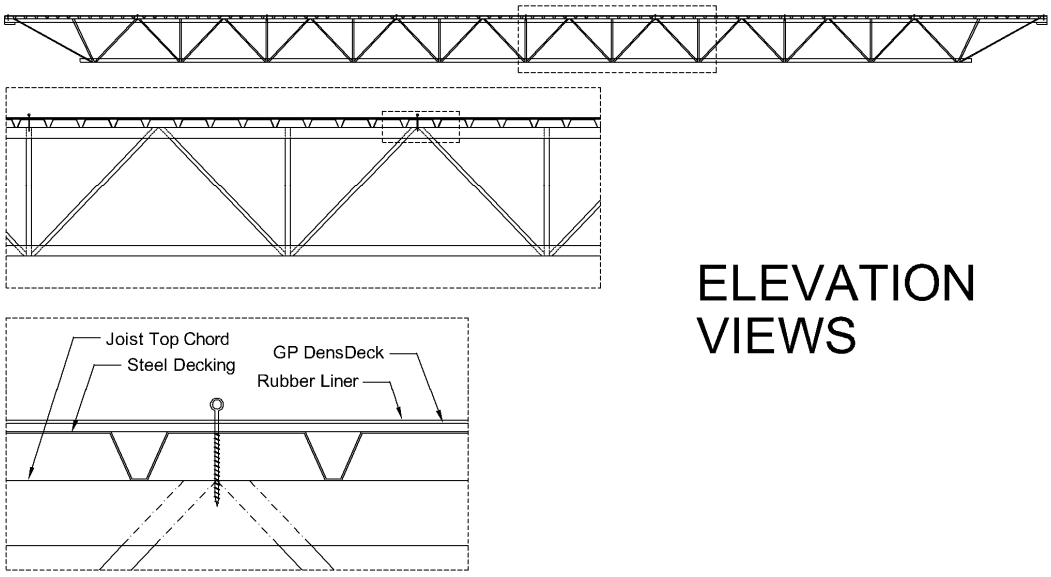

Figure 30: Joist Elevation Views

The joists supported 22 gage Wide Rib Steel Decking, a common decking material for these roof systems. The decking was welded to the top chord of the joists in a 36/4 pattern: one weld every 12 inches (30.5 cm). On top of the steel deck roofing, Georgia Pacific DensDeck was used to provide a flat roof surface on which to work. Over this, a 45 mil (45/1000 inch or 1.14 mm thickness) rubber waterproofing membrane was used to waterproof the roof. This membrane was draped over the concrete and plywood walls on all four sides and weighted to allow movement and keep it from falling into the pool. The load was applied by adding water via hoses on top of the roof.

Supports

For these experiments, the supports were pin and roller connections with no moment resistance to simplify construction and analysis. As the joist deflected, the roller end moved horizontally toward the other support due to top chord bending and compression. In

the field, joists are typically welded to both supports,which would prevent this motion, induce tension forces in the top chord and reduce the overall deformations. To eliminate these effects and use the idealized design assumptions, roller supports were used at the north end of both roofs.

Each end of the pin and roller system was supported on a twelve foot (3.66 m) W10x49 (W250x73) steel beam that carried the loads from the joists to the tank walls. The end of each of these rested on a bearing plate on top of a heavier column section that was bolted into the concrete wall. Details of this system can be seen in figures 31 and 32. The SJI code requires that for sloped joist seats at a pitch greater than ¼ on 12 the seats must be modified to accommodate the slope. It explicitly states, however, that "If slope is ¼: 12 or less, sloped seats are not required" (SJI, 2005). The slope used in this test was exactly ¼ on 12, so no modifications were made to the seats.

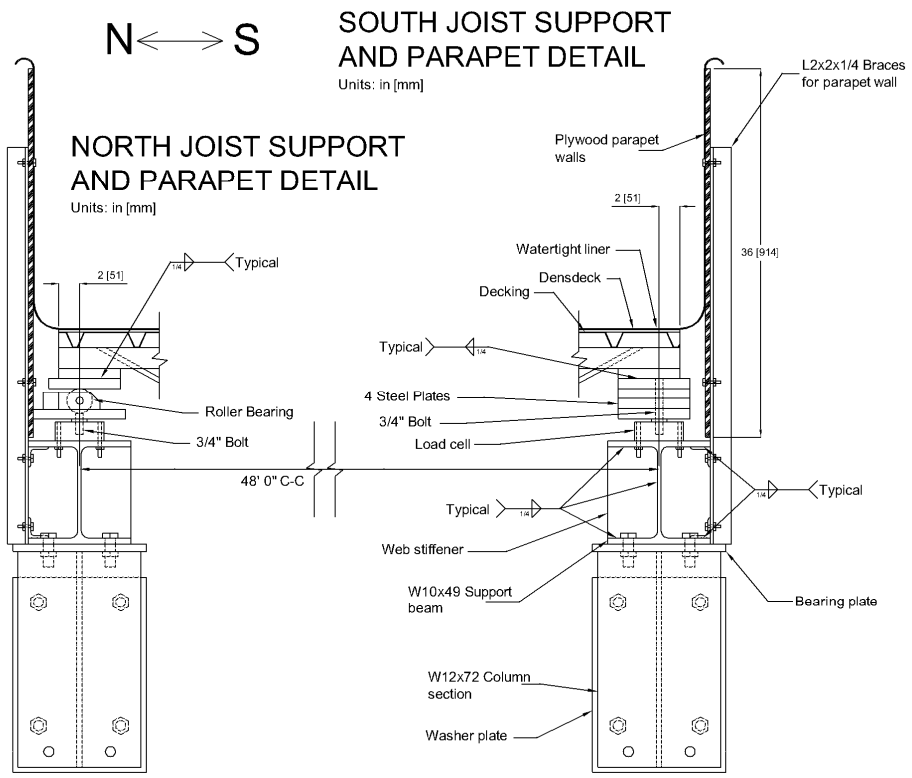

Figure 31: Joist Supports and Parapet Design

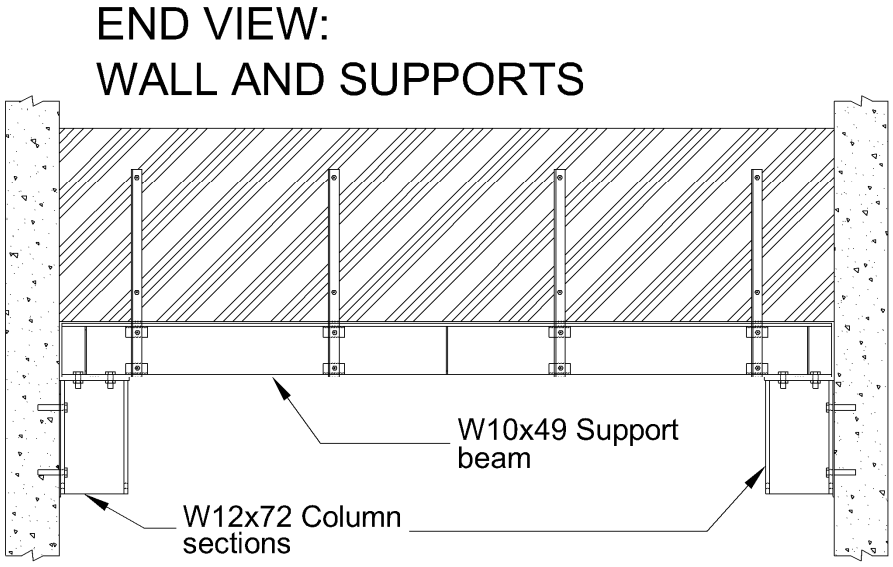

Figure 32: Parapet Wall and Supports

Bridging

Bridging elements used in these tests were 1-1/4x1-1/4x7/64 (32x32x2.8) angle sections. These were welded to the top-most edge of the bottom flange and the bottom-most edge of the top flange, leaving them out of the way of the decking and allowing them to be continuous over all three joists. The maximum allowable spacing of the bridging was 14.5 ft (4.42 m) for the center joists and 12.17 ft (3.71 m) for the side joists. These values are conservative, as they are calculated based on expected loads during construction. The limit for the edge joists was smaller because they were designed for approximately half the capacity, so smaller angle sections were used for their chords. Since the smaller number controls, none of the rows of bridging were spaced farther than 146 inches (3.71 m) apart. Based on the SJI specifications, four sets of bridging were required for these joists, the center-most of which was required to be cross bracing.

In typical construction, where the bridging terminates at the end of a set of joists, it is tied into the structure so that the entire system is laterally anchored. This could not be done for these tests, as the roof moved vertically, and tying into the concrete walls would have resisted the deflection of the roof. These roofs should be restrained laterally, but able to move freely vertically. To accomplish this, custom roller supports were built and welded to the edge joists so the rollers were in contact with the walls on either side. They are shown in figure 33:

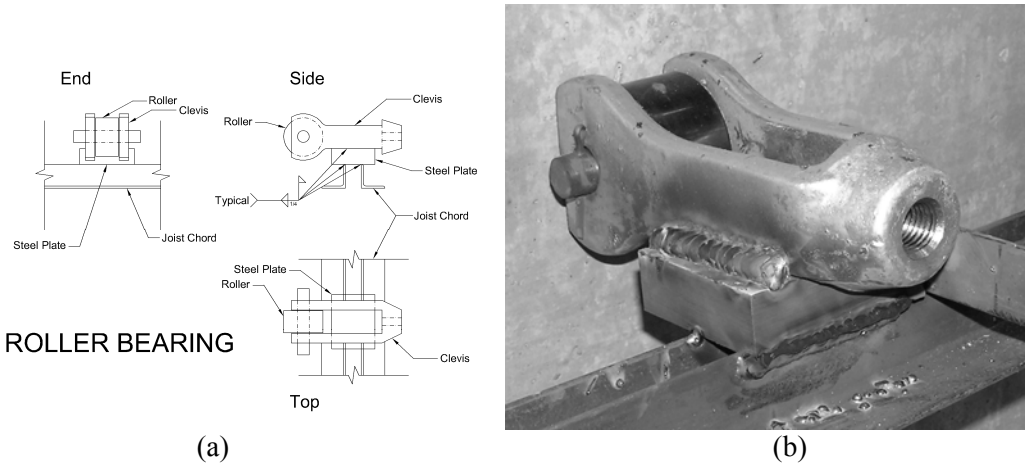

(a) (b)

Figure 33: Roller Bearing, (a) Schematic (b) Photo

There were 16 rollers laterally supporting the roofs: one at the termination of each set of bridging. For the flat test, imperfections in the walls where these rollers would rest were avoided by shifting the bridging along the length of the joists. After the flat test, it was apparent that this would not affect the outcome of the test, so in the pitched test, bridging was spaced at even intervals. The bridging spacing distances and details are shown in figures 34 and 35:

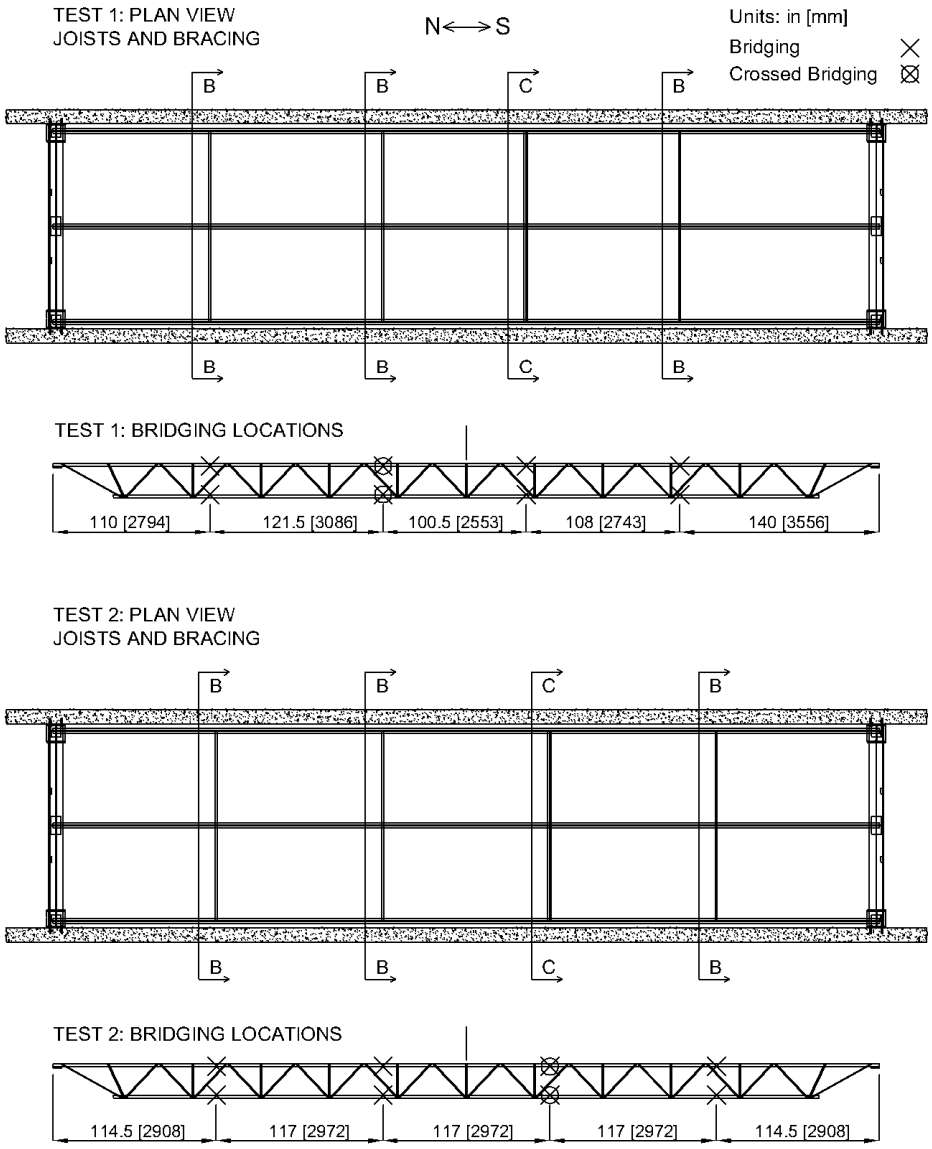

Figure 34: Bridging Locations

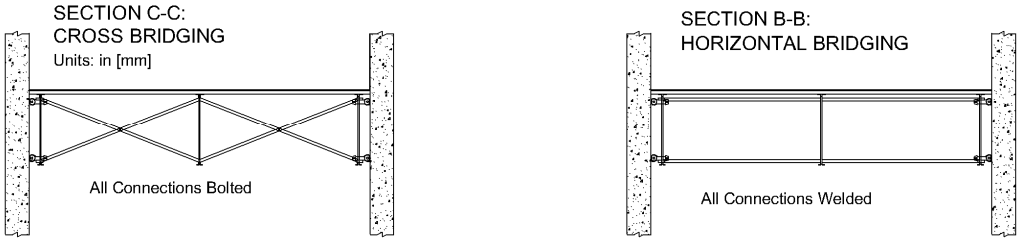

Figure 35: Lateral Bridging

Instrumentation

Several different types of instrumentation were used to measure the response of the specimens, including: strain gages, displacement sensors, load cells, a flowmeter and a sonic water level sensor. Displacement and load cell sensors were calibrated either prior to or following the tests to ensure accuracy. Strain gages were used to measure components of the internal forces in some of the joist members. Displacement sensors were used to measure the vertical motion of the roofs as they were loaded and to measure the horizontal motion of the roller supported end of the joist. A load cell was used at each joist support to measure the six joist reactions. A flowmeter was used to monitor the volume of water applied to the roof during the tests, and the water level sensor measured the water elevation over the course of the tests. Finally, during and after the test, three video cameras and a still digital camera were used to document the experiments.

Strain Gages

Strain gages were used to measure individual joist member forces. In some cases, more than one gage was required at a section in order to measure multiple force components. For details on how this was done, see appendix A. The number of gages used in different locations for the tests is summarized in figure 36 and table 6. A multiple strain gage section is shown in figure 37:

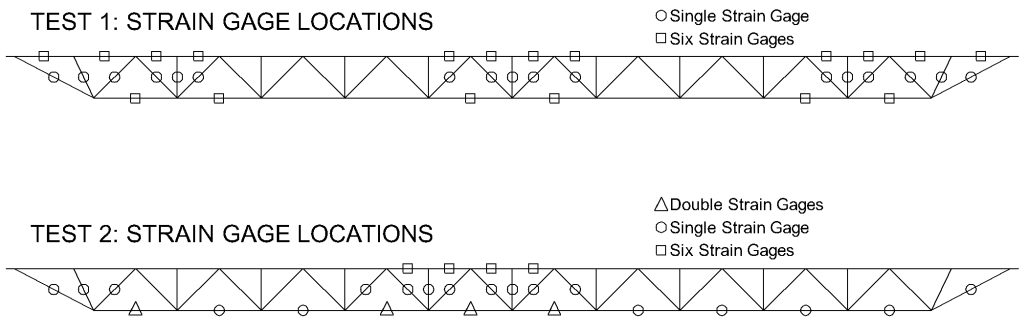

Figure 36: Strain Gage Locations

Table 6: Multiple Strain Gage Locations:

Location	First Test	Second Test
Top Chord	6	6
Bottom Chord	6	1 or 2
Web	1	1

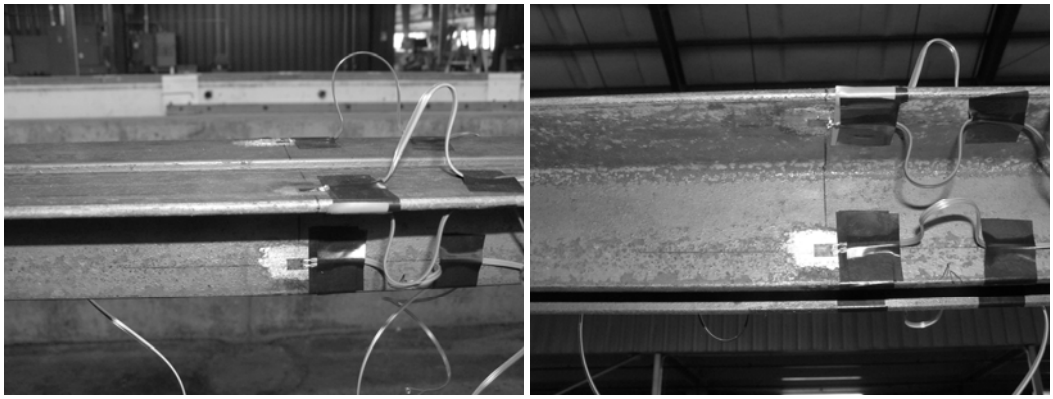

(a) (b)

Figure 37: Multiple Strain Gage Instrumentation, (a) From Above (b) From Below

The bottom chord was instrumented with six gages per location in the flat test but was found to carry only tension loads, so it was instrumented with either one or two gages per location for the pitched test. Additionally, strain gages were located on members at their midspan for two reasons: to capture the maximum bending moments, and to avoid stress concentrations at the ends.

Vertical Displacement Sensors

Vertical displacement sensors were used at 25 locations on the roof to measure the vertical roof deflection as water was added. The sensors were fastened to a rigid frame supported on the top of the concrete walls above the roof and connected by brass wire to eye bolts, screwed into the steel decking as seen in figure 38:

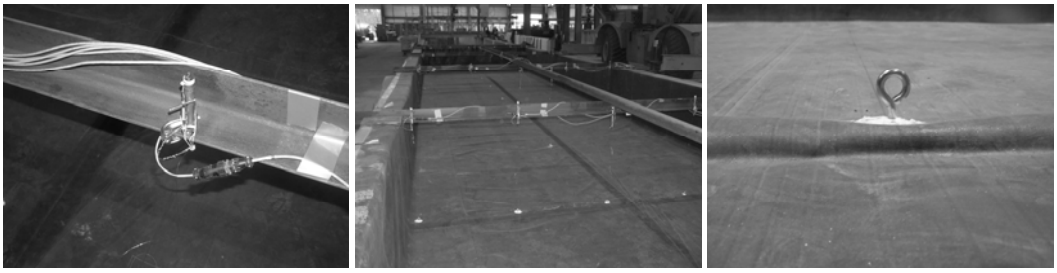

(a) (b) (c)

Figure 38: Vertical Displacement Sensors, (a) Sensor (b) Frame (c) Eye bolt

Three different types of vertical displacement sensors were used, including four inch (10.2 cm) displacement transducers, one twelve inch (30.5 cm) displacement transducer, and fifteen inch (38.1 cm) string potentiometers. The locations of each type for the two tests are illustrated in figures 39 and 40:

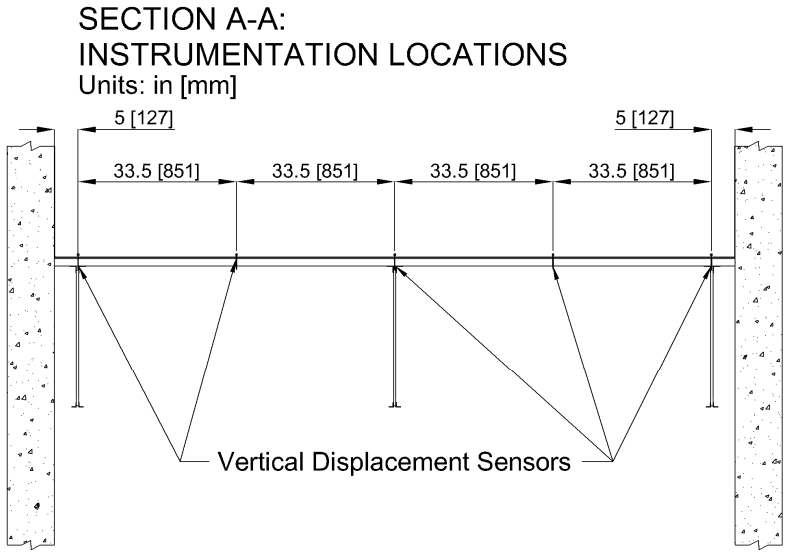

Figure 39: Vertical Displacement Sensor Locations

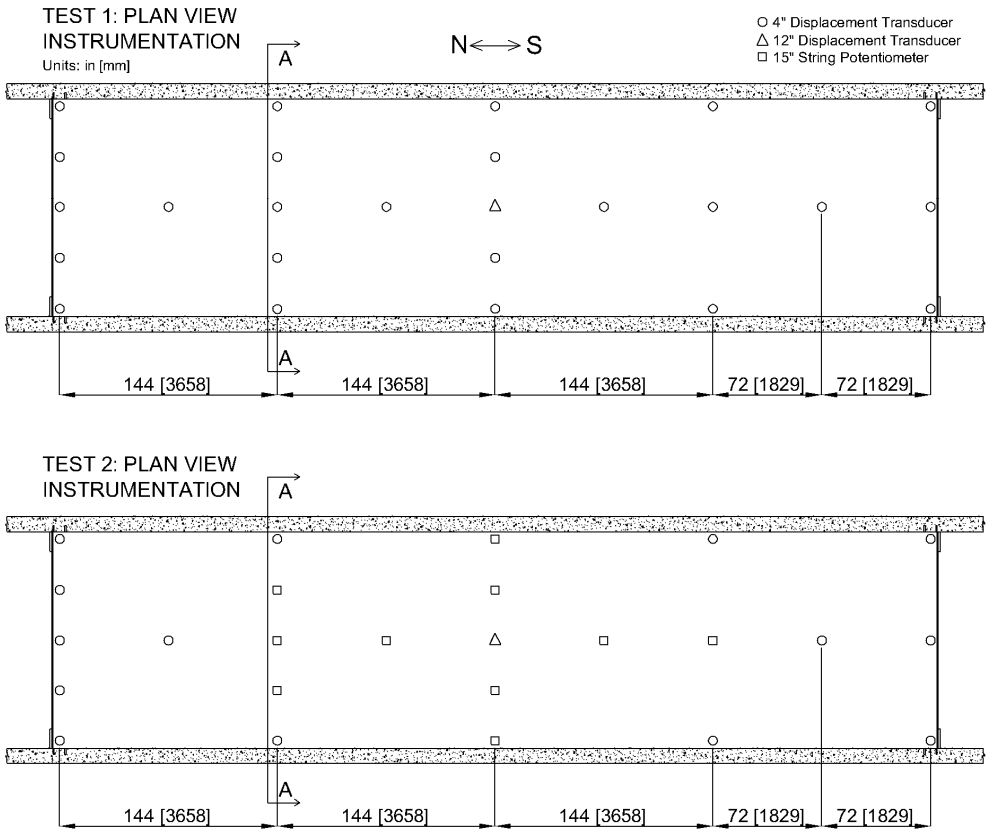

Figure 40: Plan View of Vertical Displacement Sensors

The data collected by the four displacement sensors in the corners was unreliable, as the waterproofing membrane bunched up in the corner and likely contacted the brass wires, altering these measurements.

Load Cells

Load cells were placed under the six supports of the roof. These provide each joist reaction and summed represent the total water load on the roof. The load cell installation can be seen in figures 31 and 41:

(a) (b)

Figure 41: Load Cell Installation, (a) End View (b) Side View

Horizontal Displacement Sensor

The ends of the joists that sat on rollers moved horizontally as load was applied. The magnitude of this motion was critical during testing, as there was nothing keeping the entire roof from sliding off the supports and falling to the floor if it moved too far. This measurement was made using a 1½ inch (3.81 cm) displacement transducer attached to the steel support beam, as shown in figure 42(a):

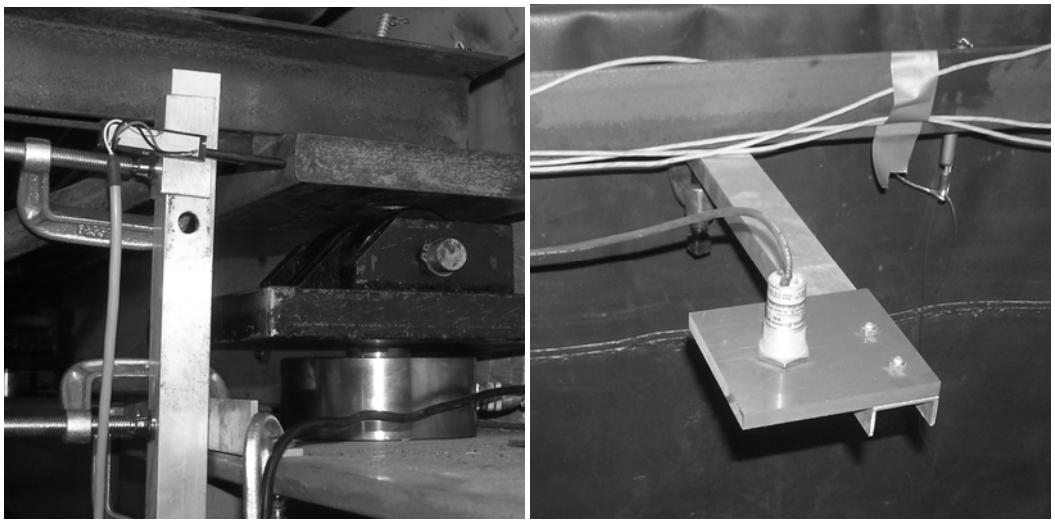

(a) (b)

Figure 42: (a) Horizontal Displacement Sensor (b) Water Level Sensor

Sonic Water Level Sensor

In order to measure the level of impounded water throughout the test, a sonic sensor was used. Because the loading was slow enough for the entire test, the surface of the water remained level in both tests until collapse, at which point the water flowed quickly toward the point of failure. In the pitched test, this sensor was installed as close to the low end as possible, at a point directly above the center joist and exactly 6½ inches (16.5 cm) from the centerline of the support. The device can be seen in figure 42(b).

Flowmeter

To give a reference value for the total amount of water applied, a flowmeter was attached to the hose feeding the roof. Over the course of the experiments, however, water leaked through the holes created by puncturing the rubber membrane to install the eye bolts for the displacement sensors, thus the values provided by the flowmeter over time did not accurately reflect the total volume of water.

Initial Conditions

When built, the first roof was expected to be exactly level, the second, straight on a 1:48 pitch. Due to joist and construction imperfections and the initial camber built into the joists, they were not perfectly flat. To determine the actual initial conditions, each roof was surveyed prior to testing. 125 measurements were taken on each roof on a grid of 25 equally spaced measurements along the length of the roof and five across the width. All

measurements were taken with a Philadelphia rod and laser level while standing directly above one of the joists. The standard deviation of all measurements taken from the flat roof was 0.0124 ft. (3.8 mm), and the standard deviation of the measurements from the pitched roof from the expected straight line was 0.0130 ft. (4.0 mm).

Experimental Methodology

After construction and instrumentation were completed and the data acquisition system was set up, the tests were conducted. Both roofs were loaded with water using a one inch (2.54 cm) garden hose attached via a flowmeter. This produced slow accumulation of water on the roofs until the eventual failure.

Test One: The Flat Roof

Testing began in the early afternoon of Friday, November 21, 2008. The data acquisition system was set to sample at 2Hz and loading continued until the water level reached approximately 1.75 inches (4.45 cm) at the supports. It was noted that the roof was slowly leaking, so the height of the water was measured to check in the morning and the flowmeter was already known to be an inaccurate measurement of the total load. With the water supply stopped, the sampling rate was reset to 0.01 Hz, attempts were made to stop the leaks, and the roof was left to sit overnight while the data files were briefly analyzed to check for any significant problems in the data acquisition.

The following morning, the water level was measured and, though the roof was still leaking, it had not made a measureable difference in the water level. All of the data looked

reasonable except that several strain gages were not working. As none of these gages were critical, the data sampling rate was reset to 1 Hz, the hose was turned on, and testing continued. Testing stopped briefly on Saturday afternoon to reset some of the displacement sensors as they became close to their capacity. Later in the afternoon, a second hose was added to speed the loading, and the roof broke at about 7:00 pm.

Test Two: The Pitched Roof

The second test was run very similarly to the first. Loading began in the late afternoon of Thursday, January 8, 2009. The sampling rate was set to 1 Hz, and the water was allowed to collect until it had reached the midpoint of the roof. The water was turned off, the data sampling rate was turned down, and the roof was left to sit overnight while the data was briefly analyzed. On Friday morning, the roof was still leaking, though the water level had not been noticeably changed. All of the data seemed reasonable, so the loading was continued. Again, the loading was stopped and sampling reduced while some of the displacement sensors were reset. Testing resumed, a second and a third hose were added, and the roof collapsed at 3:00 pm.

Design Summary

Two steel joist, steel deck roofs were built and tested to investigate ponding effects. The first test was flat while the second was on a ¼: 12 pitch. Each roof was made of a center, stronger joist, and two weaker, side joists, and was braced laterally by four sets of bridging. The experiments focused on the center joists, standard 24K9 joists. The joists were spaced at 67 inches (1.70 m) and supported by a pin-roller system on twelve foot (3.66 m)

W10x49 (W250x73) steel sections on steel column sections bolted into the concrete supporting walls. The joists supported steel decking, which supported insulation that was the foundation for the watertight liner that held the water in.

The design was a three way roof system, though it was effectively a test of a one way system. The primary system members were steel beams that had very little deflection and acted as rigid supports. The secondary system was the system of three joists, and the tertiary system was the steel decking. Because the decking did not fail before the joists, it was only important to distribute the water load to the joists. Every structural component of the test was checked to ensure it was at least as strong as the loads that it was expected to incur. These checks are included in appendix B.

EXPERIMENTAL RESULTS

Quantities measured during testing included the deflected shape of the roof, the strains in the joist members, the distribution of load at the supports, the horizontal motion of the roller supported end and the water level. These results are presented in the present chapter.

Data Reduction

Data were collected and initialized to zero. Some of the data was rescaled and the sonic water level sensor and some strain gage data were smoothed. Some other details of the data reduction process included:

- The load cell used in the southwest corner in both tests did not work properly. For the flat test, the load in this corner was taken as the average of the loads in the other three corners. For the pitched test, this measurement was taken as the same as that for the southeast corner.
- In the flat test, the strain gage on the southernmost web member was not working, so it was replaced and run through a different data collection channel. The offset value was determined from the center south load cell data.
- Element forces in the joist members were recovered from strains following the method in appendix A.
- The four corner vertical displacement measurements were taken as zero.
- The center joist support displacements were not removed from the total roof displacements because they are a significant component of the overall

displacement. The test setup consisted of a three way system (beam, joist and decking), and the data from the vertical motion of the support bending under the center joist reflects this system response.

- Some of the displacement sensors reached their stroke capacity during the test. The data after the limit was reached capacity were disregarded.
- The sonic water level sensor had an additional offset due to the position not being located directly over the support.
- Where duplicate strain gage data were collected, the average of the two sensor measurements was used.
- Where appropriate, total load on the roof was used as the independent variable for the data presentation for clarity and uniformity.

Distribution of Load

The portion of the total water weight held by each of the six support points was measured with load cells. As expected, the center joist held approximately twice as much load as each of the edge joists. The accumulation of water load at each support in the flat test is illustrated in figure 43 and the same results for the pitched test are shown in figure 44.

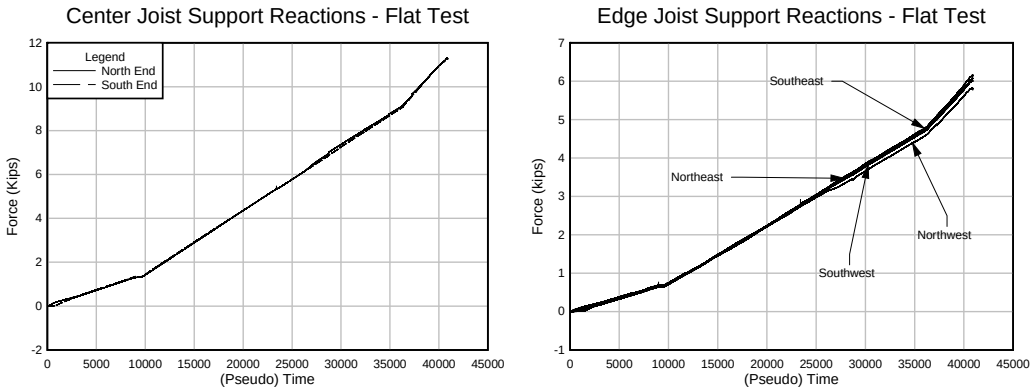

(a) (b)

Figure 43: Flat Test Support Reactions, (a) Center Joist (b) Edge Joists

For the flat test, the reaction distribution at the end of all three joists was similar throughout the test and the two side joists held very similar loads throughout the test, indicating that loading was symmetric in both directions.

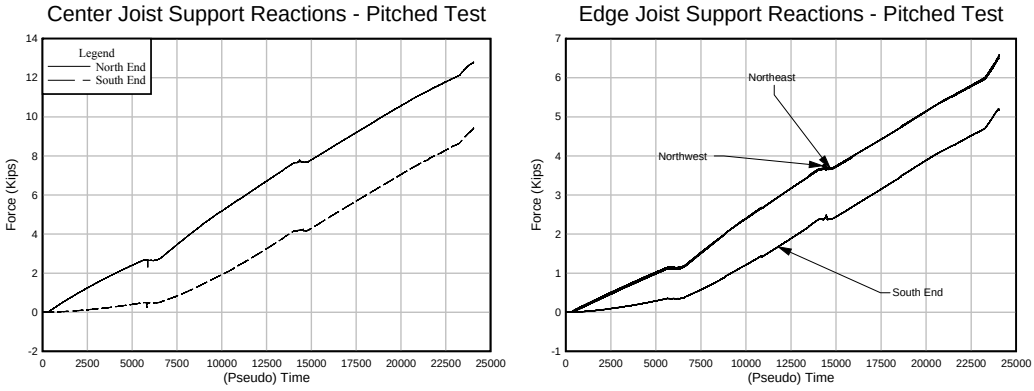

(a) (b)

Figure 44: Pitched Test Support Reactions, (a) Center Joist (b) Edge Joists

The support reactions were symmetric about the center joist for the pitched test as well, but they were not symmetric about the center of the span. This is because the water collected at the low end of the roof first, increasing the load on the north end load cells. It can be seen, however, that after a certain point (about 15,000 lb or 66.7 kN total load), the load does become more uniformly spread between the two ends and the curves representing the two opposite ends become parallel but offset due to the initial differences. A more meaningful

way of showing the distribution of the loads is to plot the reactions at each support with the sum of all six, as seen in figure 45. Results in subsequent sections will also be presented with respect to the total load on the roof.

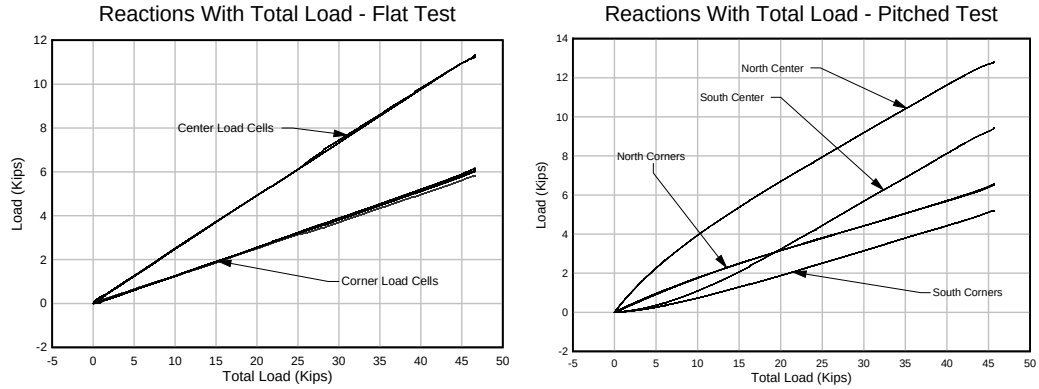

(a) (b)

Figure 45: Reactions with Total Load, (a) Flat Test (b) Pitched Test

In the flat test, the loads are distributed more evenly and increase linearly as the load distribution does not change noticeably with increasing total load. For the pitched test, however, the load distribution varied with total load, as the water conforms to the pitched roof.

From the data for the flat test, it is clear that the side joists carry more than half the load the center joist does. They were expected to carry half plus an extra amount corresponding to the 4½ inch (11.4 cm) cantilever in the decking. By checking the data at failure, the side joists combined hold 24.0 kips (107 kN) while the center joist held 22.4 kips (100 kN). These values were compared with the relative tributary areas of loading, 67 inches (1.70 m) for the center joist and 76 inches (1.93 m) for the sides combined. Computing the ratios shows that the center joist supported more load per tributary area than the edge joists. This demonstrates that the ponding effect, while clearly working along the length of the roof, was also working in the transverse direction. The center joist deflected more quickly than

the side joists, increasing its load, but it appears to be a linear relationship throughout the test. Though this could be considered a ponding effect, nonlinear load distribution was not observed.

For the pitched roof, the same ratios can be computed more easily if the reactions at the ends are summed. By summing the reactions and plotting the total weight supported by each of the three joists with the total load, linear relationships result and match those for the flat test, as shown in figure 46:

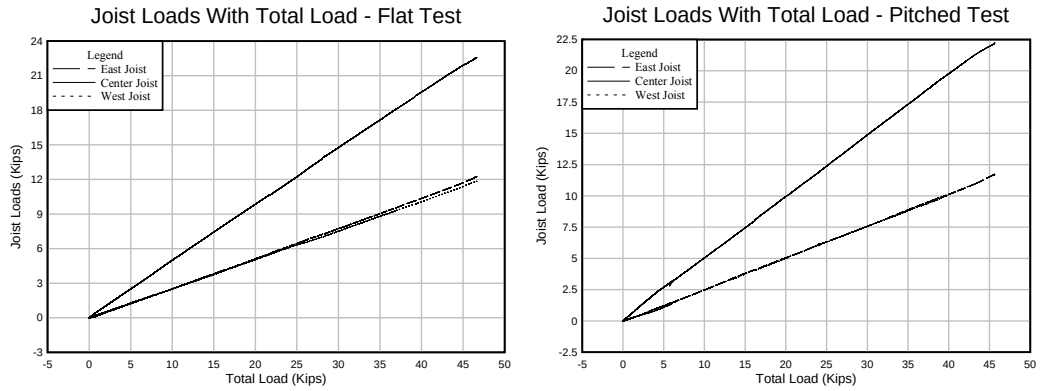

(a) (b)

Figure 46: Joist Loads, (a) Flat Test (b) Pitched Test

Based on the tributary areas supported by each joist, the center joist should support 46.9% of the total load. For the flat roof near failure, the portion of the total load held by the center joist is 48.3% and for the pitched test the ratio is 48.7%. The ratios show that the center joist is carrying a slightly disproportionately high amount of load relative to the tributary areas, and that the disproportion is similar in both tests.

Displacements

For investigation of ponding effects, the roof displacements are critical measurements. The displaced shape indicates the water load profile and also shows the overall structural response of the roof to these loads.

Joist Displacements in Profile

Figures 47 to 54 show the displacements of the three joists in both tests with a positive value indicating downward movement. For the center joists, nine measurements were taken along the length; for the side joists, five measurements were taken. The location of each measurement is at a distance measured from the north end of the roof. Symbols are shown at each of the sensor locations. As seen in the plots, the center joist displacements are not zero at their supports because the supports displace downward, and these effects were not removed. For both the flat and pitched roofs, initial geometry was removed to facilitate comparisons between the two tests.

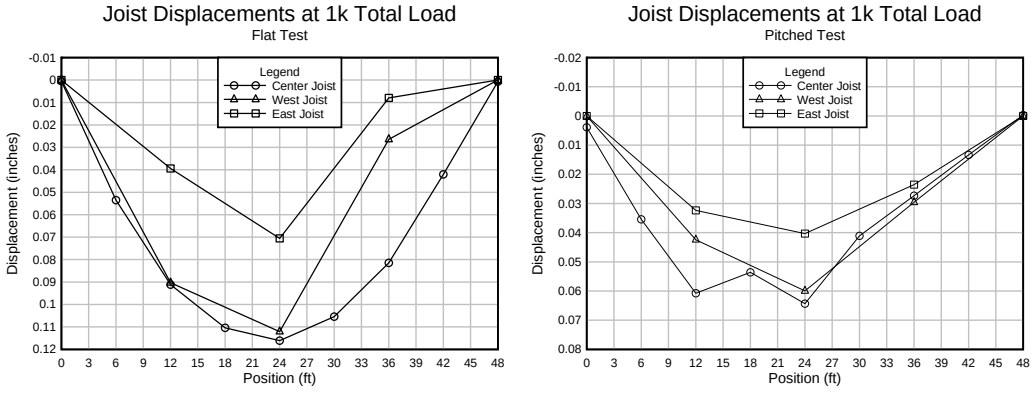

(a) (b)

Figure 47: Joist Displacements at 1 kip (4.45 kN) Total Load, (a) Flat Test (b) Pitched Test

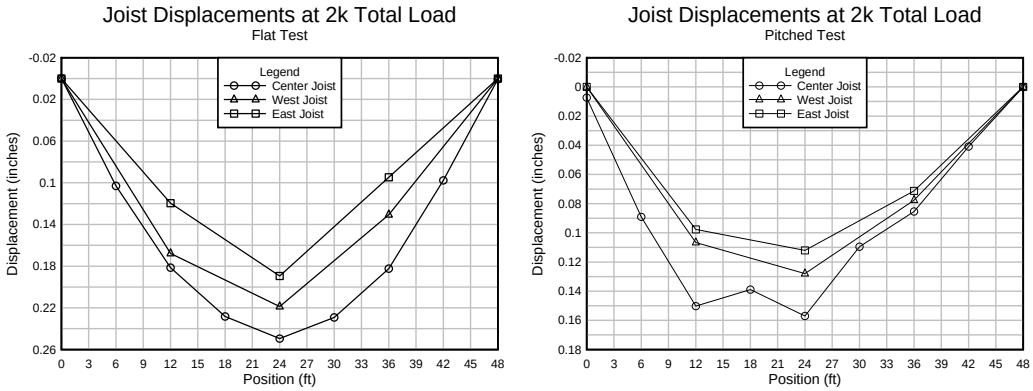

(a) (b)

Figure 48: Joist Displacements at 2 kips (8.90 kN) Total Load, (a) Flat Test (b) Pitched Test

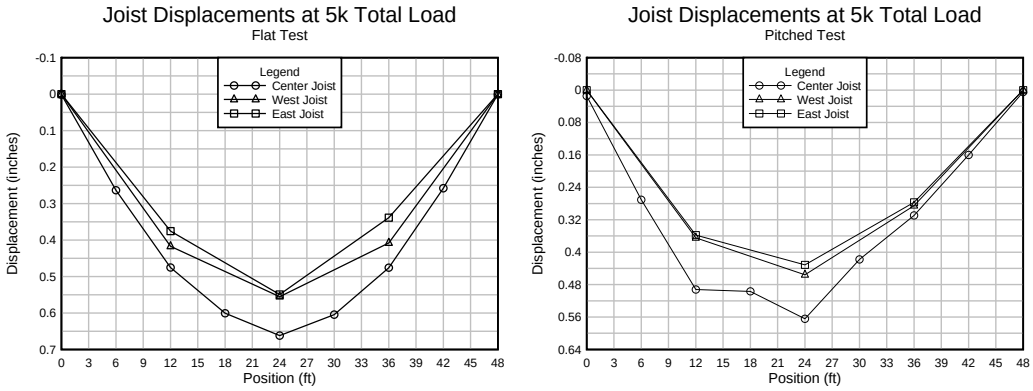

(a) (b)

Figure 49: Joist Displacements at 5 kips (22.2 kN) Total Load, (a) Flat Test (b) Pitched Test

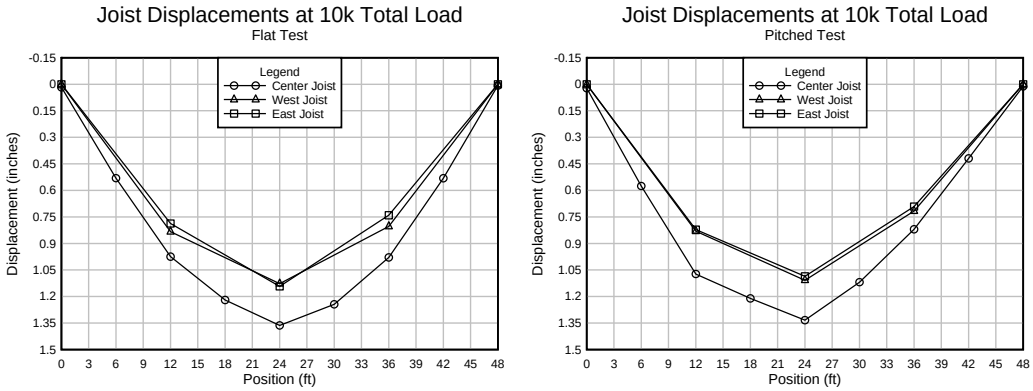

(a) (b)

Figure 50: Joist Displacements at 10 kips (44.5 kN) Total Load, (a) Flat Test (b) Pitched Test

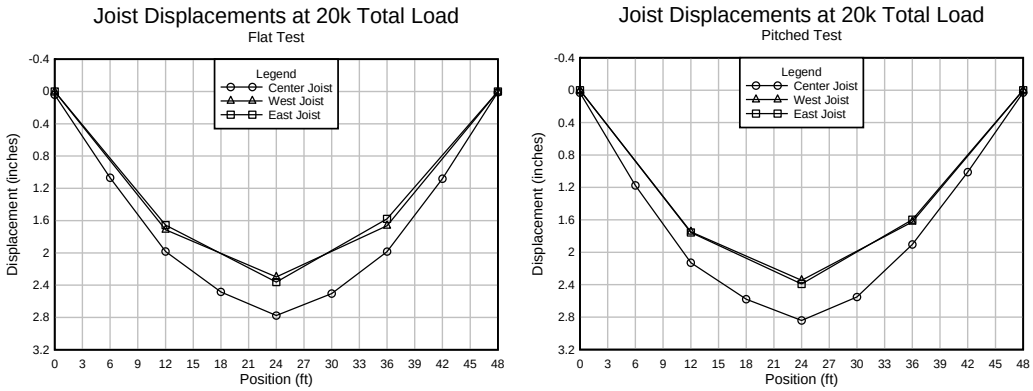

(a) (b)

Figure 51: Joist Displacements at 20 kips (89.0 kN) Total Load, (a) Flat Test (b) Pitched Test

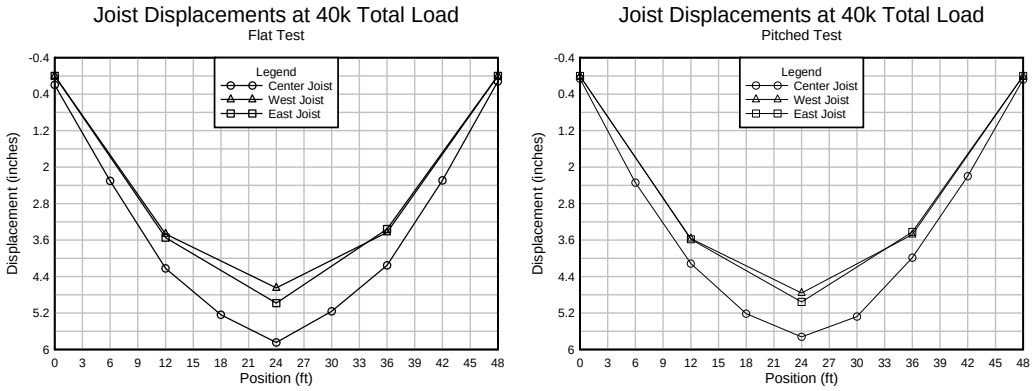

(a) (b)

Figure 52: Joist Displacements at 40 kips (178 kN) Total Load, (a) Flat Test (b) Pitched Test

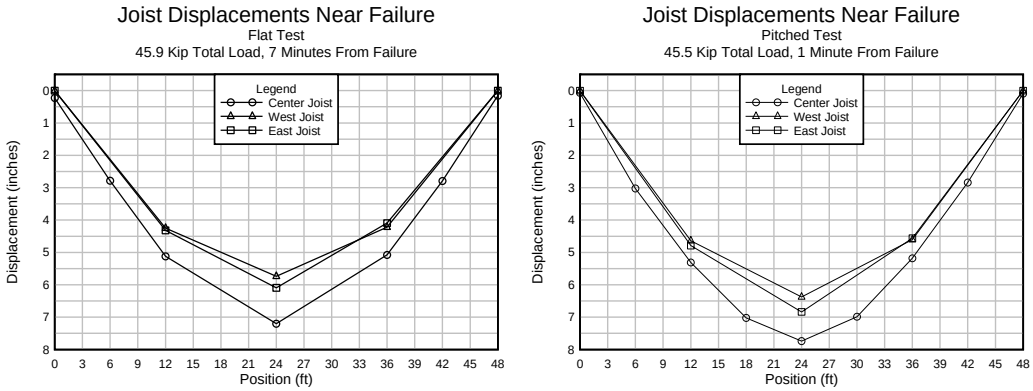

(a) (b)

Figure 53: Joist Displacements near Failure, (a) Flat Test (b) Pitched Test

Figure 53 shows the deflections shortly before collapse. Figure 54 shows the same data as figure 53(b), but includes the positions taken from the initial conditions survey.

Figure 54: Pitched Joist Elevations near Failure

Figures 47 to 54 show that the displacements for the pitched tests are asymmetrical early in the test because the load is unbalanced along the span. As the water load accumulates, the deflection profile flattens out and the difference between the two roofs becomes small. It can also be seen that the flat roof has larger deflections early in the test, but that this difference becomes less apparent with increased water load. This is because the load on the flat roof is, on average, closer to the center of the roof span.

At early stages of loading in both tests, the displacements do not exhibit the expected curve shapes. This is likely due to initial imperfections in both construction and loading. Wrinkles in the waterproof membrane led to slightly uneven distribution of water early in each test. While the initial imperfections lead to noticeable changes in the data early in the test, these become less significant as the water load increases.

Midspan Deflections

The overall performance of the joists and decking can be characterized by considering the midspan displacements of these elements. There were five displacement sensors at midspan, one over each joist and at the midspan of the decking between the joists. In the flat test, all five of the displacement sensors at midspan reached the limit of the sensor range before failure. For the midspan displacement of the center joist, the nonlinear portion of the load-deformation curve was measured and the adjacent responses were estimated from the center joist, as shown in the dashed lines in figures 55 and 56:

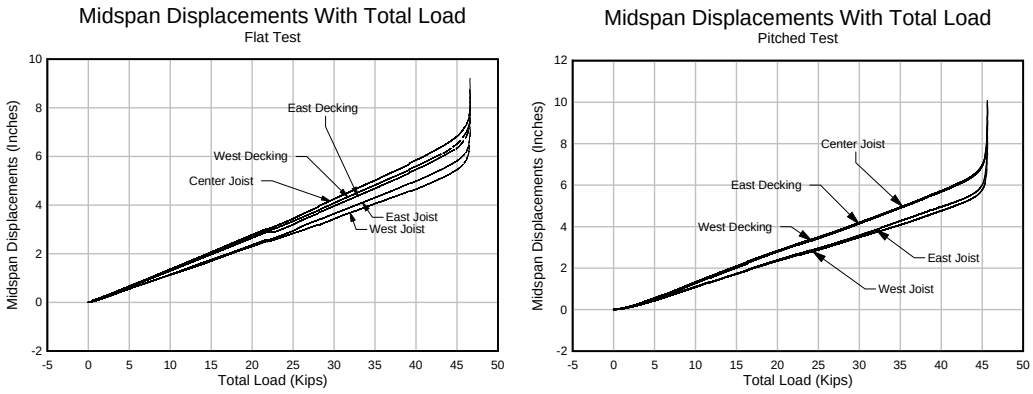

(a) (b)

Figure 55: Midspan Displacements, (a) Flat Test (b) Pitched Test

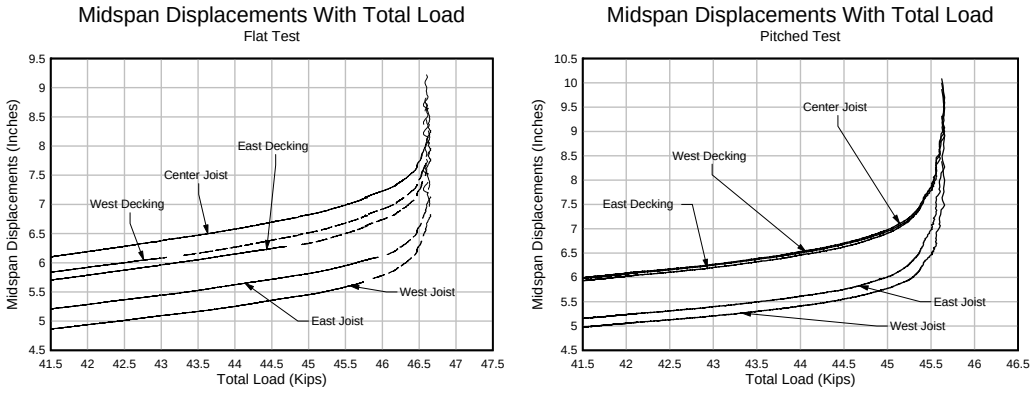

(a) (b)

Figure 56: Midspan Displacements at Failure, (a) Flat Test (b) Pitched Test

The responses of the center joist midspan displacements are plotted together in figure 57 and indicate similar overall performance:

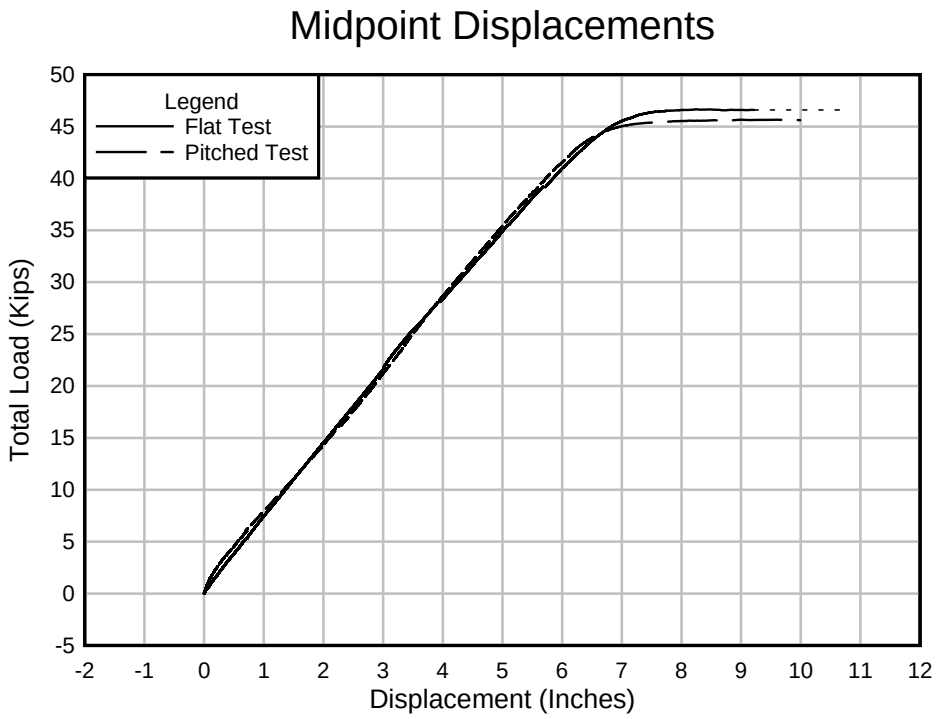

Figure 57: Midpoint Displacements

Initially, the pitched test was stiffer, but after significant load was applied, the two roof responses became similar. At failure, the flat test held slightly more total load.

The maximum moment was calculated using the deflection measurements to estimate the load profile, 62.4 pcf (9.8 kN/m^3) as the unit weight of water and the trapezoidal rule for integration. This is shown in figure 58. The moments were calculated at 5 kip (22.2 kN) total load increments for most of the test, and more frequently near the end.

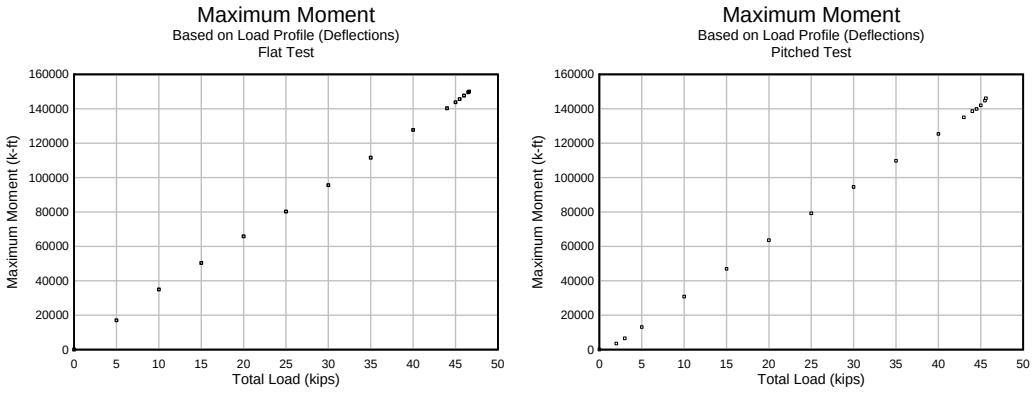

(a) (b)

Figure 58: Maximum Moments Based on Load Profile, (a) Flat Test (b) Pitched Test

The relationships illustrated in figure 58 are linear, though it appears that the moments become nonlinear at the end of the pitched test. These results further illustrate the similarity of the responses of the two specimens, even as they have different initial conditions.

Contour Plots

The roof displacement responses for the two specimens are shown in contour plots in figures 59 to 67. For the pitched roof, the net water induced displacements and the absolute elevations of the roof considering the initial geometry were both plotted. To create the absolute elevation figures, the initial conditions survey was used in combination with the test displacement data. For each roof, contours were plotted at three load steps. The in plane dimensions are in feet, and the displacements are measured in inches.

Flat Roof

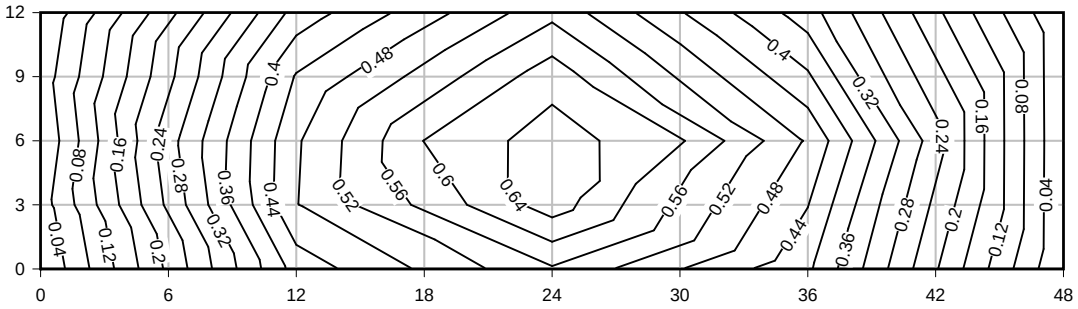

Figure 59: Flat Roof Displacements at 5 kips (22.2 kN) Total Load

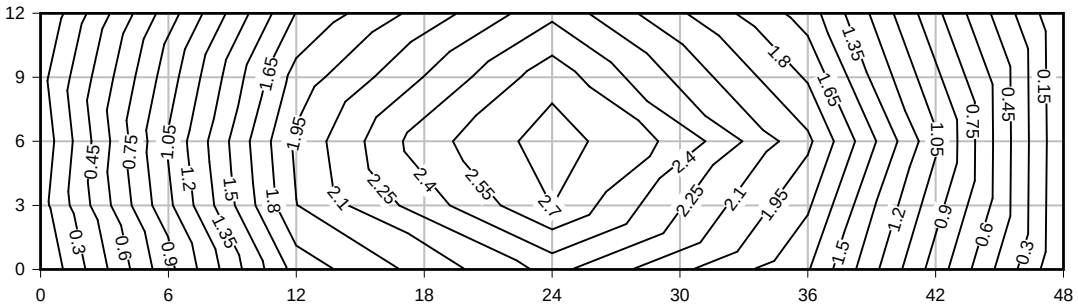

Figure 60: Flat Roof Displacements at 20 kips (89.0 kN) Total Load

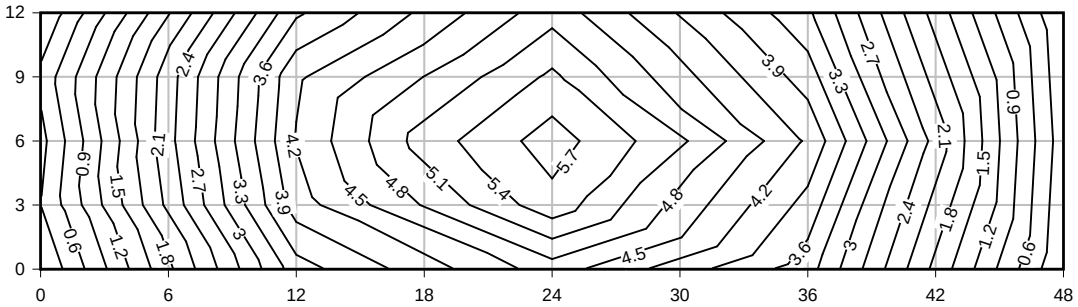

Figure 61: Flat Roof Displacements at 40 kips (178 kN) Total Load

Pitched Roof

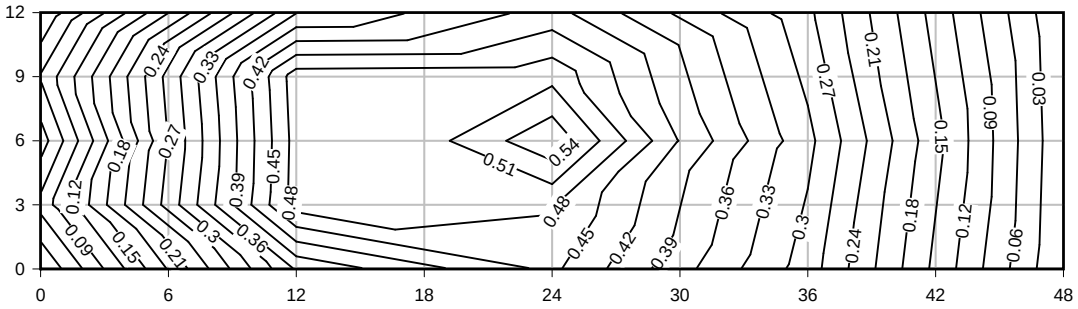

Figure 62: Pitched Roof Displacements at 5 kips (22.2 kN) Total Load

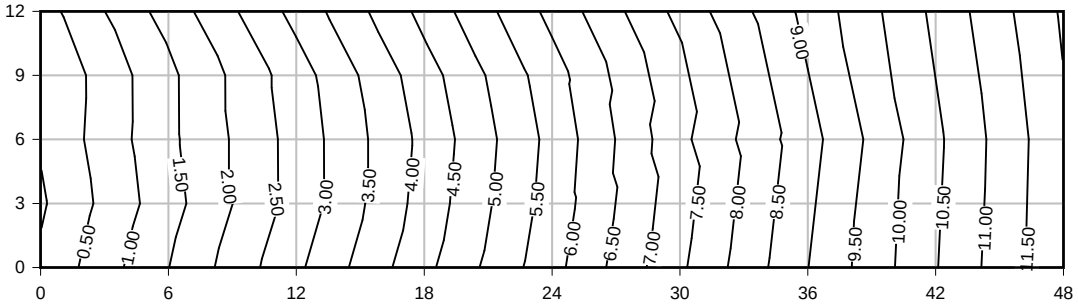

Figure 63: Pitched Roof Elevations at 5 kips (22.2 kN) Total Load

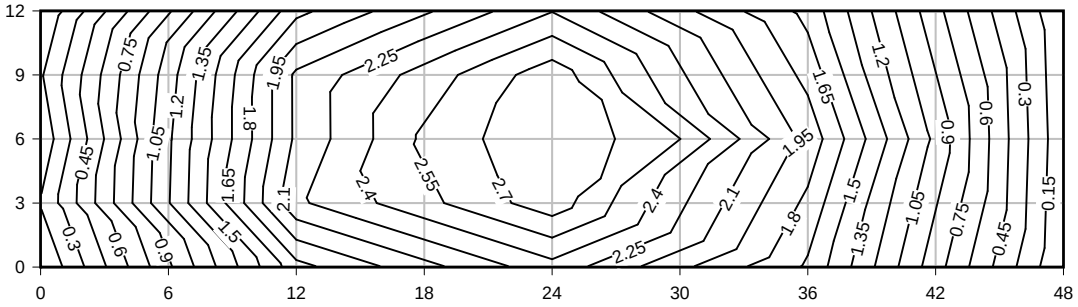

Figure 64: Pitched Roof Displacements at 20 kips (89.0 kN) Total Load

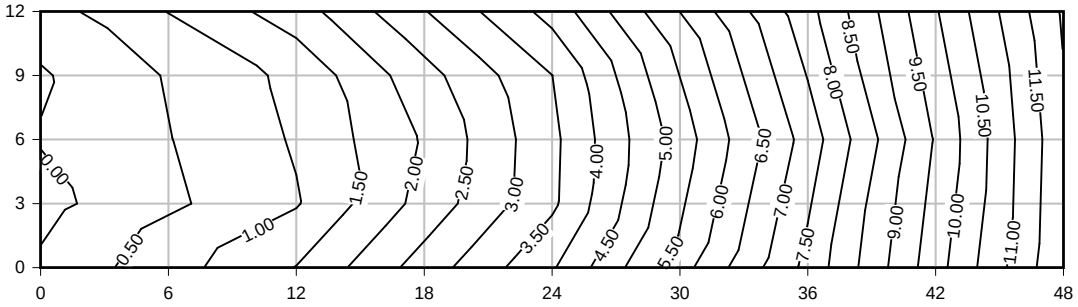

Figure 65: Pitched Roof Elevations at 20 kips (89.0 kN) Total Load

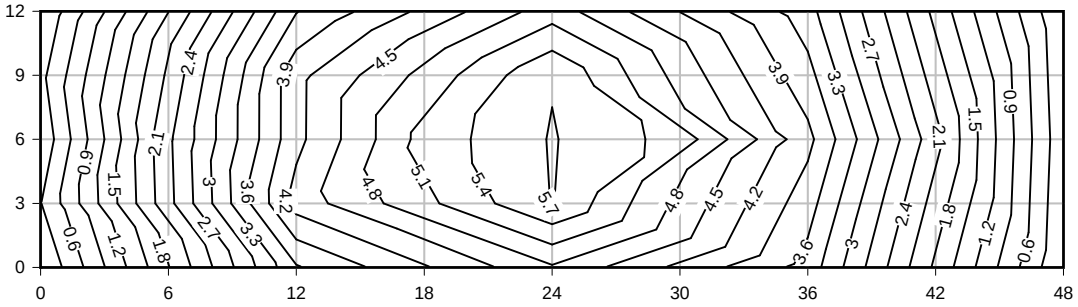

Figure 66: Pitched Roof Displacements at 40 kips (178 kN) Total Load

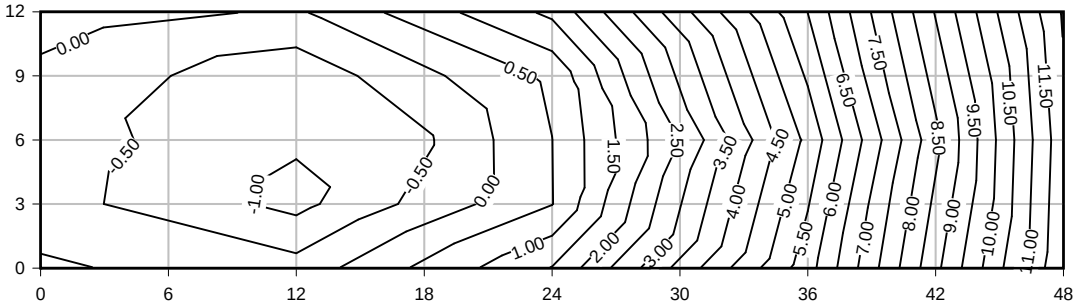

Figure 67: Pitched Roof Elevations at 40 kips (178 kN) Total Load

Support Displacements

The support displacement measurements are a combination of several effects. The largest of these is the bending induced displacement of the support beams under the center joist. In addition, support displacements could have been introduced by the compression of the support system, including the roller bearings, load cells, and column sections bolted to the concrete walls.

The total support displacements were small, but not negligible. For the flat test, the north end support displacement near failure was 0.26 inches (6.60 mm); the south end support displacement was 0.18 inches (4.57 mm). For the pitched test, these values were 0.08 inches (2.03 mm) and 0.10 inches (2.54 mm), respectively.

Decking Deflection

The third component of the three way system was the bending of the decking. It is clear from the plots of the midspan deflections that there is bending in the decking. By comparing the decking deflections with the joist deflections in both tests (though it is more apparent in the pitched test), it is easy to see that the decking deflections are closer to the center joist deflections than the side joist deflections. This indicated that the decking at these locations was below the linearly interpolated location between the joists, indicating decking bending. In the present test specimens, the decking did not fail or appear to alter the failure of the joists. For real design applications, the decking would typically be supported over three spans and tied to the adjacent decking. For these tests, the decking was supported over two spans, and was not tied into additional decking at its ends, reducing beneficial continuity effects.

Water Level

The water level response throughout the tests is shown in figures 68 and 69:

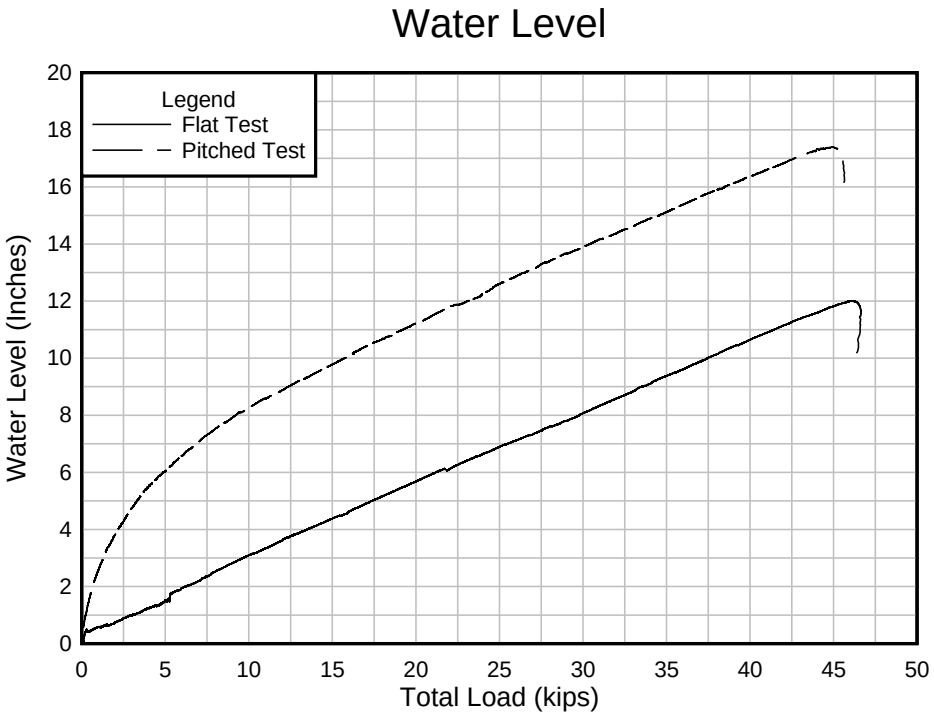

Figure 68: Water Elevation

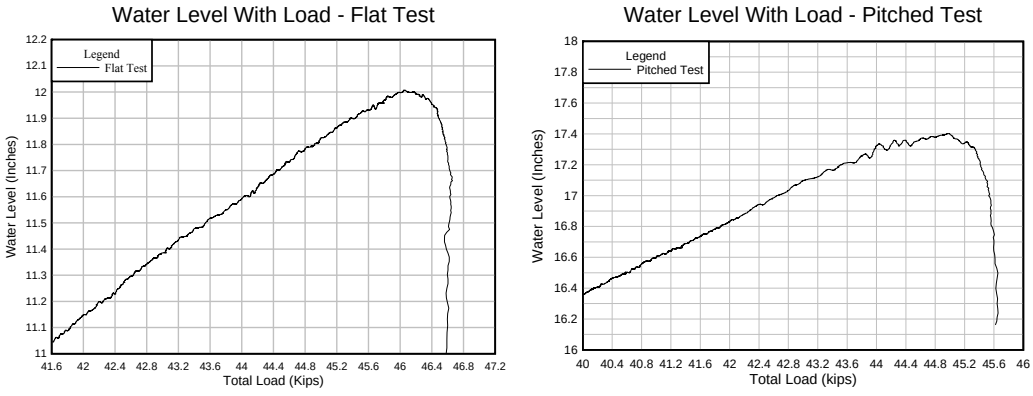

(a) (b)

Figure 69: Water Elevation at Failure, (a) Flat Test (b) Pitched Test

Figures 68 and 69 show that the water level rose most quickly in the early stages of the pitched test because the water was filling a smaller volume concentrated at the parapet wall. As the test progressed, the rate of rise of the water level for an increment of load became parallel to that for the flat test. This occurs near the point where the water has risen above the high point of the roof. At this point, the additional water filled equal areas for

both tests. The water level at the low end of the roof when the water reaches the top would be 12 inches (30.5 cm), while the water level on the flat roof that gives an equivalent load would be half that, meaning the difference between the water levels for equivalent loads once the water reaches the top would be 6 inches (15.2 cm), which is reflected in the separation of the curves. Finally, as seen in figure 69, both roofs reached a maximum point then the water elevation decreased rapidly. This occurred because the deflection of the roofs increased at a rate higher than that of the water being added to fill the roof. When the water began to flow away from the supports, it can be seen that the roof is deforming rapidly and failure is occurring.

Horizontal Motion

The horizontal motion of the end of the roof on roller supports was measured throughout both tests and is shown in figure 70. The data for these measurements shows that the horizontal motion is nonlinear with the total load throughout the test, but still displays the same rapid increase in displacement at collapse. It is interesting to note what happens to the horizontal displacement in the flat test just after 25 kips (111 kN) total load has been applied. The displacement increased quickly then returned to the same rate of change. This is likely attributable to the effects of imperfections in the roller bearings.

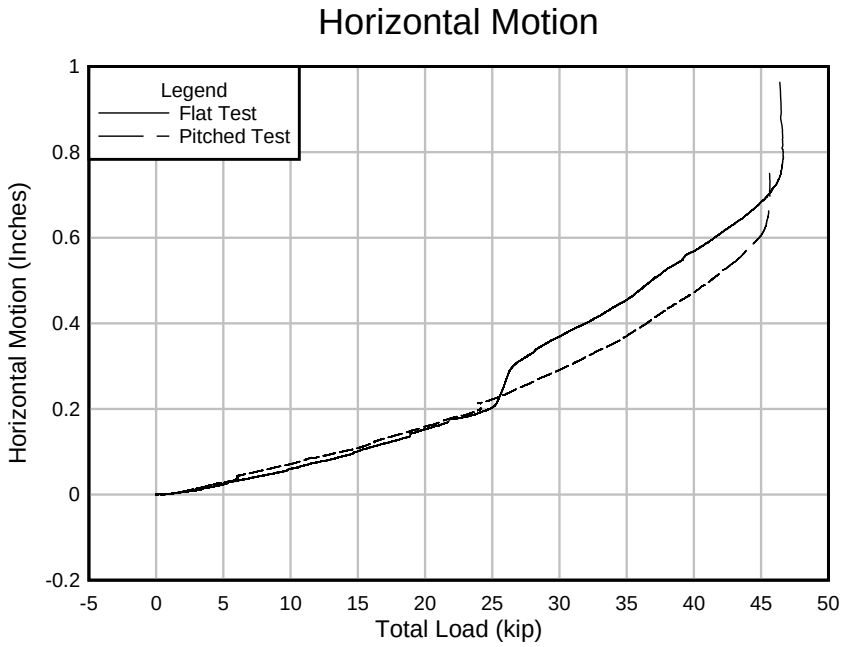

Figure 70: Horizontal Motion

Member Forces

Many of the individual joist members were instrumented with strain gages so that the individual member force components could be determined. The member axial and bending forces were recovered from the strains using the methods outlined in appendix A, with axes and sign conventions as shown in figure 71:

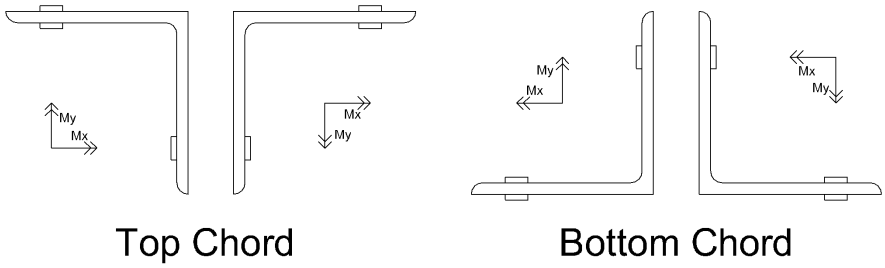

Figure 71: Angle Section Axes

With these conventions, in-plane bending is positive when putting the top of the top chord or the bottom of the bottom chord in compression, and out-of-plane bending is positive

when the angles bend toward each other. Axial forces are defined as positive in tension and negative in compression. For the purposes of this section of the report, top chord, web and bottom chord members in both tests will be referred to by a number that represents their location from the north end of the joists, as shown in figure 72. The top chord members are numbered 1 – 22, the web members are numbered 1 – 33, and the bottom chord members are numbered 1 – 10.

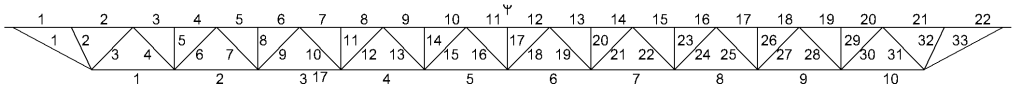

Figure 72: Joist Elevation View

Double Angle Chord Behavior

In the flat test, there were five chord locations where all six strain gages provided data. One of these was lost during testing, so only four locations (one in the top chord, three in the bottom) have complete data for the whole test. The data from the top chord location and the most representative of the three bottom chord locations are shown in figure 73:

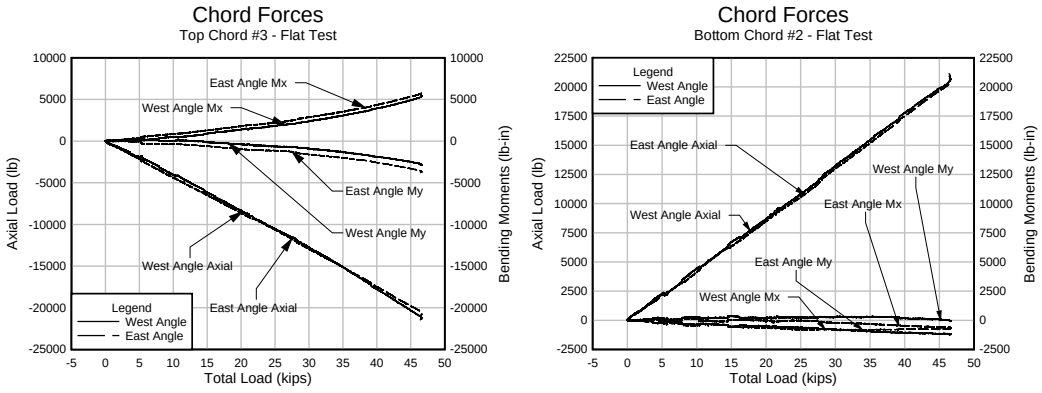

(a) (b)

Figure 73: Flat Test Member Forces, (a) Top Chord (b) Bottom Chord

For the bottom chord element in figure 73(b), the axial tension force becomes large, as expected. The bending forces in the bottom chord angles are very small. For the top chord element, the in-plane bending forces are positive, meaning that the members are bending as expected under the water pressure loads, and both angles exhibit negative out-of-plane bending moments, indicating that the two angle sections are bending away from each other. In both cases, it can be seen that both angles carry forces and moments of similar magnitude except that the out-of-plane bending moments are opposites. Similar data was observed for the pitched roof test. For the pitched test, four top chord locations were instrumented with six strain gages. Only one gave complete data for the duration of the test. There were four bottom chord locations instrumented with two gages, of which two provided good data for the durations of the test. Representative data sets from the pitched test are shown in figure 74:

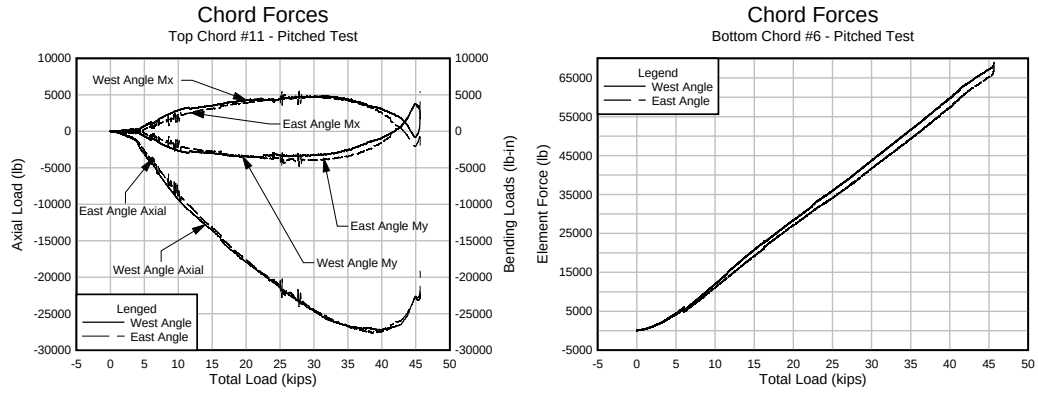

(a) (b)

Figure 74: Pitched Test Member Forces, (a) Top Chord (b) Bottom Chord

The data for this test also showed that the two angle sections in the chord members carry similar force and moment magnitudes. It can be seen in figure 74(a) where the water level rose above top chord #11, as the force and moments increase more quickly at approximately 4 kips (17.8 kN) total load. The reversal of the top chord moments and decrease in axial load observed in figure 74(a) was a result of the element shedding load to

the web members late in the test. For all three top chord locations that provided data throughout two tests, the out-of-plane bending of the angle sections in the chord always forces the angles away from each other. This was reflected in the failure and buckling of these sections.

Web Members

Example web member force responses are shown in figures 75 and 76. Central member numbering is shown in figure 77 for reference:

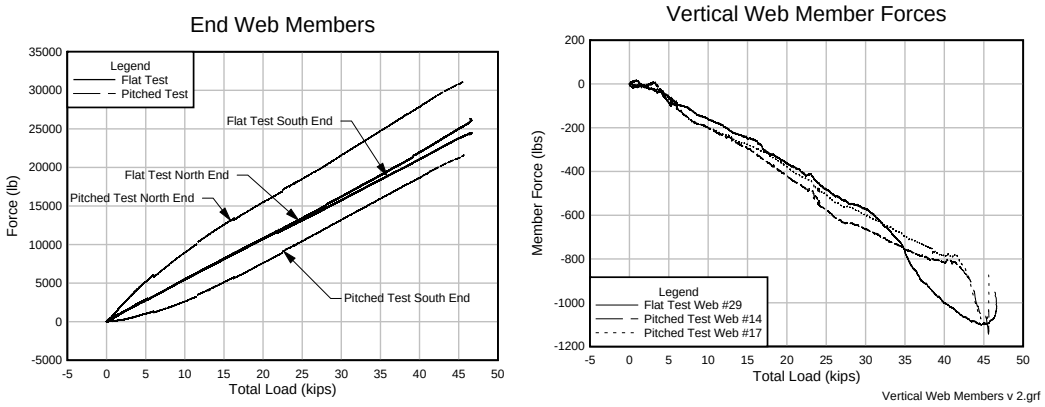

(a) (b)

Figure 75: Web Member Forces, (a) End Members (b) Vertical Members

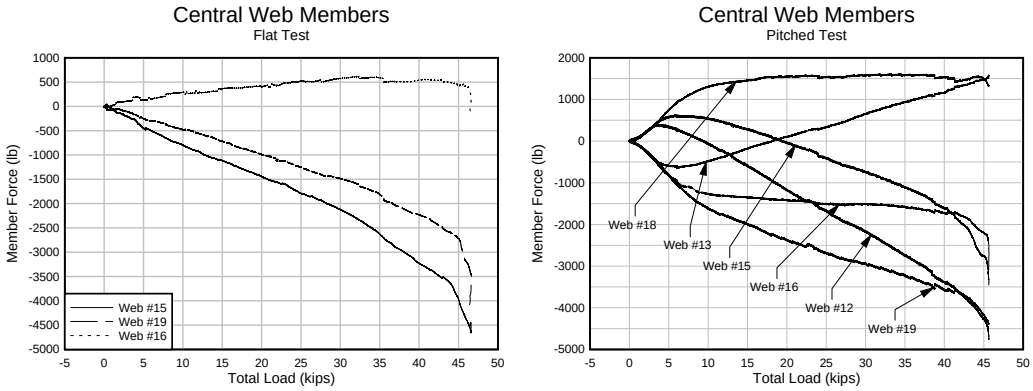

(a) (b)

Figure 76: Central Diagonal Web Member Forces, (a) Flat Test (b) Pitched Test

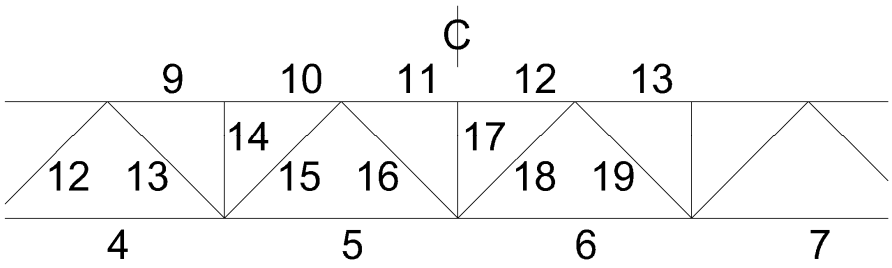

Figure 77: Central Joist Member Numbering

From these there are several interesting points to be made. The vertical members all carry approximately the same amount of compressive force. This is because they are supporting a tributary area of decking through the top chord. The vertical web member forces should be proportional to the water level above them.

From the diagonal web member data, some other interesting points can be made. In the pitched test, it can be seen that the six central diagonal web members start out in sets of three and end up as pairs. In general, the diagonal web members that angle up toward the center of the load are compressive, while those that angle down towards the center of the load are tensile. Because the center of the load moves during the pitched test, some of the elements experienced both tension and compression forces over the course of the test, as seen in figure 76(b). It can also be seen that near the end of the test, the rate of compressive loading in the web elements accelerated. This corresponds to the point where the chord members shed load in figure 74(a) and shows that load is being redistributed through the web to maintain internal equilibrium.

Bottom Chord Strains and Joist Moments

For the pitched test, the entire bottom chord was instrumented with strain gages so the moment profile could be estimated assuming the top and bottom chords carry all moments, the top and bottom chord forces are the same, and that the moment arm is the distance between the centroids of the top and bottom chord members. In the flat test, not all of the bottom chord members were instrumented, but a coarse moment profile could be determined. Shown in figures 78 to 80 are selected moment profiles based on the bottom chord strain data, with ends moments restricted to zero.

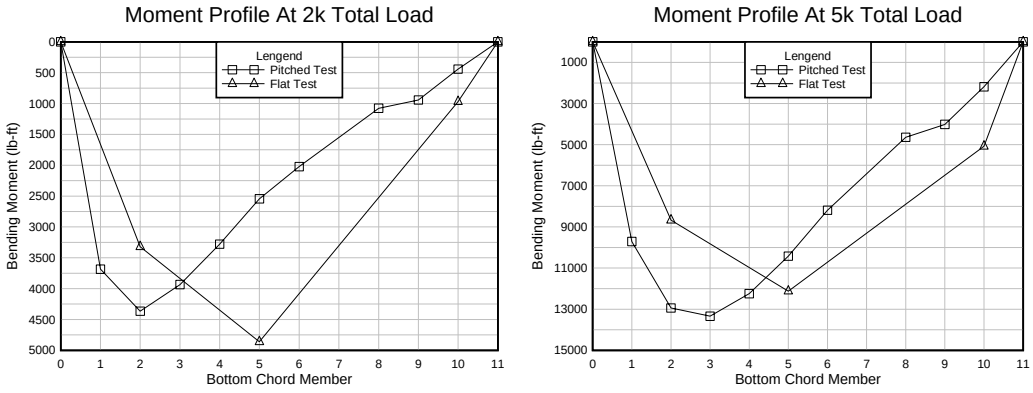

(a) (b)

Figure 78: Moment Profiles, (a) 2 kips (8.90 kN) Total Load (b) 5 kips (22.2 kN) Total Load

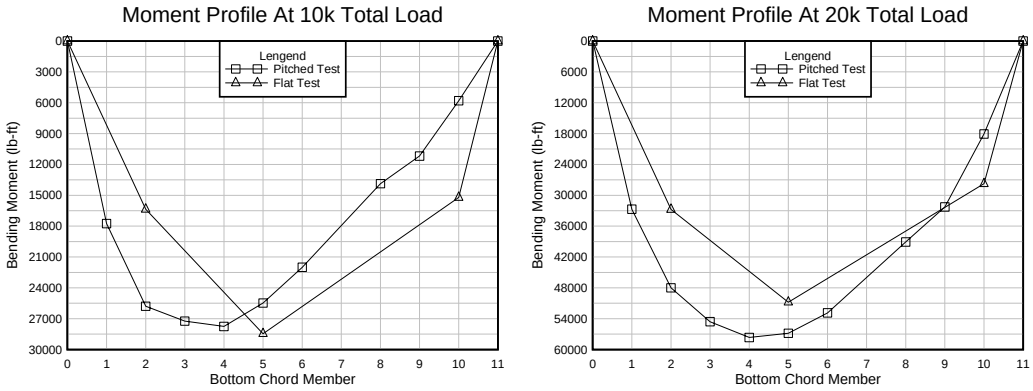

(a) (b)

Figure 79: Moment Profiles, (a) 10 kips (44.5 kN) Total Load (b) 20 kips (89.0 kN) Total Load

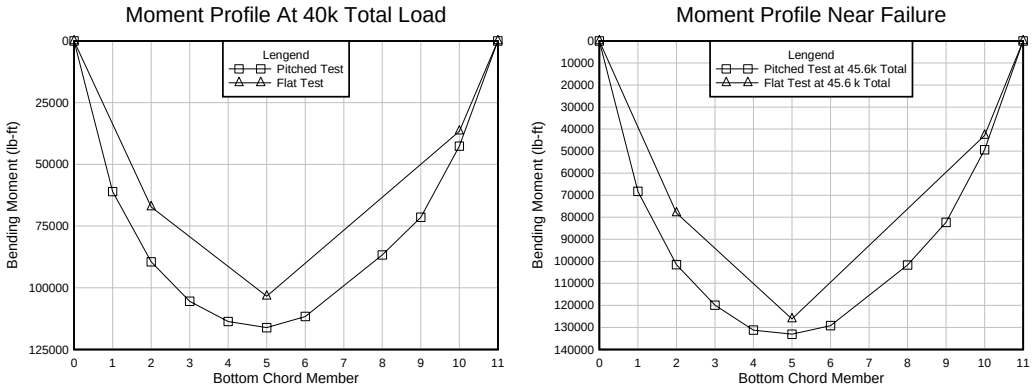

(a) (b)

Figure 80: Joist Moment Profiles, (a) 40 kips (178 kN) Total Load (b) Near Failure

Because the midspan bottom chord strains were known in the flat test, and all of the bottom chord strains were known in the pitched test, the maximum bending moment could be estimated based on the strains for each test. These are shown in figure 81:

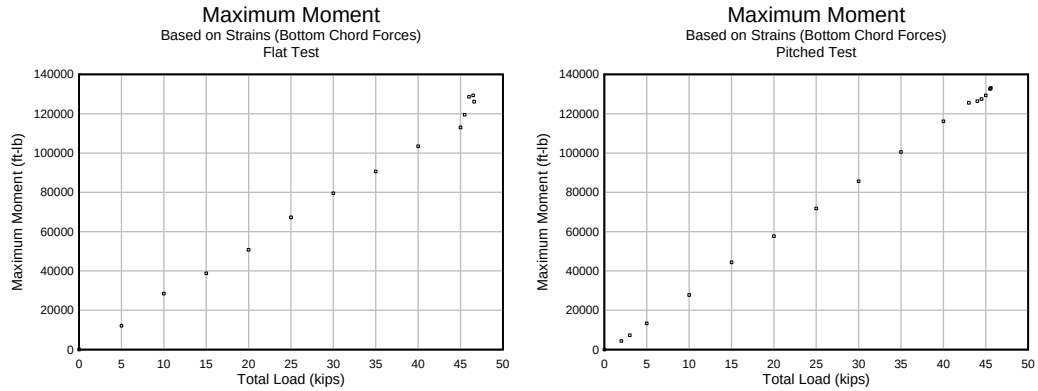

(a) (b)

Figure 81: Maximum Moment Based on Displacements, (a) Flat Test (b) Pitched Test

Failure

Both tests failed in a similar manner. The ultimate failure in both tests was initiated by buckling of the top chord of all three joists. At the onset of failure, the displacements increased rapidly, water flowed toward the center of the roof, the top chords buckled, and the north end of the joists fell off their supports. In both tests, the chord failed in the same location: the centermost section just to the north of the centerline. Photos of the buckled members are provided in figures 82 and 83:

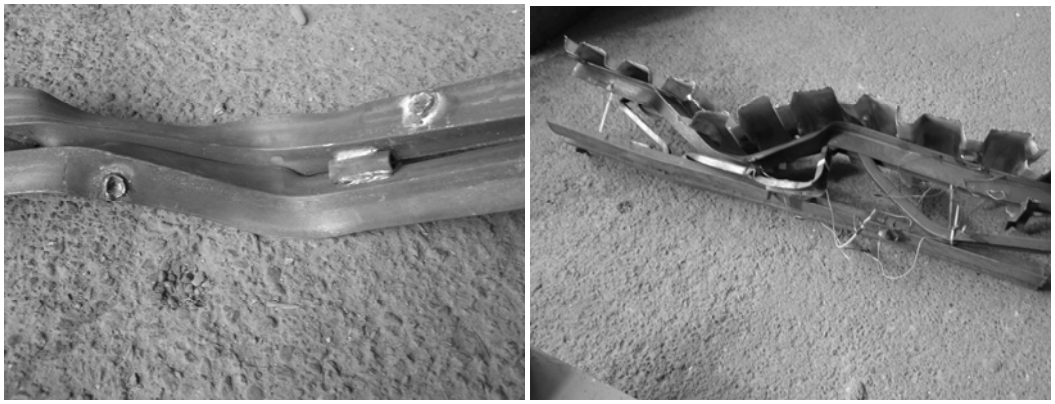

(a) (b)

Figure 82: Failed Members, (a) Flat Test Side Joist (b) Flat Test Center Joist

(a) (b)

Figure 83: Failed Members, (a) Pitched Test Center Joist (b) Flat Test Center Joist

Failure Mode

The buckled double angle members failed under a combination of biaxial bending and axial compression. The minor y-axis bending was small compared to the x-axis bending and was disregarded in the subsequent analysis. The design strengths of the double angle section were computed per Chapter H of the AISC steel design code. The nominal compressive strength is P_c = 57.0 kips (254kN) and the nominal moment capacity is M_c = 40.0 kip-ft (54.2 kN-m). Based on these design strengths and the loads measured during the test, the ratio of load to capacity for this section was calculated throughout the test and is plotted against the total load in figure 84:

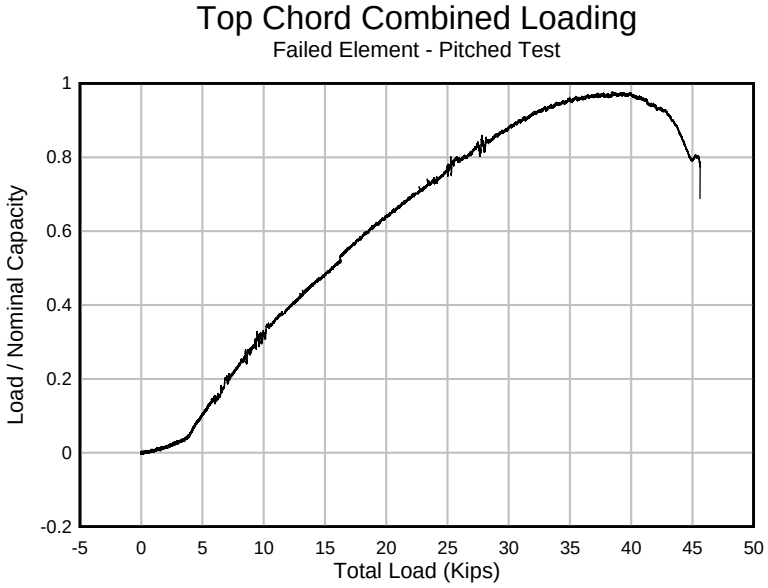

Figure 84: Failed Member Combined Loading

Additional details for these calculations are shown in appendix C. As seen in figure 84, the load to capacity ratio reaches a maximum value of 0.98. Note the early change in the slope of the plot that results from the water level reaching the level of the location of the failed element. Near the end of the test, this member begins to shed load, which has already been shown to be transferred to the web members.

Strain Condition in Top Chord at Failure

By reversing the procedure used to calculate the double angle member forces, the maximum strain in the failed element was calculated. The maximum strain in the top chord angle members occurred in the corners, due to the combined biaxial bending and compression forces. When most heavily loaded, the failed double angle section carried 54.98 kips (244.6 kN) axial compression, 6.83 kip-in (0.772 kN-m) in-plane bending and 3.92 kip-in (0.443 kN-m) out-of-plane bending. Based on these loads and the double angle section properties, the maximum strain in the corners was 1796 με. The yield strength of

this steel section, measured to be 60 ksi (414 MPa), indicates that the member should yield at 2067 με. This data shows that the failed element was elastic through collapse. See appendix A for the calculations in detail.

Decking Strength

As shown in appendix B, the decking was strong enough to support 12.9 inches (32.8 cm) of water. During the pitched test, the water level at the lower end of the roof exceeded 17 inches (43.2 cm). The water at the bottom of the pitched roof was over 14 inches (35.6 cm) deep when the design strength (including the factor of safety) was reached. This illustrates a potential issue for design of the decking on pitched roofs that may be subjected to ponding loads. This decking was chosen to match the strength of the joists for a flat roof. In the case of a pitched roof, however, water builds up more quickly in the lower areas, thus the design could lead to understrength decking at lower elevation areas. This could be remedied either by designing decking in a tiered system, providing stronger decking where needed, or by designing all the decking for the loads at the lowest elevation.

Lasting Displacement Effects

During the flat roof test, loading was suspended to attempt to stop water leakage by adding marine grease around the membrane punctures that allowed the displacement sensor attachment. As personnel walked on the roof to do this, additional deflection of the roof and horizontal motion was observed, and when the additional load was removed from the roof, some additional deformations, while small, remained. The data for the midspan

displacement of the center joist and horizontal motion were representative of the motion of the roof, and are shown in figure 85 for the first eight hours of the overnight data.

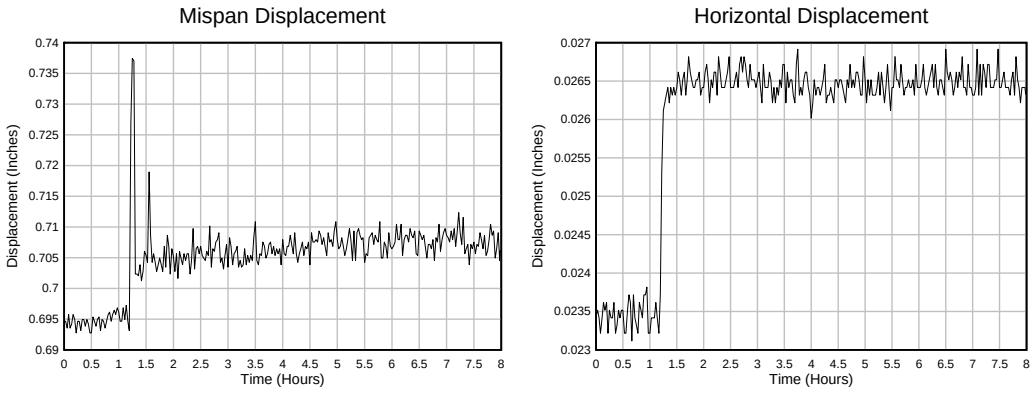

(a) (b)

Figure 85: Lasting Displacement Effects, (a) Midspan (b) Horizontal

It can be seen that the difference in the vertical displacement was approximately 0.015 inches (.381 mm), and in the horizontal displacement was about 0.003 inches (0.076 mm). These resulted from an additional live load of approximately 350 lbs (1.56kN). This is important because it shows that if additional loads are applied to a roof with ponded water, the additional deformations produced do not simply go away when the additional loads do. If a roof with ponded water were also subjected to wind loads, for example, wind pressure induced deformations will cause additional, lasting displacement effects.

Shear Deformations

The AISC specifications require a 15% reduction in the moment of inertia of trusses and steel joists to account for shear deformations. The data collected in this test allowed for the effect of shear deformations to be estimated in two independent ways. First, the bending deformations were calculated from the load profile given by the displacement data using the reduced moment of inertia. These deformations and the measured values were then

compared to estimate the impact of shear deformations. Second, shear deformations were evaluated directly from the diagonal web member strains.

Shear Deformations Based on Displacement Data

The load on the roof can be estimated throughout the tests based on the displacements and the water level data. Using this data, it was possible to reconstruct the load profile, the reactions and shears, the bending moments and eventually the displaced shape. This calculated displaced shape was then checked against the same displacement measurements to determine how well they matched. The data is summarized in tables 7 and 8:

Table 7 Calculated and Measured Displacements, Flat Test:

Total Load	Calc. (in)	Meas. (in)	Diff. (in)	%
5k	0.781	0.662	-0.120	-18.1
10k	1.604	1.363	-0.241	-17.7
15k	2.310	2.069	-0.241	-11.6
20k	3.021	2.777	-0.244	-8.8
25k	3.684	3.440	-0.244	-7.1
30k	4.385	4.248	-0.136	-3.2
35k	5.117	5.012	-0.105	-2.1
40k	5.856	5.848	-0.008	-0.1
45k	6.594	6.822	0.228	3.3

Table 8: Calculated and Measured Displacements, Pitched Test:

Total Load	Calc. (in)	Meas. (in)	Diff. (in)	%
5k	0.521	0.564	0.043	7.6
10k	1.330	1.335	0.005	0.4
15k	2.082	2.096	0.015	0.7
20k	2.860	2.842	-0.018	-0.6
25k	3.586	3.494	-0.092	-2.6
30k	4.296	4.198	-0.098	-2.3
35k	4.996	4.936	-0.060	-1.2
40k	5.715	5.722	0.007	0.1
43k	6.161	6.267	0.106	1.7

From the data in tables 7 and 8, it can be seen that there are significant deviations in the two data sets early in the tests, as the load is small. As the load increases, however, the two data sets match well, typically to within two or three percent. Data from late in the test is omitted, as nonlinearities affect the results. This data shows that for much of the test, the fifteen percent reduction in the moment of inertia is a good estimate for the shear component of the total deformation.

Shear Deformations Based on Strains

Because the strains in the diagonal web members are known throughout the test, the shear displacements can be calculated directly from the data. See appendix D for details of these calculations. The vertical panel deformations at the end of each test are shown in figure 86:

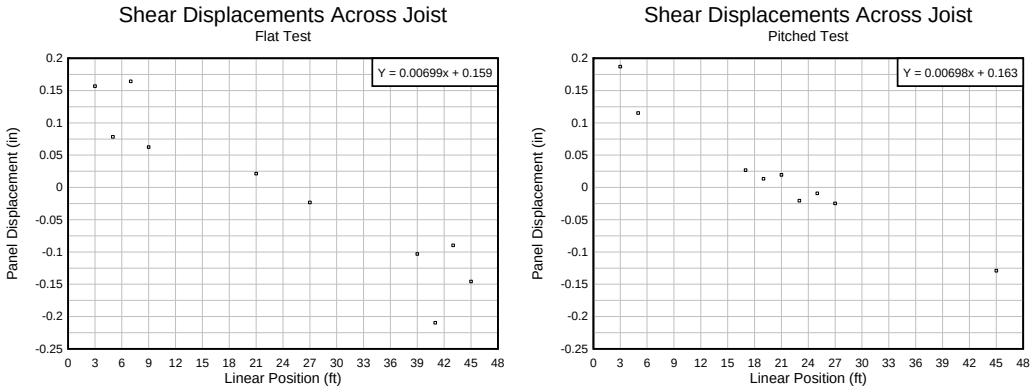

(a) (b)

Figure 86: Shear Displacements across Joist, (a) Flat Test (b) Pitched Test

Based on figure 86, a best fit linear function was found that allowed the shear deformations in all panels to be determined. By summing these, the contribution of the shear deformations to the total midspan displacement was calculated. This process was repeated for several total load steps (later in the pitched test to avoid large load imbalance early in the test) and it was found that the shear deformations make up 11.2% of the total

displacement in the flat test and 13.8% in the pitched test. The larger contribution in the pitched test can be attributed to the load imbalance which produces higher shear deformations at low roof elevations. This data indicates that the 15% estimate to account for shear deformations appears reasonable.

Comparative Analysis

End Reactions

At the supports of the center joist in each test, the vertical end reaction was measured by the load cells. These forces are opposed only by the small vertical load (shear) carried in the top chord to the support, and by the large axial force in the end diagonal. The data for these two forces for both ends in both tests were compared, and it was found that in all four cases, their relationship was linear, except the south end early in the pitched test. For the flat test, the ratios of the local member forces to the support reactions were 2.25 at the north end and 2.16 at the south end. For the pitched test, the ratios were 2.42 and 2.20, respectively. Based on the member geometry, the force in the end diagonal should be 2.24 times the support reaction. The pitched roof and the rotations of the joist at the supports changed the geometry slightly, but the ratios of the forces in all four cases are all fairly close to those predicted.

Midspan Displacements

The midspan displacements were calculated at varying water levels using the analysis program described in the numerical analysis chapter and the joist stiffness modified by

15% for shear displacements. The predicted displacements were compared to the measured midspan displacement values in figure 87:

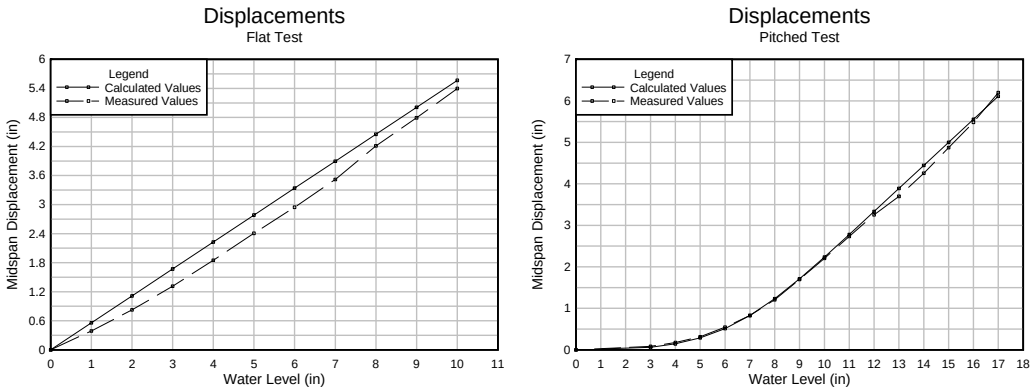

(a) (b)

Figure 87: Displacement Comparisons, (a) Flat Test (b) Pitched Test

From figure 87, the predicted displacements were reasonably close, especially in the pitched case.

Total Load

The total load was measured over the course of the test in multiple ways. The flowmeter was intended to give a direct measurement of the total water volume, thus load, but due to water leakage, was not a reliable measure. The load cells allowed measurement of the total water by weight. A third measurement of the total load is the volume of the water calculated from a combination of the deflected shape and the water level. Using the displacement data from the center joist to determine the load profile, the total weight of water was calculated and plotted with the total weight of water from the load cells in figure 88:

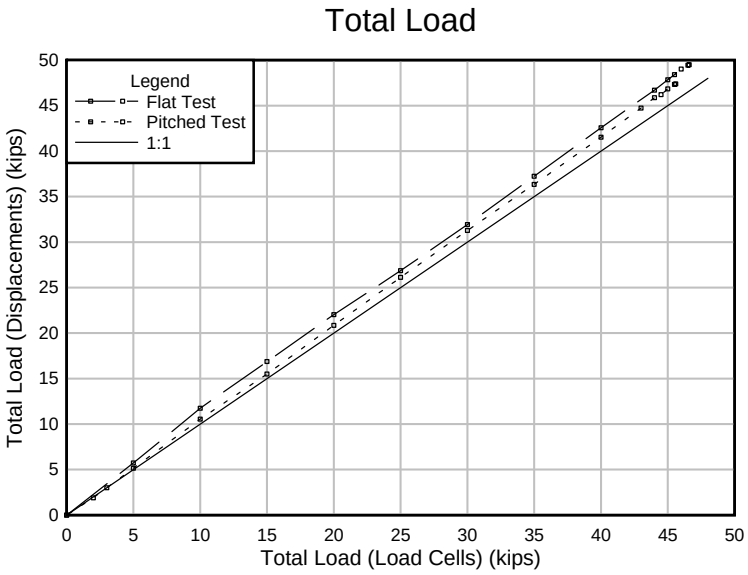

Figure 88: Total Load Calculation Comparison

For both tests, the displacements predict slightly higher load than that measured with the load cells. The slight over-estimation provided from the displacements is a result of the choice of the center joist because it had slightly larger displacements than the edge joists.

Design Applications

Two effects amplify the maximum joist moment when ponding is involved. First, the load is heavier in the center due to the roof deflection; second, the roof deflections allow a greater amount of water to collect if the basic premise is that water is available to fill the roof to a certain height. The results of these effects, calculated from both the load profile taken from the displacement data and the strain data from the bottom chords can be seen in figure 89:

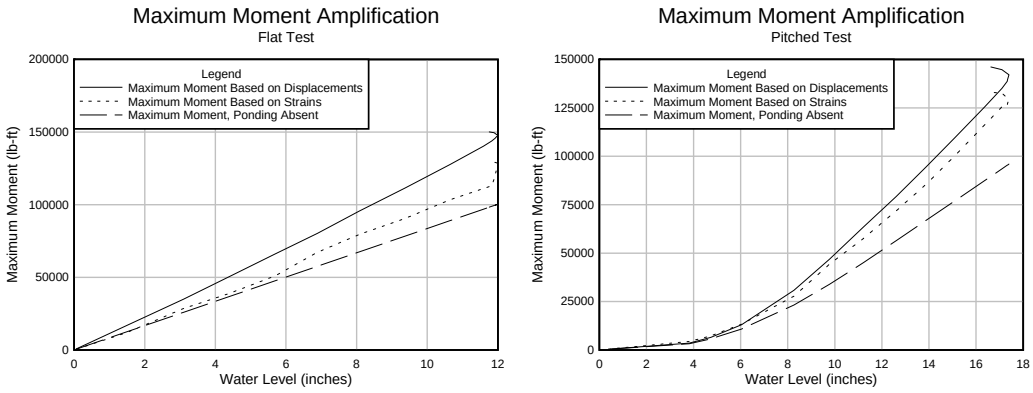

(a) (b)

Figure 89: Maximum Moment Amplification, (a) Flat Test (b) Pitched Test

For both tests, the moment amplification factor due to ponding was 1.45 based on the displacement data. For the flat test, the amplification factor is 1.18 and for the pitched test it is 1.34 when the strain data is used. The data from the displacements show that the moment due to ponding diverged very early from the no-ponding results, while the strain data showed that it took longer for the second order effects to become noticeable. For both tests, the moments calculated from displacement data are larger than the moments calculated from the strain data, in the flat case by a factor of 1.21, in the pitched case by a factor of 1.10.

Another way of comparing the results of these tests to the design process is to show load-deformation response along with predicted results based on the specified moment of inertia, modulus of elasticity and design strengths of the joists. These results are illustrated in figure 90:

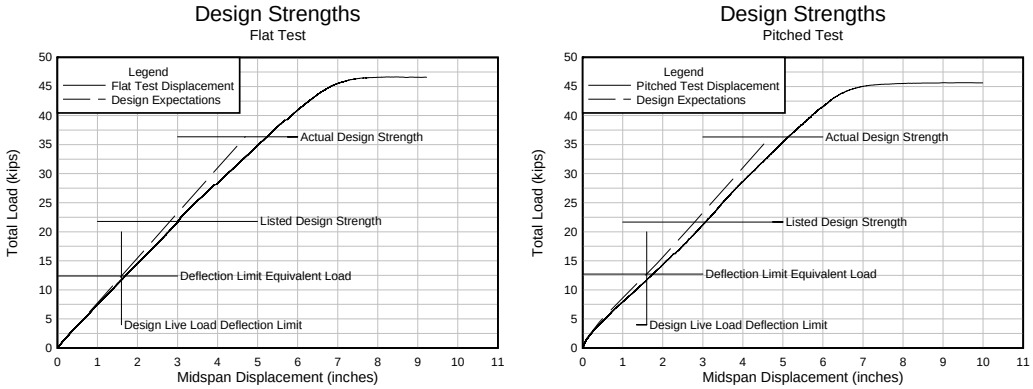

(a) (b)

Figure 90: Design Strength Comparisons, (a) Flat Test (b) Pitched Test

For the flat test, the design strengths were based on the prescribed values established by the manufacturers, while for the pitched case they were converted from the flat case based on the maximum resulting moment. The values are very close for both cases. From figure 90, it is clear that for both tests, the joists deflect more with ponding load than anticipated by the design parameters. The joist response remained approximately linear beyond the projected strength (including the 1.67 factor of safety) in both tests.

CONCLUSIONS

Conclusions and Recommendations

Research on ponding behavior and collapse was performed. Analytical models were created and used to numerically investigate ponding stability. Additionally, two full-scale steel joist roof systems were designed, built, and tested to failure using water loads to investigate the ponding response. The experimental roofs did not exhibit ponding instability, but did show ponding load amplification effects and eventual collapse under ponding water. Based on the experimental and analytical results, the following conclusions are drawn and recommendations and suggestions for future work are presented:

Analytical Conclusions

- The original ponding stability criteria published by Haussler was confirmed
- Increased roof slope does not improve ponding stability until the roof pitch gets much steeper than the current AISC ¼ on 12 pitch requirement.

Experimental Conclusions

- Early in the experiments, the behavior of the two roof systems were different based on the initial geometries. After significant ponding load was added, however, the responses became similar in terms of moment profiles and displaced shapes.
- Nearly all response quantities appear to be linearly related to the total load on the roof until it is near collapse. The horizontal motion of the roller supported end of

the roof, however, exhibited a nonlinear response relative to the total load throughout both experiments.

- Near the point of collapse in both experiments, the water elevation starts to decline as the volume created by the displaced shape exceeded the volume provided by adding new water to the system.
- The double angle sections that make up the top chords carry biaxial bending and axial loads. The only significant loads carried in the bottom chord double angles are tension forces. The magnitudes of these components were similar in paired angle sections.
- Of the biaxial bending forces in the top chord, the in-plane bending is the larger of the two moments resulting from the loads applied by the decking on the top of the joist. The out-of-plane bending is smaller, and the direction of the moment tends to move the angle sections away from each other.
- In both experiments, the failure mode was buckling of the joist top chord members due to combined compression and bending forces that resulted in gross changes in geometry and increased loads due to water flow.
- The maximum water pressure on the decking occurred at midspan in the flat test and near the third point in the pitched test. These local pressures are significantly larger than the pressure equivalent to the uniformly loaded joist strength.
- If an additional load is temporarily superimposed over water loads in a ponding situation, the displaced shape is permanently altered until the water is removed. The additional load leads to a change in the distribution of water loads, which creates the lasting displacement effects. This finding indicates there are possible

deleterious effects of wind pressure surcharges that could occur concurrently with water loading.

- The factor by which the ponding effect amplified the maximum first order joist moment was calculated most reliably from the displacement data. In both roof tests, the amplification factor was 1.45.
- The current practice of using a 15% reduction in the joist moment of inertia to account for shear deformations was reasonable and appeared slightly conservative when compared with experimentally measured responses.
- For real in-situ cases, the large amount of water available in the area surrounding the collapsing section would further accelerate failure, resulting in local rather than global roof collapse.

Recommendations

- Recognize that the code requirement of a 1: 48 pitch to prevent ponding does not ensure roof stability or increase load capacity.
- Current design code treatment of ponding load effects requires only sufficient plumbing and a slight pitch. This may not adequately protect against ponding for all roof systems. A foolproof approach would be to design the roof to support ponding loads up to the top of the parapet walls.
- Steel decking should be designed to hold the maximum water load, which will be larger than the pressure equivalent to the uniformly loaded joists' strength.

Areas for Further Research

There are additional research needs to improve understanding of roof behavior and design under ponding loads. Presently, much of the research is focused toward finite element modeling and development of analytical tools. There are also a number of opportunities for further experimental research.

Analytical Tools

The analysis program developed for this thesis works for simple conditions. A short list of possibly useful additions is provided here. An updated program could:

- Analyze truss deflections explicitly rather than use beam theory
- Include serviceability checks
- Allow for variations in loads (Point loads, two sets of loads, uplift etc.)
- Allow for initial imperfections
- Include material nonlinearity
- Account for multi-directional roofing systems
- Allow varied support conditions and include catenary action
- Explicitly account for shear deformation contributions to overall deflection
- Calculate a rate of convergence for stable systems to determine a safety factor

One other item that needs more work in the future is the determination of a general equation for the stability condition in the pitched case. Results from the program have been presented for this, but no closed form analytical solution has been found.

Experimental Work

There are several topics related to the ponding effect that require future research, including:

- Ponding effects on different green roof designs
- Ponding effects in water insulating systems on roofs
- The seismic response of green roofs with ponding loads
- Ponding response under a combination of rain and snow loads
- The effect of different support conditions and catenary action in ponding response
- Wind effects on the ponding response

BIBLIOGRAPHY

"A dash of Cold Water." *Engineering News Record*, June 4, 1981

Adams, Staley F., Chinn, James, and Mansouri, Abdulwahab H. "Ponding of Liquids on Flat Roofs." *Journal of the Structural Division.* (May, 1969): 797-807.

Ahmadi, Goodarz, and Glockner, Peter C. "Effect of Imperfection on Ponding Instability." *Journal of Engineering Mechanics*. (August, 1984): 1167-1173.

American Institute of Steel Construction. Manual of Steel Construction. USA: AISC, 2005.

American Society of Civil Engineers and the Structural Engineering Institute. Minimum Design Loads for Buildings and Other Structures. Reston, Virginia: American Society of Civil Engineers, 2005.

Avent, R. Richard. "Deflection and Ponding of Steel Joists." *Journal of the Structural Division.* (July, 1976): 1399-1410.

Avent, R. Richard, and Stewart, William G. "Rainwater Ponding on Beam Girder Roof Systems." *Journal of the Structural Division.* (September, 1975): 1913-1927.

Avrahami, Yair, Doytsher, Yerach, and Raizman, Yuri. "Semi-Automatic Approach Toward Mapping of Flat-Roofed Buildings Within a Non-Stereoscopic Environment." *The Photogrammetric Record.* (March, 2007): 53-74.

"Background." <http://heron.tudelft.nl/heron.html> (March, 2009)

Bergeron, Ananda, Green, Perry S., and Sputo, Thomas. "Improved Ponding Criteria for Cantilever Framing Systems." Presented: Structures Congress and Exposition, Nashville Tennessee. Archived: ASCE. (2004)

Blaauwendraad, Johan. "Modified Method for Rainwater Ponding on Flat Roofs." *Journal of Constructional Steel Research.* (March, 2009): 559-568

Blaauwendraad, Johan. "Ponding on Light-Weight Flat Roofs: Strength and Stability." *Engineering Structures.* (2007): 832-849.

Bohannan, Billy, and Kuenzi, Edward W. "Increases in Deflection and Stresses Caused by Ponding of Water on Roofs." *Forest Products Journal.* (September, 1964): 421-424.

Burgett, Lewis B. "Fast Check for Ponding." *AISC Engineering Journal.* (1973): 26-28.

Carter, Charles, and Zuo, Jiahong. "Ponding Calculations in LRFD and ASD." *AISC Engineering Journal.* (1999): 138-141.

Chang, Bin, and Chong, Ken. “Minimum Slope on Flat Roof Systems.” *Forest Products Society.* (July, 1977): 35-37.

Chang, Bin, and Chong, Ken. “Ponding of Sloped Roof Systems.” Presented: World Congress on Space Enclosures. Archived: Concordia University, Montreal. (July, 1976)

Chao, Ta. “Stability of Trusses Subjected to Ponding Loads.” *ASCE Journal of the Structural Division.* (June, 1973): 1327-1332.

Chinn, James “Failure of Simply-Supported Flat Roofs by Ponding of Rain.” *AISC Engineering Journal.* (April, 1965): 38-41.

Chinn, James, and Mansouri, A.H. “Generalization of a Single Span Beam for Ponding.” *Journal of Engineering Sciences.* (1980): 1-9.

Colombi, Pierluigi. “The Ponding Problem on Flat Steel Roof Grids.” *Journal of Constructional Steel Research.* (November, 2005): 647-655.

Colombi, Pierluigi, and Urbano, Carlo. “Ponding Effect on Nearly Flat Roofs of Industrial or Commercial Single Story Buildings.” Presented: Second European Conference on Steel Structures, Prague. Archived: Prague Technical University. (May 1999)

Derks, J., Locht, J, and Schouten, A. "Evaluation of Ponding Analysis Methods Using 3-D Finite Element Modelling." *Heron.* (2006, Volume 51): 183-200

Factory Mutual Insurance. "Public Data Sheet 1-54." (September, 2006)

Fijneman, H.J., Snijder, H.H., andVan Herwijnen, F. "Structural Design for Ponding of Rainwater on Roof Structures." *Heron.* (2006, Volume 51): 115-150

Fisher, James and West, Michael. "Steel Design Guide 3: Serviceability Design Considerations for Steel Buildings, Second Edition." USA: AISC, 2004

Folz, Bryan, and Foschi, Ricardo O. "Reliability of Timber Beams Subjected to Ponding." *Journal of Structural Engineering.* (February, 1990): 490-499.

Fridley, K.J. and Rosowsky, D.V. "Reliability Based Design of Wood Members Subject to Ponding." *Journal of Structural Engineering*. (November, 1993): 3326-3343.

Haussler, Robert W. "Roof Deflection Caused by Rainwater Pools." *Civil Engineering.* (October, 1962): 58-59.

International Code Council. International Building Code. USA: ICC, 2006.

Marino, Frank J. "Ponding of Two-Way Roof Systems." *AISC Engineering Journal.* (July, 1966): 93-100.

Kaminetzky, Dov. Design and Construction Failures. New York, New York: McGraw-Hill, 1991.

Katsikadelis, John T. and Nerantzaki, Maria S. "Ponding on Floating Membranes." *Engineering Analysis with Boundary Elements.* (June, 2003): 589-596.

Milbradt, K. P. "Discussion of Ponding Calculations in LRFD and ASD" *AISC Engineering Journal.* (2000): 167-169.

Moody, Martin L. and Salama, Ahmed E. "Response of Nonlinear Beams and Plates to Ponding." *Engineering Mechanics Division* (February, 1969): 195-209.

Moody, Martin L. and Salama, Ahmed E. "Analysis of Beams and Plates for Ponding Loads." *Journal of the Structural Division* (February, 1967): 109-126.

Ruddy, John L. "Ponding of Concrete Deck Floors." *Modern Steel Construction.* (September, 2005): 35-42.

Sawyer, Donald A. "Ponding of Rainwater on Flexible Roof Systems." *Journal of the Structural Division*. (February, 1967): 127-147.

Sawyer, Donald. "Roof Structure Roof Drainage Interaction." *Journal of the Structural Division.* (January, 1968): 175-199.

Steel Joist Institute. Standard Specifications. USA: SJI, 2005.

Steel Joist Institute. "Technical Digest 3: Structural Design of Steel Joist Roofs to Resist Ponding Loads." (May, 1971)

Steel Joist Institute and Steel Deck Institute. "Exploring Building Design with Steel Joists, Joist Girders, and Steel Deck." (April, 2008)

"The Risk of Roof Collapse." <http://www.senteck.com/need/> (May, 2008)

Urbano, Carlo. "Ponding Effect on Nearly Flat Roofs." *Structural Engineering International.* (2000): 39-43.

Vambersky, J. "Roof Failures Due to Ponding - A Symptom of Underestimated Development." *Heron.* (2006, Volume 51): 83-96

APPENDICES

Appendix A: Chord Member Forces

Force Recovery from Multiple Strain Gages

The top and bottom chords of the center joist were instrumented in several locations in both tests. The top chord members looked like this:

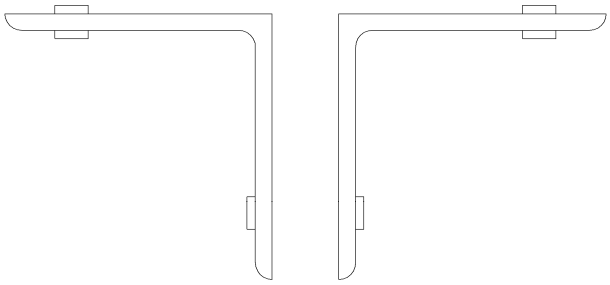

Figure 1: Double Angle Cross Section

The bottom chords members were similar: they were inverted, so figure 1 is upside down, and they were made of slightly thinner angle sections. The sizes of the sections will be reflected in the calculations. The protrusions from the sections in the figure 1 represent the locations of the six strain gages. Six strain gages were used for each segment of the truss in the flat test that was expected to have axial and bending forces. Each angle requires three strain gages, as each could have independent measures of axial forces and bending forces in two directions. Six strain gages per location allow recovery of all three of these components for each angle section. The results of the flat test showed that the bottom chord really only experiences tension, so in the pitched test, only the top chord locations were instrumented with six gages.

Figure 2 will facilitate the coming calculations that will allow recovery of element forces from individual strain measurements:

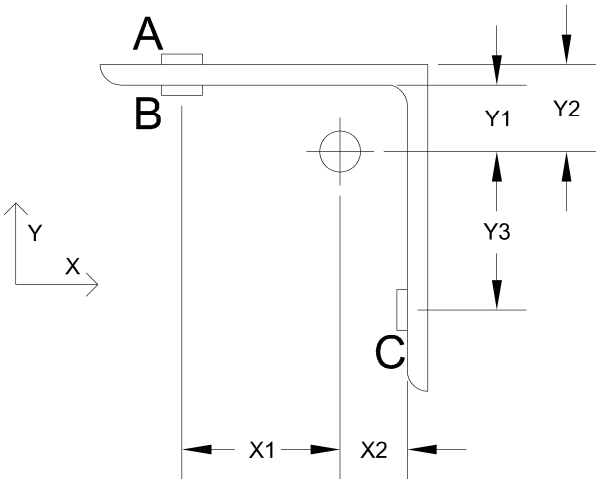

Figure 2: Chord Angle Dimensions

Here, the locations of the gages are defined by their position on the element relative to its center of mass. For the physical testing, all strain gages were placed on the same faces, as shown in both figure 1 and figure 2, at a position exactly one half inch (1.27 cm) from the end of the angle section.

Section properties were provided by the manufacturer for the majority of the sections used in building the joists. The only section properties that were used that were not provided were those for the end web members, which have a circular cross section, and the moment of inertia about the weak axis of the joist. These were calculated by hand, and the provided values were checked by hand calculations. The angle section properties are for the double angle section that makes up the chord members. For these calculations, values for one angle alone were used. The relevant sections properties are as follows:

Center Joist:

1. Top chord:

- Angle Size: 2L 2x2x0.166 (2L 51x51x4.2)
- A = 1.272 in^2 (8.21 cm^2)
- I_x = 0.490 in^4 (118 mm^4)
- I_y = 1.924 in^4 (462 mm^4)
- R_x = 0.620 in (1.57 cm)
- y_c = 0.562 in (1.43 cm)

2. Bottom Chord:

- Angle Size: 2L 2x2x0.142 (2L 51x51x3.6)
- A = 1.096 in^2 (7.07 cm^2)
- I_x = 0.426 in^4 (102 mm^4)
- R_x= 0.624 in (1.58 cm)
- y_c = 0.552 in (1.40 cm)

The problem is defined:

Define: Tension positive, moment positive by right hand rule

Known: Modulus of Elasticity, Section area, moment of inertia, strains at A, B, C.

Find: Axial force, bending moments about X and Y axis.

Step One: By Hooke's Law, Stresses are known at A, B, C:

$$\sigma_n = E\varepsilon_n \tag{7.1}$$

Step Two: Determine expressions for stresses in terms of the forces:

$$\sigma_A = \frac{P}{A} - \frac{M_x Y_2}{I} - \frac{M_y X_1}{I} \tag{7.2}$$

$$\sigma_B = \frac{P}{A} - \frac{M_x Y_1}{I} - \frac{M_y X_1}{I} \tag{7.3}$$

$$\sigma_C = \frac{P}{A} + \frac{M_x Y_3}{I} + \frac{M_y X_2}{I} \tag{7.4}$$

Step Three: Write this in matrix form:

$$\begin{bmatrix} \sigma_A \\ \sigma_B \\ \sigma_C \end{bmatrix} = \begin{bmatrix} \frac{1}{A} & -\frac{Y_2}{I} & -\frac{X_1}{I} \\ \frac{1}{A} & -\frac{Y_1}{I} & -\frac{X_1}{I} \\ \frac{1}{A} & \frac{Y_3}{I} & \frac{X_2}{I} \end{bmatrix} \begin{bmatrix} P \\ M_x \\ M_Y \end{bmatrix} \tag{7.5}$$

Step four: Invert the matrix, substitute section property values, and write in three equations:

For the bottom chord:

$$P = 2.075E\varepsilon_A - 1.91E\varepsilon_B + 0.3825E\varepsilon_C \tag{7.6}$$

$$M_X = -1.499E\varepsilon_A + 1.499E\varepsilon_B \tag{7.7}$$

$$M_Y = 1.499E\varepsilon_A - 1.656E\varepsilon_B + 0.1568E\varepsilon_C \tag{7.8}$$

For the top chord:

$$P = 2.076E\varepsilon_A - 1.888E\varepsilon_B + 0.447E\varepsilon_C \tag{7.9}$$

$$M_X = -1.475E\varepsilon_A + 1.475E\varepsilon_B \tag{7.10}$$

$$M_Y = 1.475E\varepsilon_A - 1.659E\varepsilon_B + 0.184E\varepsilon_C \tag{7.11}$$

Notice that the numbers in the equations are similar for the different chords, as the difference in the thickness is small. These equations were used in the data reduction to determine the element forces throughout the test from the strains as collected by the strain

gages. In doing so, it is important to note the units used. Strain gage data was collected in microstrain, the section properties used in these conversions have units in inches and the modulus of elasticity of steel is taken as 29,000 ksi (200 GPa). These units will be used in the data reduction.

Maximum Strain from Member Forces

The maximum strain in the top chord was determined from the maximum loads using equations 7.12 and 7.13.

$$\sigma = \frac{54.98}{1.272} + \frac{6.83(0.562)}{0.490} + \frac{3.92(0.5)}{1.924} = 52.1 \tag{7.12}$$

$$\varepsilon = \frac{52.1}{29 * 10^3} = 0.001796 \tag{7.13}$$

Appendix B: Design Calculation Checks

In this section, every structural element involved in the test will be checked to ensure that everything can support more load than the center joist. It would be unfortunate if something other than the center joist failed first and little data was gathered regarding ponding or the failure was able to be collected. For these calculations, the joist design factor of safety (1.67) will be taken into account.

Check the strength of McGill CYR 2½ inch (6.35 cm) Roller Bearings for Strength

These bearings serve as the rollers of the pin-roller system, and as the rollers held in the clevises at the termination of bridging elements. The greatest load occurs at the end of the center joist:

$$R = \frac{1}{2}\left(211\,plf * 48'\right)\left(1.67\right) = 8457lb \tag{7.14}$$

As there are two rollers under each support, each roller must be able to hold 4228 lbs (18.8 kN). From McGill literature, these roller bearings are rated at 32900 lb (146 kN) static, 11720 lb (52.1 kN) dynamic loads. The bearings should therefore be fine under these loads.

Check Georgia Pacific ½ inch (1.27 cm) DensDeck for Strength

This product is rated at 500 psi (3.45 MPa) and 2-5/8 inch (6.67 cm) flute spanability. The 1½ inch (3.81 cm) Wide Rib decking used for the tests has flutes that are 2½ wide. Based on the strength, the allowable height of water can be calculated:

$$h = \frac{500\,psi}{62.4\,pcf}\frac{(12in)^3}{ft^3} = huge \tag{7.15}$$

Based on these two criteria, the DensDeck material is strong enough for the tests.

Check Edge Joists for Possible Failure

From SJI, the moment of inertia of the joists is directly proportional to their live load capacity:

$$I = w_{ll} L^3 * 26.767 * 10^{-6} \tag{7.16}$$

From the test setup, the spacing between joists was 67 inches (1.70 m). Space between edge joists and the wall was about 4½ inches (11.4 cm). Based on this, the tributary area of loading for the center joist is 67 inches (1.70 m), and for the edge joists is 38 inches (0.965 m). The center joist was rated at 101plf (1.47 kN/m) live load, the edge joists, 58 plf (0.846 kN/m). The factor of safety against the side joist failing is the ratio of their deflections under a uniform load:

$$\frac{\frac{67}{101}}{\frac{38}{58}} = \frac{0.663}{0.665} = 1.013 \tag{7.17}$$

The factor of safety here is very small, which is good. The goal was to use joists that were as close to balanced as possible, so the roof would deflect together. The problem is that when they are perfectly balanced, any of the joists could break first. This result shows that the center joist is expected to fail first, but that the joists are balanced enough that they should act as a unit. One percent may seem small, but as the load collects on the joists, any initial differences will begin to be exaggerated by the ponding effect, so any factor of safety, regardless of how small, should be fine. Experimentally, this is representative of a field condition where identical joists are used side by side, but due to manufacturing

inconsistencies, one is slightly weaker than its neighbors: it will start to collect load more quickly.

Check the Decking for Failure

As the center joist should fail first, the decking that was sent with the joists from the manufacturers should be checked to make sure it is strong enough to withstand the maximum loads. First, the maximum expected load will be calculated:

$$\frac{\left((1.67)(211)-12\right)plf}{67in} = 61.0\,psf \tag{7.18}$$

The decking used was 22 gage 1½ inch (3.81 cm) wide rib decking. At 6 ft (1.83 m) spacing with a double span condition, the Steel Deck Institute Design Manual load tables show that this decking can support up to 67 psf (3208 Pa). Based on this, it appears the decking should be safe from failure. The pitched roof complicates this, however. Because the water will be deeper at the low end of the roof, decking at this end will carry more load than decking at the high end. A more appropriate way to check the strength of the decking is to determine the allowable height of water at any point on the roof:

$$\frac{67\,psf}{62.4\,pcf} = 1.07\,ft = 12.9in \tag{7.19}$$

If the water level at any point in the structure becomes greater than 12.9 inches (32.8 cm), then the decking may fail. It is not known how high the water will get, so this check will be revisited in the results section of the report.

Check the Steel Support Beam for Failure, Deflection

The only significant force acting on the W10x49 (W250x73) steel beam is the reaction of the center joist. The maximum expected force can be calculated, including the built in 1.67 factor of safety:

$$\frac{(211\,plf)(1.67)}{67in} = 63.1\,psf \tag{7.20}$$

$$63.1\,psf\,(6\,ft)(24\,ft) = 9088lb \tag{7.21}$$

Conservatively rounding this to 10k, the maximum shear and bending moment in the beam should be 5 kips (22.2 kN-m) and 30 kip-ft (40.7 kN-m), respectively. From the Manual of Steel Construction, table 3-10, the moment capacity is 238 kip-ft (323 kN-m) and from table 3-2 the shear capacity is 102k. These strength values both provide large factors of safety against failure of the beam, but the question remains, will the beam deflection be significant? Again from the manual of steel construction, the moment of inertia of the beam is 272 in^4 (6.53 cm^4). The deflection can then be calculated:

$$\Delta = \frac{PL^3}{48EI} = \frac{(10k)(12\,ft)^3}{48(29000ksi)(272in^4)}\left(\frac{12in}{ft}\right)^3 = 0.0789in \tag{7.22}$$

So the deflection in the beam, for the conservatively calculated expected loads, is very small.

Check the Steel Column Sections for Strength

Each of the steel beams is supported on two column sections which are bolted into opposite walls. The load each needs to support is:

$$P = \frac{(12\,ft)(48\,ft)(63.1\,psf) + (49\,plf)(24\,ft)}{4} = 9380kip \qquad (7.23)$$

The column section is at least a W12x72 (W310x107), and is 21 inches (53.3 cm) long. Checking the Manual of Steel Construction table 4-1, it is clear that because these column sections are so short, there is no way they will fail.

Check Bolts Holding the Entire Structure to the Walls

Each column section is bolted into the support walls with four, one inch (2.54 cm) diameter bolts. The load each must carry is one quarter the load on a column section plus the weight of the column section, or 2377 lbs (10.6 kN). Assuming the bolts used are the weakest structural bolts, then from the Manual of Steel Construction, table J3.2, A307 bolts' shear strength is F_{nv} = 24ksi (165 MPa). The strength of one bolt can then be calculated:

$$F = (24ksi)\left(\pi(.5in)^2\right) = 18.8k \qquad (7.24)$$

This shows that each bolt is strong enough to support the required loads by a large factor.

AISC Ponding Check

The only independent set of code provisions published anywhere for checking ponding is in appendix two to the AISC manual of steel construction; every other code provision references this one for ponding. There are two methods presented in this appendix. The "Improved Design for Ponding" provisions are based on the properties of the roof and the expected dead and rain load, and provide the engineer with the ponding contribution to the load. As this test is expected to go to failure, there is no design rain load. For the purposes

of this report, only the "Simplified Design for Ponding" provisions of the AISC code will be checked (AISC, 2005).

According to this section of the code, a roof is considered stable if, for English units:

$$C_p + 0.9C_s \leq 0.25 \tag{7.25}$$

$$I_d \geq 25S^4 10^{-6} \tag{7.26}$$

Where:

$$C_p = \frac{32L_s L_p{}^4}{10^7 I_p} \tag{7.27}$$

$$C_s = \frac{32SL_s{}^4}{10^7 I_s} \tag{7.28}$$

And I_d is the moment of inertia of the decking and S is the spacing between the members supporting the deck. Because the test is treated as a one way test of the single joist, these requirements simplify to the single equation:

$$\frac{32DL^4}{10^7 I} \leq 0.25 \tag{7.29}$$

Where D is the distance between the joists in feet, L is the length in feet and I the moment of inertia in inches^4. For the joist tested in this experiment. This is essentially the same requirement that has been repeated throughout the literature with a factor of safety of four against instability. The code states that for trusses and steel joists, the moment of inertia should be reduced by fifteen percent for this check, and the numbers provided by the manufacturers include this reduction. By running the numbers for the joist tested, with length of 48 ft (14.6 m), spacing of just under six ft (1.83 m), and a moment of inertia of 309.33 in^4 (7.43 cm^4), the equation becomes:

$$.307 \leq 0.25 \tag{7.30}$$

So the roof that is being tested does not pass the ponding requirements of the code. This means that there is less than a factor of safety of four against the joist used being unstable in ponding loading. This should not affect the tests, for several reasons. First, the factor of safety of four is completely arbitrary; the joist is still stable by the theory. Second, the test is not investigating failure due to instability, or the assumptions that the theory was based upon. Whether or not the structure used for this test is stable against ponding loads, the contribution of these effects to the overall loads and stresses developed can still be determined.

Appendix C: Failed Member Design Strength Calculations

Calculations of the design strength requirements for the failed member, the top chord double angle section are presented here. All equations and explanations given here are taken from the AISC steel construction manual. The known data regarding the failed member that are required for these calculations are presented here:

b = 2 in (5.08 cm)	t = 0.166 in (4.22 mm)
E = 29000 ksi (200 GPa)	F_y = 50ksi (345 MPa) (nominal)
$\Phi_b = \Phi_c = 0.9$	A_g = 1.272 in^2 (8.21 cm^2)
R_x = 0.620 in (1.57 cm)	L = 24 in (61.0 cm)
I = 0.490 in^4 (118 mm^4)	y_c = 0.562 in (1.43 cm)

AISC Chapter H1.1

The design of a double angle section in compression and bending is controlled by either equation H1-1a or equation H1-1b, depending on the loading. These equations both require the calculation of P_c, M_{cx} and M_{cy}. The moments about the Y-axis are ignored because they are small and the member is restrained in this direction: the member fails (buckles) as a result of the combination of compression and in-plane bending.

AISC Chapter B4

First, it was determined that the double angle section is a slender element. Based on table B4.1, the limiting width-thickness ratio for slenderness is:

$$\frac{b}{t} < 0.45\sqrt{\frac{E}{F_y}} \tag{7.31}$$

The double angle section fails this check, so it is slender.

AISC Chapter E7.1

Based on chapter E, the following equations are given: $P_c = \Phi P_n = \Phi F_{cr} A_g$. Chapter E7 addresses slender elements and the calculation of F_{cr}. The equations require the determination of K, Q and F_e. Because the structure was designed as a truss all connections are treated as hinges and K is one. Because equation 7.32 is true and there are no stiffened elements, Q is one as well:

$$\frac{b}{t} \le 0.56\sqrt{\frac{E}{F_y}} \tag{7.32}$$

Because the failure mode is flexural buckling, F_e can be determined by:

$$F_e = \frac{\pi^2 E}{\left(\frac{KL}{r}\right)^2} = 191 ksi \tag{7.33}$$

Based on K and Q, the governing equation can be determined. Because the inequality is true:

$$\frac{KL}{r} \le 4.71\sqrt{\frac{E}{QF_y}} \tag{7.34}$$

F_{cr} is determined by:

$$F_{cr} = Q\left[0.658^{\frac{QF_y}{F_e}}\right]F_y = 44.8 ksi \tag{7.35}$$

Based on this, P_c can be calculated:

$$P_c = \Phi F_{cr} A_g = 51.3K \tag{7.36}$$

AISC Chapter F9.3

Based on chapter F9.3, $M_c = \Phi F_{cr} S_{xc}$. S_{xc} is the section modulus referred to the compression flange:

$$S_{xc} = \frac{I}{y_c} = 0.872 \tag{7.37}$$

Because the double angle is a slender section, F_{cr} is calculated:

$$F_{cr} = \frac{0.69E}{\left(\frac{b_f}{2t_f}\right)^2} = 551ksi \tag{7.38}$$

Then M_c can be calculated:

$$M_c = \Phi F_{cr} S_{xc} = 36kft \tag{7.39}$$

Summary

Returning to the specifications for combined loading and keeping in mind that the compressive force reaches more than 50 kips (222 kN), the governing equation for the interaction of the axial and in-plane bending is:

$$\frac{P_r}{P_c} + \frac{8}{9}\frac{M_{rx}}{M_{cx}} \le 1.0 \tag{7.40}$$

$$\frac{P_r}{51.3k} + \frac{M_{rx}}{40.5kft} \le 1.0 \tag{7.41}$$

The same equation, using the unfactored strength values, is shown in equation 7.42. This is the equation that is referred to in the text of the thesis regarding the strength of the failed element.

$$\frac{P_r}{57.0k} + \frac{M_{rx}}{45.0kft} \leq 1.0 \tag{7.42}$$

Appendix D: Shear Displacement Calculation

The shear displacements were calculated panel by panel based on the strains in the diagonal web members. The calculations use the dimensions shown in figure 3, where the panel shear displacement is shown as S:

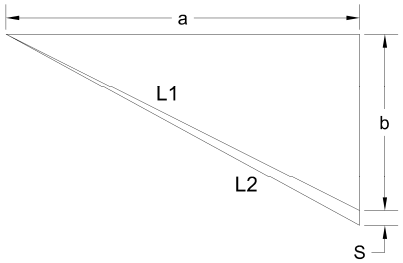

Figure 3: Shear Displacement

From geometry:

$$L_1 = \sqrt{a^2 + b^2} \tag{7.43}$$

$$L_2 = \sqrt{a^2 + \left(b + S\right)^2} \tag{7.44}$$

From mechanics:

$$L_2 = L_1\left(1 + \varepsilon\right) \tag{7.45}$$

From these three equations, set up for a tension diagonal and modified for a compression member by changing two signs, the shear displacements are found by:

For a tension diagonal:

$$S = \sqrt{\left(a^2 + b^2\right)\left(1 + 2\varepsilon + \varepsilon^2\right) - a^2} - b \tag{7.46}$$

For a compression diagonal:

$$S = b - \sqrt{\left(a^2 + b^2\right)\left(1 - 2\varepsilon + \varepsilon^2\right) - a^2} \tag{7.47}$$